PREDICTING CHANGES IN LAND USE AND LAND SURFACE TEMPERATURE USING CELLULAR AUTOMATA BASED ALGORITHM

A N M FOYEZUR RAHMAN

A THESIS SUBMITTED

FOR THE DEGREE OF MASTER OF SCIENCE IN CIVIL ENGINEERING

DEPARTMENT OF CIVIL ENGINEERING

MILITARY INSTITUTE OF SCIENCE AND TECHNOLOGY

2020

DECLARATION

I hereby declare that this thesis is my original work and it has been written by me in its entirety. I have duly acknowledged all the sources of information which have been used in the thesis.

This thesis has also not been submitted for any degree in any University previously.

A N M Foyezur Rahman

CERTIFICATION OF APPROVAL

The thesis titled **"Predicting Changes in Land Use and Land Surface Temperature Using Cellular Automata Based Algorithm"** by A N M Foyezur Rahman, has been accepted as satisfactory in partial fulfillment of the requirement for the degree of MSc in Civil Engineering (Env).

BOARD OF EXAMINERS

1.

Dr. Md. Tauhid Ur Rahman — Chairman
Professor — (Supervisor)
Department of Civil Engineering, MIST

2.

Brig Gen Md Abul kalam Azad, psc — Member
Dean & Head — (Ex-officio)
Department of Civil Engineering, MIST

3.

Maj Dr. Mohammad Shafiul Azam — Member
Instructor Class B
Department of Environmental, Water Resources, and Coastal Engineering, MIST

4.

Maj Dr. Kazi Shamima Akter — Member
Instructor Class B
Department of Environmental, Water Resources, and Coastal Engineering, MIST

5.

Dr. Md. Mafizur Rahman — Member
Professor — (External)
Department of Civil Engineering, BUET, Dhaka

ACKNOWLEDGEMENT

All praises to Allah the benevolent, the Almighty and the kind. I wish to particularly express my profound gratitude and sincere appreciation to my supervisor, Dr. Md. Tauhid Ur Rahman, Professor, Department of Civil Engineering, Military Institute of Science and Technology (MIST), for his proper guidance, valuable advice, encouragement and untiring help in the preparation of this research work. Virtually, he was the main source of inspiration whose continuous encouragement and valuable suggestions made it possible to carry out this work. Also, I am thankful to Bangladesh Meteorological Department (BMD) for their informative support. I am also grateful to the entire respondent who all has participated in the field visit and also for their informative support and inspiration.

During the entire process of my research work, I tried to collect accurate information and analyzed the relevant data carefully. Although I made every effort to formulate an error-free text and numbers, some errors may find their way into the research. I will be grateful to the readers who have comments or suggestions concerning the content.

ABSTRACT

More than half of the world population lives in Cities, therefore, urbanization has made a significant contribution to the global warming. In rapidly rising Mega-Cities results in a major change in land use and land cover (LULC) and substantial impact in land surface temperature (LST). Abrupt rise of LST has also adversely impacted some of the urban phenomenon. The aim was to analyze the pattern of LULC and LST change in Mirpur and its surrounding area for the last 30 years using Landsat Satellite images and remote sensing indices and develop relationship between LULC types and LST and analyze their impact on local warming. Later prediction of LULC and LST change for next 20 years was carried out using this analyzed data. Landsat-4 & 5 (TM) and Landsat-8 (OLI) images were used to track the relation between the LULC changes and LST from 1989 to 2019 at an interval of five years. The LULC and LST maps were simulated for the year 2039 by Cellular Automata based Artificial Neural Network (CA-ANN) algorithm. Two environmental indices such as Normalized Difference Vegetation Index (NDVI) and Normalized Difference Built-up Index (NDBI) were analyzed to show their interrelationship with LST. Findings of relationship among LST and LULC types signify that built up area increases LST by replacing natural vegetation with non-evaporating surfaces. Increasing trend of average surface temperature has been found and it has been rising gradually for last 30 years. For the year 2019 it was found that approximately 86% area was converted to built up area so far and 89% area had LST more than 28°C. The simulation shows that if the present trend continues, 72% of Mirpur area is likely to experience temperature close to 32°C in the year 2039. Further, LST showed a strong and positive correlation with NDBI and negative correlation with NDVI. The overall accuracy for LULC was over 90% where the result of the Kappa coefficient was 0.83 that was more than 0.75. The study may help urban planners and environmental engineers to understand and recommend effective policy steps and plans for LULC adjustments to reduce its consequences.

TABLE OF CONTENT

LIST OF FIGURES

LIST OF TABLES

LIST OF ACRONYMS

ANN: Artificial Neural Network

AVHRR: Advanced Very High-Resolution Radiometer

BMD: Bangladesh Metrological Department

BNBC: Bangladesh National Building Code

CA: Cellular Automata

DMP: Dhaka Metropolitan

GIS: Geographic Information Systems

IGBP: International Geosphere and Biosphere Program

IHDP: Human Dimensions Program

ISA: Impermeable Surface Area

LST: Land Surface Temperature

LULC: Land Use Land Cover Change

NDBI: Normalized Difference Built-up Index

NDVI: Normalized Difference Vegetation Index

UHI: Urban Heat Island

CHAPTER 01: INTRODUCTION

CHAPTER 01: INTRODUCTION

1.1 Background of the Study

Bangladesh is one of the heavily populated countries in South Asia and, over the past century, it has also experienced rapid population growth. The explosion of population growth mainly took place in the City areas. It is estimated that, almost all other men, women and children will be living in urban areas in future [16]. Study was conducted for Mirpur and surrounding area in the context of Dhaka. Being the capital of Bangladesh, Dhaka is one of the fastest growing mega-cities of the world [1-3]. Therefore, although it is likely that such rapid urbanization in Dhaka has a major impact on land cover changes and consequently on the urban micro-climate, little is known about these trends. It is also the home of more than 16 million people with a total land area of approximately 304.16 km2. The population of this city has increased by approximately 11 million in the past two decades [2]. Due to this population explosion mainly due to rural-urban migration and partially due to natural growth, Dhaka is expanding both vertically and horizontally and these expansions have been identified one of the major contributors of LST increase [20].

Urbanization refers to the process of the change of country area to a City area, which is the result of population immigration, administrative services, construction of new infrastructure, and development of industry and service sector. Over the past few years, the LULC change mechanism at national and local level has also drawn the attention of researchers. It is reported that LULC's global spatial dynamics also reveal the connection between land use change and human activity [4-7]. Some scholars emphasized on the effects on LULC changes by urbanization, believing that population growth and economic development contributed to urban expansion and the large number of water and agricultural land transformations into built-up areas. This transition also affects the local, regional and global ecosystem, including habitat quality, green areas and destruction of the environment [4, 8-10]. The mechanism of LULC transition is complex as the relationship depends on different scales in of natural and socio-economic factors [11-13]. The associated factors have an impact on the change in LULC due to the scale effect and vulnerability of the land system dynamics and it is therefore vital to understand its relation. Meanwhile, accurate prediction for future land use is essentially required in

order to avoid unexpected urbanization, which is necessary to plan and manage land use [7, 14-16].

Human migration to Cities causes urban areas to grow every year and creates rapid changes to their ecosystems, biodiversity, natural landscapes and the environment [12]. More than 70% of the world's population is anticipated to live in urban areas in the next 30 years [16-21]. While this development is a sign of economic growth and economic stability in the region, it has several short and long-term consequences. Over the last decade, geographers, urban planners and climate scientists have been paying considerable attention to elevated LST over urban areas [19, 22-26]. Several studies suggest that population expansion appears to increase the average LST in urban environment by 2-4°C in contrast with rural areas [27-30]. Increased LSTs and Urban Heat Island (UHI) impact have been associated with high energy consumption, air pollution, and health issues, including the deaths of children and elders from asthma and heat stroke [22, 31-36].

According to "Bangladesh Delta Plan 2100", Bangladesh is one of the highly populated country in the world. According to 2011 census data, the total population density is about 1,015 people per square kilometer. According to the recent UN data, approximately 25% of Bangladesh's current population lives in urban areas. Out of this urban population, more than half live in the four largest Cities: Dhaka, Chittagong, Khulna and Rajshahi. The population density is now believed to have reached around 34,000 people per km^2, making Dhaka amongst the most densely populated cities in the world. The area under rural settlement was estimated 885,637 ha in 1976 occupying 6.1% of the total area of the country. The rural settlement area consistently increased over time at a faster rate and become 10.0% (1,458,031 ha) in 2000 and 12.1% (1,766,123 ha) in 2010 [37].

Examining LULC change in the last few decades has become an increasing concern because of biodiversity decreasing, habitat changing and altering the regional and global climate patterns and composition [9, 38, 39]. It can be challenging, complicated and likely to yield contradictory results to detect and tests changes in LULC through direct field visits [5, 24, 25]. Over the past few decades, developments and integration of Remote Sensing and Geographic Information System (GIS) technologies have overcome most of the constraints and are now powerful methods for assessing, monitoring changes in LST and LULCs [6, 40-42]. Even since the early 1970s, the use of remote sensing techniques to measure LSTs and investigate the development and spatial distribution of

UHIs has been quite successful. Research has identified that massive change of various LULC components (water bodies, vegetation and agricultural land) contribute to the increase in LST which significantly stimulus the generation of UHI effect [1, 22, 43]. In fact, LST is recognized as one of the main factors for urban microclimate warming. A number of local issues are closely linked to the LST, such as biophysical hazards (e.g. heat stress), air pollution and public health concerns [44-47]. As the rise in surface temperature contributes significantly to the deterioration of the ecological balance, it is therefore important to obtain LST as a first and primary step and then to model possible LST so that policies can be implemented to mitigate the negative environmental impact [16, 18, 31, 32, 48, 49].

As LST is largely dependent on LULC therefore, prediction of LULC for evaluating future change in LST is needed. CA -ANN model provides a solid understanding of the complexities of the spatial system to evaluate and predict LULC changing pattern. For the purposes of monitoring previous and existing LULC and determining the potential impacts of LULC on the city area, this study mainly focuses on predicting future changes of LULC and identifies its impacts on future LST. Using a CA-ANN model, the simulation of future land cover can be analyzed. The CA- ANN model, together with the geographical information system, is widely regarded as the most powerful tool for modeling the probabilities of spatiotemporal shift in LULC [56, 57].

Under these circumstances stated above, the research is primarily planned to investigate LULC and LST shifts in the past two decades (1989-2019) through the use of recent and historically archived Landsat satellite images in Mirpur and its surrounding area. Also, a simulation will be done by using ANN based CA algorithm to predict the future growth and surface temperature of the Mirpur and its surrounding area for the year 2039.

1.2 Objectives of the Study

Following objectives were set for the study:

1. To analyze the LULC and LST change in Mirpur and its surrounding area for last 30 years using Landsat images and employing remote sensing indices.
2. To develop relationship between change in land cover types and LST and analyze the effects of land use change on local warming.
3. To predict the land use changes and estimates their impacts on LST for next 20 years.

1.3 Scopes of the Study

Global warming is an underlying environmental consequence which affects the global climate adversely all over the world. One of the main reasons for global warming is increase of LST due to unplanned urbanization through systematic destruction of the greeneries and water bodies. LST increases global average temperature that causes melting of north and south polar ices. As a result, sea level rise is common that causes flooding of lower region all over the world. This study analyzes urbanization rate by analyzing land cover changes and Surface temperature rise from satellite images. The analysis tries to make a relationship between these two major changing events using current technology for past, present and future eras. Also, environmental indices such as NDVI and NDBI that have correlation with LST, are analyzed too. Furthermore, as ground monitoring stations are not available all over the world, the study shows an alternative technology to monitor and analyze these important indicators for global problem. Environmental researchers, civil engineers, policy makers, and other governmental and nor-governmental institutions can use the study findings as the study evaluates one of the most burning issues in Dhaka city area. LST is related to enormous developing sectors such as urban planning, infrastructural development, and extent of building development permission and so on. These sectors are extensively related to the LST and LULC change study.

The analyzed data reveals increasing trend of past 30 year's land cover and LST data which can be used for further urban, strategic and policy planning. The LST and LULC data are estimated and predicted using Landsat Satellite Images which can be downloaded from USGS archive. LSTs are estimated using different LST retrieval techniques using Landsat thermal bands from reviewed literatures. Maximum Likelihood Supervised Classification and CA-ANN are used to classify LULC and predict the data, respectively. Furthermore, the study will introduce a free and cost-effective approach to analyze the issues therefore, it can be helpful for young researchers to think outside the box and analyze more and more in these sectors.

1.4 Limitations of the Study

Despites many benefits of this study, there are some disadvantages regarding this method of analysis. The major limitations regarding the study are given as follows.

- Due to 30m resolution of Landsat images, classification may not be 100% accurate.
- We could have collect smaller resolution images since satellite images beyond 1999 were not available. Also budget would not permit to procure those images.
- Due to time constraint whole Dhaka could not be studied.
- In summer and monsoon seasons, most of the satellite images are covered by clouds. That is why satellite images during winter season were considered only.

1.5 Thesis Structure

Thesis is structured into following manner:

- Chapte-1: Introductory chapter.
- Capter-2: This chapter summarizes the reviewed literature related to history of Dhaka City, expansion of Dhaka city, land use types and LULC classification, estimation of LST, Prediction methods, rationale for adopting CA-ANN.
- Capter-3: It gives a comprehensive overview of the Mirpur and surrounding are and past and present state of Dhaka City.
- Capter-4: This Chapter portrays the comprehensive research methodology. Downloaded Landsat images were classified into four broad LULC classes by ArcGIS. Method of estimation LST is discussed. Finally, LULC and LST prediction methods using CA-ANN for the year of 2039 with the help of MOLUSE plug-in QGIS are discussed.
- Capter-5: This Chapter sequentially discusses about the analyzed results of the classification of LULC and LST and validation of results. Association of LULC and LST, relationship among LST, NDBI and NDVI, future prediction of LULC and LST and finally validation of predicted result.
- Capter-6: Conclusions and Recommendations are made at the end

CHAPTER 02: REVIEW OF RELATED LITERATURES

CHAPTER 02: REVIEW OF RELATED LITERATURES

2.1 Introduction

This chapter summarizes the reviewed literatures related to LULC classification, LST estimation and LST prediction and their different methods of estimation using satellite images. It will also sequentially discuss few methods and related literatures of LST estimation and process of estimating some environmental indices related to LST. Finally, some prediction procedures of LST and LULC including CA-ANN method will be discussed.

2.2 Historical Background of Dhaka City

Dhaka first emerged as a thriving city during the Mughal period. Making Dhaka the capital of Bengal was the catalyst for its rapid growth. Even though Dhaka was already a budding city during Afghan rule, it truly came into its own during the Mughals period. Dhaka became an important metropolitan, attracting traders and dignitaries from all over the world. The area known today as 'Puran Dhaka' was the focal point then [12]. It was also during the British rule that the Dacca Municipality was established. Also, a 'Committee for improvement of Dacca' was established to organize better and develop the city. As a result of both, the inner city saw widespread rebuilding activities of houses and roads. However, this development of Dhaka was mostly unplanned [43]. The rising population and the ever-increasing demand led to the formation of several new residential areas in Dhaka. Elites of the city began building houses in Dhanmondi, and it became the most valuable real estate for residence. Development of Dhaka, particularly Mirpur road and the highlands around it helped the government create the first planned residential area in Mohammadpur. Creation of several satellite towns quickly followed this. Gulshan Model Town was the first one; Banani, Uttara and Baridhara Model Town came after them. They were designed to accommodate middle-class citizens of Dhaka [62].

2.3 Expansion of Dhaka City

Dhaka experienced a massive boom after the country gained independence, both in terms of area and population. DIT was re-christened as RAJUK, and many urbanization projects took place under its banners [43]. The expansion of Dhaka continued with the filling up of swamp and marshland to satisfy the growing demand for housing. It largely followed plans left by the Mughals. Private land developmental projects began to play a major role

in the creation of residential areas for the city. Areas such as Malibagh, Banasree, Rampura, and Mirpur began to take shape as promising places to live in Dhaka. Most of the growth of Dhaka was organic in nature, and very little intervention from the government took place. The rapid growth of Dhaka has propelled the metropolitan to the ranks of a megacity. It is now the 11th largest megacity in the world [12]. High-rise buildings have become necessary to accommodate the vast population of Dhaka. Most of the citizens, however, are migrates to the city. According to Power and Participation Research Centre (PPRC), only 21% of residents in urban Dhaka were born here [17]. As such, urbanization of Dhaka is moving at an accelerated pace. The expansion of Dhaka is now focused eastward, and a host of new development projects are taking place in areas such as Purbachal and Uttar Khan. These areas and others will be the frontier for a more global Dhaka. The core city only comprises 30% of the entire greater Dhaka. This eastern push is in line with the decentralization of Dhaka and expanding the reach of the core city [12].

2.4 Land Use types and LULC Classification

Land cover change is defined as the loss of natural areas, particularly loss of forests to urban development [2, 58-61]. Urbanization creates pressure in cities and brings changes in ecosystems, biodiversity, landscape and environment [12, 43, 62]. Although urbanization is a sign of economic development and prosperity, it also creates short and long-term negative consequences in cities [18, 27]. Changes in LULC scenario and increase in the city's LST are the main long-term consequences [27, 63]. There are several published reviews of raster imagery-based on two dates change detection methods on the use of remotely sensed data or pre-existing map datasets from remotely sensed data [5, 6, 20, 36, 46, 60, 64-66]. These methods include: (1) image rationing (2) image differencing (3) Principal Components Analysis (PCA) (4) multi-date classification (5) Change Vector Analysis (CVA) (6) post classification comparison. The choice of method can depend on such factors as the input data used for deriving the change map dataset and the kind of change map (e.g., general forest change or more specific LULC change). Excluding the post-classification method, most change detection mapping methods require that remotely sensed imagery from two or more dates as input to a data processing workflow in order to derive a change map [4, 9, 67-70]. Identification of LULC transitions is an effective approach to address the problems regarding unregulated urbanization and environmental degradation [71-73]. Besides, to ensure proper management and sustainable distribution

of environmental resources, a detailed analysis of the evolving trend of LULC change is essential, which can be achieved through the implementation of Remote Sensing (RS) techniques [74-77]. RS techniques facilitate modeling of the upcoming LULC change pattern and helps to develop an understanding of the continuous LULC transitions [78]. It further helps to analyze and develop the land management regulations. Different topographical features such as demographic information, past pattern of LULC transition, positions of various facilities, etc. are considered to model the possible location of the LULC transition. The change in LULC subsequently increase the LST and urban heat island (UHI) formation which have been directly linked with high energy consumption, air pollution, and human health risks, such as high blood pressure, asthma and heat-stroke related deaths for both elders and children [33, 79, 80]. The systematic implementation of mitigation approaches for LULC and LST is, therefore, a crucial political priority for minimizing urban warming and improving living environments, public health and community well-being.

2.5 Estimation of LST

Researchers have analyzed the LST characteristics (per LULC categories) in different urban settings using the different thermal infrared sensors available that can collect data at different spatial resolutions [52, 81-83]. Xiao et al. (2008) assessed Landsat TM sensor LSTs and calculated their statistical relationships for Beijing City with several biophysical and demographic variables [84]. Li et al. (2012) have noted that in Beijing, the similarities between the Spatio-temporal patterns in LSTs obtained from the Landsat TM sensor and the green spaces configuration (classified as SPOT imagery) [85]. By capturing and comparing LSTs from the AVHRR sensor with land coverage identified from SPOT-HRV data, Dousset and Gourmelon in 2003 analyzed the relationships between different land cover and LSTs in Los Angeles and Paris metropolises [86].

Recently, in the border cities of Calcutta (India) and Khulna (Bangladesh), Chaudhuri and Mishra (2016) compared the LSTs (from Landsat data) between different types of land coverage [68]. Ahmed et al. (2012) have calculated the LSTs and the decadal shifts in the metropolitan area of Dhaka and Khulna from Landsat sensors for the first time in Bangladesh [14, 53]. They simulated the future growth of the city and LSTs of the built-up areas for 2029 [33]. Kafy et al. (2020) identified the impact of LULC change on LST by modelling approach using ANN and MLP-MC method in Rajshahi City [60].

Among the cities of the Middle East, El Abidine et al. (2014) modelled the heat waves by analyzing the interactions between LST and the differences in the LULC groups in Qatar [26]. Rasul et al. (2015) have carried out a similar study using Landsat 8 data to compare LSTs in different LULC groups in the northern Iraqi city of Erbil in northern Kurdistan [55]. Lazzarini et al. (2013) combined data from MODIS, ASTER, and Landsat ETM+ and formed a relationship between LST, NDVI, and UHI surface at the city and district level for the city of Abu Dhabi, UAE [87]. For the Kingdom of Bahrain, a mixture of Landsat images, statistics and weather station information was used by Radhi and Sharples in 2013 to investigate spatial trends and their impacts in the formulation of UHIs over the past decades [88]. Scientists have used the National Oceanic and Atmospheric Administration (NOAA) data in the recent past to extract LST and therefore to calculate UHI for national scale studies [89, 90]. Nonetheless, thermal infrared (TIR) data from Landsat Thematic Mapper (TM) and Enhanced Thematic Mapper Plus (ETM+) have often been used in smaller-scale experiments in recent years [45, 91, 92]. Some studies used mixed types of images. For example, in order to extract UHI strength in Hong Kong city, Liu and Zhang (2011) analyzed Landsat TM and ASTER images [93]. The following steps and algorithms were selected for LST classification:

a. Top of Atmospheric Spectral Radiance: Top of Atmospheric Spectral Radiance (TOA) was retrieved by using following equation 4.1 [93].

$$L_\lambda = M_L \times Q_{cal} + A_L \quad \text{---------- (2.5.1)}$$

Where M_L was represented as the band-specific multiplicative rescaling factor, Q_{cal} was the Band 10, A_L is the band-specific additive rescaling factor.

b. Sensor Brightness Temperature Estimation (T_i): First and foremost, conversion from the spectral radiance of thermal infrared band to active radiance sensor brightness temperature was calculated by equation 4.2 [16, 22, 93, 94].

$$T_i = \frac{K_2}{\ln\left(\frac{k_1}{L_\lambda}+1\right)} \quad \text{---------- (2.5.2)}$$

Here, K_1 and K_2 are the calibration constant K1 in W/(m^2.sr.μm) and K2, in kelvin, respectively. The value of K_1 and K_2 for Landsat 4-5 and Landsat 8 are given as following table 4.3 [93].

Table 2.1: Landsat Thermal Bands Calibration Constants

Constant	Unit K1: W/(m^2.sr. μm)	Unit K2: Kelvin
Landsat 4-5 TM	607.76	1260.56
Landsat8 TIRS (band 10)	774.8853	1321.0789
Landsat8 TIRS (band 11)	480.8883	1201.1442

c. Retrieving LST: The thermal infrared band measures Top of Atmosphere (TOA) radiance. Meanwhile, atmospheric effects such as upward emission and downward irradiance reelection from the surface should be corrected to obtain accurate land surface brightness temperature. Calculation of land surface spectral emissivity (Ɛ) is a way for the above correction. Meanwhile, there are some factors such as water content, chemical composition, structure and roughness which control the surface emissivity [26]. Many researchers described that surface emissivity is closely related to NDVI and therefore the emissivity can be estimated by using NDVI [33].

NDVI can be calculated the values of reflectance of the Visible and Near Infrared bands using the following equation 4.3 [33].

$$\text{NDVI} = \frac{B_{NIR} - B_{RED}}{B_{NIR} + B_{RED}} \quad \text{---------- (2.5.3)}$$

Where, B_{NIR}, B_{RED} were the pixel values of near-infrared and red bands. Using the NDVI value the Proportion of Vegetation (Pv) can be calculated to measure land surface emissivity (Ɛ) by using equation 4.4 [93].

$$P_v = \left(\frac{NDVI - NDVI_{min}}{NDVI - NDVI_{max}}\right)^2 \quad \text{---------- (2.5.4)}$$

Using Pv, land surface emissivity (Ɛ) can be measured by following equation 4.5 [95, 96].

$$\varepsilon = 0.004 \times P_v + 0.986 \quad \text{---------- (2.5.5)}$$

The land surface temperatures corrected for spectral emissivity (Ɛ) was computed by the following equation 4.6 [20, 68, 97, 98].

$$LST = \frac{T_i}{1 + \left(\lambda \times \frac{T_i}{\rho}\right) \times \ln(\varepsilon)} \quad \text{---------- (2.5.6)}$$

Here, LST represents land surface temperature, T_i was the sensors brightness temperature. The emitted radiance's wavelength was indicated as λ and Ɛ indicates the land surface spectral emissivity.

In addition,

$$\rho = h\frac{c}{\sigma} \quad \text{---------- (2.5.7)}$$

Here, the value of ρ is 1.438×10^{-2} mk. Where h indicates Plank's constant which is equal to 6.626×10^{-34} Js, c indicates the velocity of light, which is equal to 2.998×10^{8} ms^{-2} and σ is the Boltzmann constant (5.67×10^{-8} Wm^2k^{-4} = 1.38×10^{-23} JK^{-1}) [26].

for the validation of LST temperature data of Bangladesh Meteorological Department located at Agargaon, Dhaka to be used [29]. .

2.6 Relationships between LST and Environmental Indices

Using Landsat TM data collected from Twin Cities, Minnesota, Yuan and Bauer, an analysis was established about the relationships between LSTs, the uniform vegetation difference index (NDVI) and the percentage of impermeable surface area (ISA) [99]. In order to investigate the associations between land cover changes and LST, different types of land cover indices were also created [46, 99]. Among the different indices, studies found a strong association between the normalized difference vegetation index (NDVI), normalized difference built-up index (NDBI), normalized difference water index (NDWI), and normalized difference bareness index (NDBaI) with LST [22, 100, 101]. Worldwide, NDVI is used to evaluate plant abundance, measure drought, monitor and forecast agricultural production, assist in forecasting dangerous fire areas, and model desert invasion [99, 102]. NDVI creates a single-band dataset that reflects predominantly healthy biomass. This index value is between −1.0 and 1.0, where any negative values are produced primarily from clouds water and snow, while values close to zero are created primarily from rock and bare soil Rather small NDVI levels (0.1 and below) are similar to desolate fields of farmland, gravel, sand or snow [103, 104]. Moderate values reflect parks, shrubs and grasslands (0.2 to 0.3), while high values display temperate and tropical rainforests (0.6 to 0.8) [103, 104]. NDWI means vegetation water content and vegetation water condition [105, 106]. NDBI is responsive to the environment being built up. Previously, it has been used as a proxy for the magnitude of built-up areas [106]. Similar barren fields are listed by NDBaI [107]. Such indexes are used by setting the correct threshold values to distinguish different types of land cover [11].

The LST-NDVI interaction was extensively documented in the literature [108]. The urban thermal climate is correlated with a decline in vegetation coverage [97]. Relationship of

LST is quite strong in nature as NDBI is a sensitive indicator to monitor and isolate built-up areas. LST is extreme where commercial and industrial land uses are located in Toronto, i.e., correlation exists between NDBI and LST [109]. NDWI and NDBaI are being studied to assess water content in vegetation and soil bareness which are also responsive with LST [107, 109]. The LST level is directly related to the level of urbanization, patterns of land use and intensity of development [43]. LST is linked to land use/cover transition patterns such as the configuration of the built-up area, vegetation and water bodies [107].

2.7 Prediction Methods

An urban area is a dynamic system which is a complex configuration. A City's development depends on various driving factors such as financial, economic, socioeconomic, political, spatial, cultural, and other phenomena [8, 62, 110]. Over the years, numerous methods have been developed to help forecasting improvements in urban growth and land use. Some of the prominent packages are Geomod [111], SLEUTH [112], Land Use Scanner [113], Environment Explorer [114], SAMBA [115], Land Transformation Model and CLUE [116], among others. Again, these techniques use a number of methods to model shifts in ground cover such as Markov Chain [117], Cellular Automata [56], Logistic Regression [118], and Artificial Neural Network (ANN) [50]. Numerous studies have used a CA model to analyze the simulation of land-use change patterns. There are many researchers who gave a descriptive and methodological overview of CA-ANN algorithm. They successfully predict LULC for the future and recommended CA-ANN method for simulation. The accuracy of CA-ANN was satisfactory as well. Moreover, Parsa et al. (2016) successfully used the CA-Markov model in the Arasbaran Biosphere Reserve-Iran to predict the future LULC, which will serve land-use planners and policymakers to make suitable decisions about future land use challenges [119]. They found out that the use of a CA-Markov model can be useful in the design of land use policies and can also be used as an early warning system. Additionally, Ozturk (2015) provided a comparison between the CA-Markov chain and the multi-layer Perceptron-Markov chain (MLP-MC) models to predict future LULC transition in Turkey's Atakum, Samsun urban growth simulation [120]. The MLP-MC model gave superior results for projected simulation of scenarios than the CA-Markov model, according to the Authors. Regmi et al., (2014) on the other side, linked CA-Markov and GEOMOD models to examine and model the dynamics of LULC in Nepal's

Phewa lake watershed [121]. They observed that in forecasting potential LULC scenario, CA-Markov chains were quite successful as an organizational model. In these models, multiple driving factors were used, such as infrastructure and socio-economic drivers (road network & human settlement) and Digital Elevation Model (DEM driven slope) terrain physical drivers. The results show that the driver forces influenced watershed LULC's spatial structure.

2.8 Adaptation of CA-ANN

Artificial neural networks (ANN), the branch of artificial intelligence, date back to the 1940s, when McCulloch and Pitts developed the first neural model [22, 50]. Since then the wide interest in ANN, both among researchers and in areas of various applications, has resulted in more-powerful networks, better training algorithms and improved hardware. The basic problem solved by ANN is the inductive acquisition of concepts from examples. ANN is biologically inspired computer programmes designed to simulate the way in which the human brain processes information [48, 52, 122]. ANN gathers knowledge by detecting the patterns and relationships in data and learns through experience, not from programming, and there lies the basic difference between ANN and other classical computer programmes. Another significant difference between ANN and other computer programmes is that the algorithms used for data analysis are flexible [22, 50]. They can be changed anytime during the progress of analysis. The distinctive feature of ANN is their ability to deal effectively with multidimensional problems, including several thousands of features. An ANN is formed from hundreds of single units, i.e. artificial neurons or processing elements, connected with coefficients (weights), which constitute the neural structure and are organized in layers. The ability of neural computations comes from connecting neurons in a network. The better the neurons are connected in networks, the better is the prediction as output. The activity of a neural network is determined by transfer functions of its neurons, by the learning rule, and by the architecture itself [123, 124]. ANN is made of three layers namely input layer, output layer, and hidden layer/s [52, 125-127]. There must be a connection from the nodes in the input layer with the nodes in the hidden layer and from each hidden layer node with the nodes of the output layer. The input layer takes the data from the network [50, 52, 125]. The hidden layer receives the raw information from the input layer and processes them. Then, the obtained value is sent to the output layer which will also process the information from the hidden layer and give the output. The interconnection of the nodes

between the layers can be divided into two basic classes, namely the feed forward neural network and recurrent neural network. In the feed forward ANN, the information movement from inputs to outputs is only in one direction. On the other hand, in the recurrent ANN, some of the information moves in the opposite direction as well Achievement of successful result from ANN studies depends on minimization of prediction error by optimization of inter unit connections during training [50, 52, 123, 127]. By doing so as trial and error, the network reaches the specified level of accuracy. Once the network is trained with minimum prediction error and tested, it may be used with new input information to predict the output. The information in ANN is encoded in the strength of the network's 'synaptic' connections [22, 48, 122-124]. Latest studies on ANN are mainly centered on designing new network types by changing transfer connection of neurons, by changing learning rule, and by initiating new connection formula [50, 123, 124, 126]. The CA model was used for the simulation of future LULC changes using MOLUSCE plugin in open-source QGIS 3.1 software. The CA model encompasses both static and dynamic aspects of LULC transformation at a high degree of precision [20, 56, 60, 128, 129].

. A number of studies, applied different integrated modeling approach to identify the relationship between LULC and LST [14, 18, 23, 33, 42, 53, 54]. Mishra et al. (2018) recently assessed and compared the application of the Stochastic Markov chain (ST-MC), CA and MLP-MC models to observe, simulate and predict future LULC scenarios in the district of Varanasi, India [54]. Rahman, Aldosary and Mortoja (2019) used Landsat imageries and CA model to investigate the effects of LULC changes on LST for the Saudi Arabia Eastern Coastal City of Dammam [16]. Maduako, Yun and Patrick (2016) simulate and predict future LST trend in Ikom city of Nigeria using the ANN method [22]. For, Bangladesh, Ahmed et al. (2013) first calculated decadal shifts of LULC and LST from Landsat sensors in Dhaka metropolitan area. Eventually, they modeled the city's growth and simulated the built-up area LST for 2029 [33]. Islam and Ahmad (2011) also evaluate and predict the LULC change using MLP-MC techniques in Dhaka City [41]. Zine El Abidine et al. (2014) model urban heat waves in Middle Eastern cities (Qatar) by establishing correlations between LST and LULC categories [26]. Rasul et al.(2015) also focused on a parallel study using Landsat 8 data to compare LST with various LULC categories in the Iraqi city of Erbil [55].

2.9 Field Verification Techniques of LULC

Overall accuracy, producer accuracy, user accuracy and the Kappa coefficients are the part of the accuracy parameters. The overall accuracy is calculated by dividing in the error matrix with the total corrected number of samples (equation 5.1). Traditionally, the 'producer's accuracy' is referred to as the division of the total number of the correct sample units within a category by the total number of sample units in that category (equation 5.2). This measure of accuracy concerns the possibility to correctly identify a reference sample unit and is a true measure of omission error. On the other hand, the total number of correct category sample units is divided into that category on a map (e.g., the total number of row sample units), then this result is a commission error measure. This measure is called "user's accuracy" or reliability and indicates the probability that a sample unit identified in the map is in reality in the ground (equation 5.3). After calculating all the accuracy parameters, the Kappa coefficient was measured by following equation 5.4 [69, 130-132].

$$Overal\ Accuracy = \frac{Total\ number\ of\ corrected\ classified\ pixelx\ (diagonal)}{toal\ number\ of\ reference\ pixels} * 100 \text{ --- (2.9.1)}$$

$$Producer\ \ Accuracy = \frac{number\ of\ correctly\ classified\ pixelxs\ in\ each\ catagory\ (diagonal)}{total\ number\ of\ reference\ pixels\ in\ each\ catagory\ (column\ total)} * 100 \text{ ------ (2.9.2)}$$

$$User\ \ Accuracy = \frac{number\ of\ correctly\ classified\ pixelxs\ in\ each\ catagory\ (diagonal)}{total\ number\ of\ reference\ pixels\ in\ each\ catagory\ (row\ total)} * 100 \text{ ---------- (2.9..3)}$$

$$Kappa\ Coefficient\ (T) = \frac{Total\ number\ of\ Sample * Total\ Number\ of\ Corrected\ Sample - \sum(col.tot * row\ tot)}{(Total\ number\ of\ Sample)\text{^}2 - \sum(col.tot * row\ tot)} * 100 \text{ ----- (2.9.4)}$$

2.10 Summary

On the basis of above review in order to address the objectives of the study the following techniques to be adopted: Firstly, LULC classification will be done through Landsat imageries for its easily accessibility and moderate resolution. Secondly, the LST will be

estimated using the Landsat imageries also. The equations for retrieving LST will be taken from related literatures. Thirdly, presently many literatures are available in which only prediction of LULC has been done by some prediction algorithms. Simulation of LST using prediction algorithm is new and very few literatures are available in internet. Therefore, prediction of LST will be challenging for this study. In addition, both LULC and LST will be predicted using CA-ANN algorithm in this study. Finally, validation of all the generated data will be done using ground observation data, Kappa coefficient and other related methods.

CHAPTER 03: STUDY AREA PROFILE

3.1 Introduction

A comprehensive overview of the study area will be discussed here in this chapter. Mainly study area profile including geographical location, brief discussion of Dhaka city, existing condition of study area, visited area in the field will be highlighted here.

3.2 Location of the Study Area

"Dhaka City" is popularly known as "Dhaka Metropolitan Area (DMP)", which is located almost at the geographical center of Bangladesh at 23°43′0″ North latitude and 90°24′0″ East longitude (Figure 3.1), on the eastern bank of the Buriganga River [33]. DMP covers a total area of 306.04 km^2 [53].

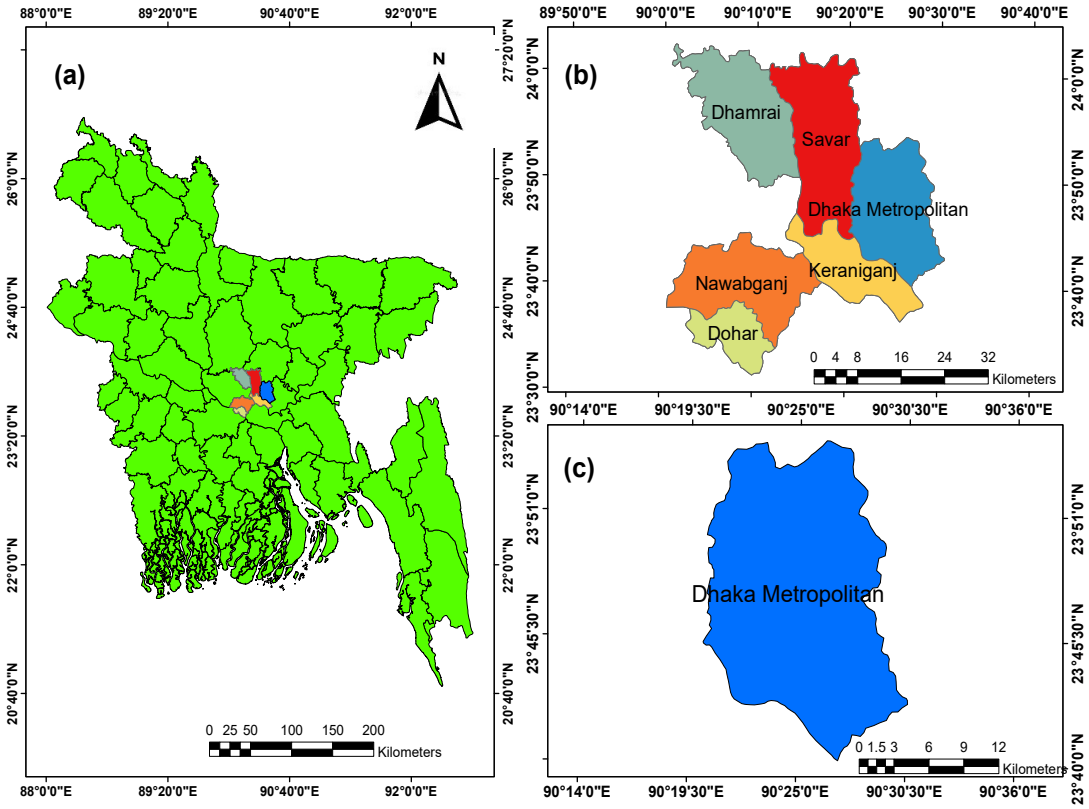

Figure 3.1: Location of DMP (a) Bangladesh, (b) Dhaka District and (c) Dhaka Metropolitan Area (DMP)

There are some old images are shown in figure 3.2 to have an idea the past condition of Dhaka city. The Buriganga river was very lively in old days and the surrounding areas were also non-urbanized (Figure 3.2).

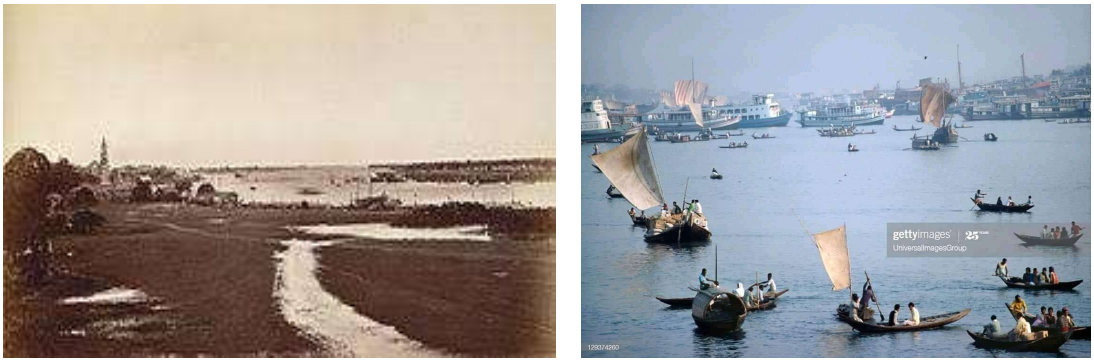

Figure 3.2: Glimpse of Old Dhaka City [Ahmed et al, 2013]

Mirpur and its surrounding area faced tremendous change in LULC and LST for last 30 years. Therefore, Mirpur and its surrounding area has been selected for the main study area of this analysis.

Geographic location of the study area is located between 90°21'42.195"E to 90°21'27.465"E and 23°50'55.249"N to 23°44'46.334"N. The study area is total 48.834 km^2. The area of interest is situated in DMP area. Eight (8) Thana boundaries such as Mirpur, Adabor, Mohammadpur, Pallabi, Darus Salam, Shah Ali, Kafrul and Sher-e-Bangla Nagar cover the study region. The Figure 3.2 shows the location of the study area (Figure 3.3).

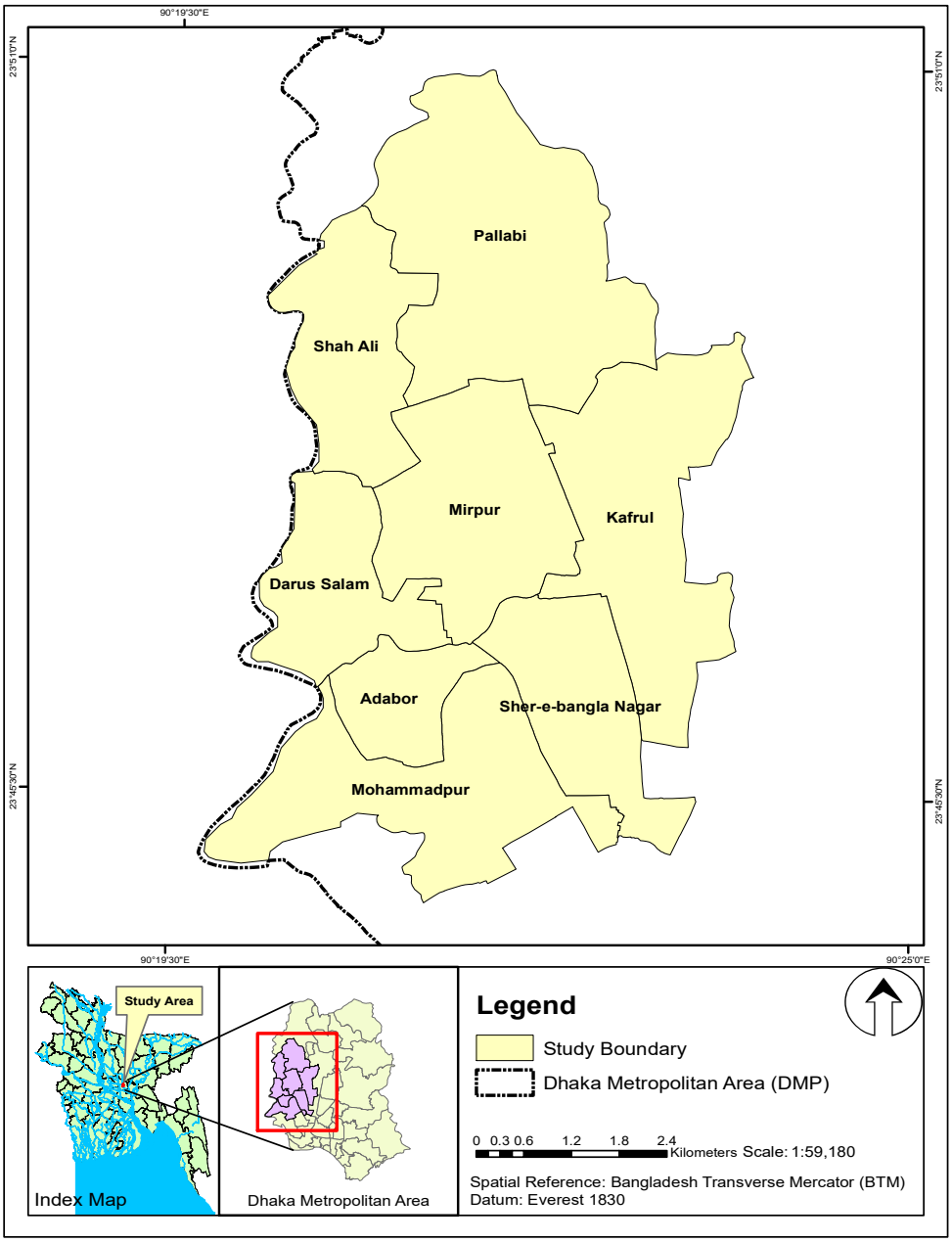

Figure 3.3: Location of the Study Area

3.3 Existing Scenario of the Study Area

3.3.1 Gradual Expansion of Dhaka City

Since its establishment, Dhaka has grown mostly without adequate planning interventions; substantially organic in nature. The patterns of areal expansion and the urban form of Dhaka have been largely dominated by the physical configuration of the landscape in and around the city, particularly the river system and the height of land in relation to flood level. There are two dominant general patterns in the historical evolution

of urban old Dhaka or the historic core, and new Dhaka or northern expansion. The latter is actually post-colonial development, an effect of modernization, still spontaneous and organic in the nature. Besides these two dominant factors, five distinct and mutually exclusive spatial patterns are found simultaneously existing in an explicit composition. Dhaka reached its present status through a series of dynamic changes it underwent during different phases of history. The phases and consequent changes over the years have shaped Dhaka to its present structure. The growth of Dhaka from 1949 to 1989 largely followed the limits determined by the Mughals (i.e. towards north up to Tongi, up to Mirpur in north-west, up to Postagola in south- east). The growth of modern Dhaka reached its apex just after the liberation war. The growth caused many low lands filled up owing to scarcity of land and consequent rise in its price. All the low lying areas on the eastern and western side came under occupation. In the course of time, land use pattern was

Dhaka city is exponentially growing; specially after 1971 it became the capital of the independent Bangladesh. The key factors of urban population growth are (1) unequal infrastructure and national strategies, environmental threats and lack of opportunities for jobs in rural areas (2) the geographical expansion of current urban areas and a reform of the concept of metropolitan areas (3) the rural to metropolitan migration, (4) the rapid development of native city's (5) the geographical expansion of new towns, and (6) rural to urban migration. Owing both to the pull factors and the push factors in Bangladesh between 1974 [133, 134]. Bangladesh saw a rise in urban population growth of 10.03%. Those are job prospects, higher salaries and profits, improved working standards, educational opportunities, means of travel, relatively better social welfare, etc. To the benefit of the pull effects, they are Poverty and lack of employment in rural areas is, on the other hand, motivating forces. There are no higher education institutions; there are also natural disasters such as cyclones, flooding, river erosion, etc. Migration is thus the key driver of rapid growth (up to 70 percent) in the city of Dhaka among urban populations [6, 41]. World Bank (2007) has shown that new migrants (about 300,000-4000, 000) come to Dhaka City in past years [135].

3.3.2 Present Condition of the Study Area

Mirpur and its surrounding area is one of the most growing part of Dhaka city. Past 30 years, this area faced enormous changes both in physically and environmentally. Dhaka city mainly gown up beside the Buriganga River but the extent of expansion is gradually

increasing in the northern part along with the river. Loss of water bodies, vegetation lands are the common scenario in this area except National Zoo and Botanical garden. To conduct this research, regular field visit has been done to evaluate the present and past condition of the study area. Field visits were also conducted for validation purposes.

Analyzing past urbanization trends, some hotspots were selected where LULC were changed mostly. Hotspots were selected by analyzing the Google Earth Images and secondary data from internet. The places which went under large LULC changes have been selected as hotspots for field visit. The hotspots for field visit are shown in Figure 3.4. Riverside lands were considered minimally as hotspots because of existence of water bodies. Most of the water bodies were occupied by several developing purposes such as sand filling for urbanization, direct urbanization and slum development and so on.

Figure 3.5: Ancient View of Dhaka City (Hart & Sailor, 2009)

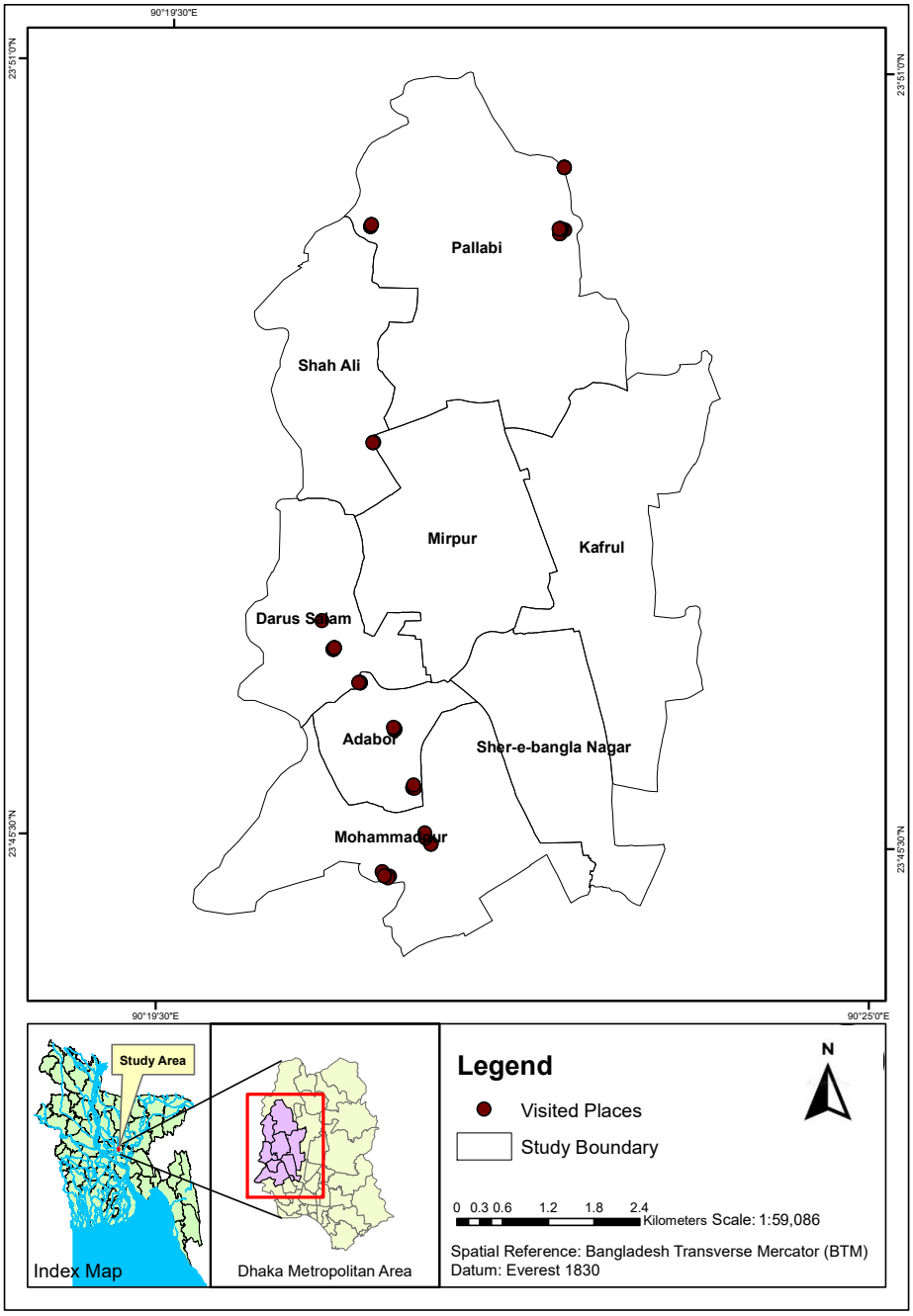

Figure 3.4: Selected Hotspot Locations for Field Visit

The main purpose of field visit was to conduct a focus group discussion with 5-10 local respondents to know the past and present condition of that region. Eight focus group discussion with 5-10 local respondents were generated in eight different places to know the past trend of urbanization in their local areas. As the local respondents are the active witnesses for these changes, therefore, talking with them, the Author evaluated how and what extent the changes was occurred in that particular area. The sequential information

which were come from focus group discussion are presented below with necessary Figures.

Bosila Area is situated near to the Buriganga River. In past, the area was covered by water, agricultural lands and greeneries and so on. But now the place is gradually becoming an urban hub. According to local respondent, development of residential buildings, local bazars, shops, showrooms are now a common phenomenon here. They added that it was a beautiful before and full of water, fish, canals, agricultural lands available all around in the past. There was a big canal in this area which disappeared almost nearly 15 years ago. The place was a village before. The area was started to urbanized from 90's and still it is going on (Figure 3.5).

Figure 3.5: Existing condition of Bosila Area, Mohammadpur

Kedarabad Housing is a residential hub of Mohammadpur Area which is being under development in. The area was covered under water body and agricultural land till past 5-10 years. Though 40 years ago, the area was declared as City Corporation Area but the area was a village for the long time. The area was started developing from 5-10 years earlier. Developing of residential building is rapid here, but most importantly, the developers do not follow the basic Bangladesh National Building Code (BNBC). Therefore, they built the houses by not maintaining minimum spaces between the building (Figure 3.6).

Japan City Garden is a modern residential hub which was developed recently. It has high quality of living facilities where people very eager want to live. The area is infested with several high rise buildings those are the residences of large number of people (Figure 3.7). Hence, some greenery can be seen here but the area was not urbanized before. The

area had a lot of greeneries which provided cold weathers, shadows, oxygen, shelter for species and so one.

Figure 3.6: Existing Condition of Kedarabad Housing, Mohammadpur

Figure 3.7: Existing Condition of Japan City Garden, Mohammadpur

Baytul Amal Housing, Adabor is highly urbanized residential and commercial area. Earlier it was known as a place for fish cultivation and crop production (Figure 3.8) area. In the high elevated land, rice and several crops used to be grown there. The area is situated near a water canal. In the low lying areas, fish cultivation was very popular just besides the canal in earlier time. Now the canal is nearly dead. Household and commercial wastes are thrown into the canal. Also, the canal had lost its shape and turned into narrower one. Local peoples informed that present temperature is much higher than earlier.

A natural water canal is existed in the Darus Salam Area, but the canal seems to be dead due to household and commercial waste. A huge slum area was grown beside the canal to support excessive livelihood. The household and living condition for the slum area is unhygienic (Figure 3.9).

Figure 3.8: Existing Condition of Adabor (left) and Darus Salam (Right)

Ranikhola Bazar is situated near National Zoo and Botanical Garden. The area was not much urbanized before. The place was full of watrer features specially ponds in the past. Local respondents told that the overall land use change of this area is slower than others places. The temporal condition of this area is comparatively lower because of the zoo and Botanical garden. Many respondents also added that the area will be urbanized in near future to meet the increasing demand (Figure 3.9).

Figure 3.9: Existing Condition of Ranikhola Bazar, Shah Ali

Eastern Housing is situated at the eastern portion of Mirpur area. The area is under a housing project and it is developing rapidly for the past few years. Earlier it was a rural area with full of water bodies, agricultural lands and grass land. The area used to go under water during rainy season. The area has undergone development work since 1996.

The existing condition of this area is destructive. All the cultivated lands are gone. Meanwhile, the water canal had lost its shape by getting narrower than previous. Most of the land are used for housing purposes (Figure 3.10).

Figure 3.10: Existing Condition of Eastern Housing, Mirpur

Pallabi, is an important place for Dhaka city which is known as modern high raised developed area. A lot of high raised buildings are developing from the past few years. The area was near the Mirpur Cantonment and most of the construction buildings are done under the supervision of Bangladesh Army. Due to rapid urbanization, all greeneries are gone forever. Impervious surfaces are everywhere which increases surface temperature (Figure 3.11).

The field visits were conducted to evaluate the present condition of the study area and to learn previous condition too by talking to the local inhabitants. Most of the respondent informed that due to rapid and unplanned urbanization they are feeling the negative impact on the local environment. They also mentioned that average temperature is increasing every day. Now it is getting intolerable during summer. Because of deforestation and loss of water bodies, they feel lack of cold air flow and they agreed that unlike economic benefit, they are missing the old condition of Dhaka city where they have grown up.

Figure 3.11: Existing Condition of Pallabi

CHAPTER 04: RESEARCH METHODOLOGY

CHAPTER 04: RESEARCH METHODOLOGY

4.1 Introduction

This Chapter portrays the comprehensive research methodology. The obtained Landsat images were classified into four broad LULC classes by ArcGIS. Method of estimation LST is discussed. Finally, LULC and LST prediction methods using CA-ANN for the year of 2039 with the help of MOLUSE plug-in QGIS are discussed.

4.2 Data Collection

The overall methodology of the study was mainly based on satellite images. Satellite images cover larger area with significant spectral bands which could be used for several environmental analysis. On the other hand, satellite image also can provide previous data which is significant for past to present and future trend analysis [85].

Presently different satellite images are available. These are unique by different spatial, spectral, temporal and radiometric resolution. A list of prominent presently available satellite images are shown in Table 4.1 [86].

Table 4.1: List of Presently Available Satellite Images

Spaceborne sensors[2]	# of bands	Spectral regions	Nominal spatial resolution (m)	Swath width @ nadir (km)	Quantization (bits)	Temporal resolution (days)
Coarse Resolution						
MODIS	7	blue, green, red, NIR, SWIR (3)	250, 500	2330	12	1
VIIRS	6	pan, red, NIR, SWIR, MWIR, LWIR	375	3000	12	1
VÉGÉTATION-P	4	blue, red, IR, SWIR	333, 666	2285	12	2
Sentinel-3 OLCI	21	modifiable band position and width	300	1270	12	2
Medium Resolution						
AWIFS	4	green, red, NIR, SWIR	56	740	12	5
HYPERION	220	visible, NIR, SWIR	30	7.5	12	16
Landsat 7 ETM+	8	pan, blue, green, red, NIR, SWIR (2), LWIR	15, 30, 60	185	8	16
Landsat 8 OLI	9	pan, violet, blue, green, red, NIR, SWIR (3)	15, 30	185	12	16
ASTER	14	green, red, NIR, SWIR (6), LWIR (5)	15, 30, 90	60	8	8 [3]
LISS-3	4	green, red, NIR, SWIR	23.5	141	10	24
SLIM6	3	green, red, NIR	22	650	10	1-3 [3]
Sentinel-2 MSI	13	visible (3), red edge (3), NIR, SWIR	10, 20	290	12	5
Spot 5 HRG	5	pan, green, red, NIR, SWIR	2.5, 10, 20	60x2	8	1-5 [3]
High Resolution						
Rapideye REIS	5	blue, green, red, red edge, NIR	6.5	77	16	1 [3]
Spot 6 (and 7) NAOMI	4	pan, visible (3), NIR	1.5, 6	60x2	12	1-3 [3]
ResourceSat-2 LISS-4	3	green, red, NIR	5.8	23.9	10	5 [3]
Kompsat-3 AEISS	5	pan, blue, green, red, NIR	0.7, 2.8	16	14	1-4 [3]
Pleaides HIRI	4	pan, blue, green, red, NIR	0.5, 2	20	20	1-2 [3]
Geoeye-1 GIS	5	pan, blue, green, red, NIR	0.5, 2	15.2	11	4 [3]
Worldview-3 WV110	9	pan, violet, blue, green, red, red edge, NIR(2)	0.3, 1.2	13.1	11	1 [3]

Not all satellite images are freely available and also all satellite images do not provide past 20-30 years data. Santinel-2 image is freely available and gives 10-20 m spatial resolution, but it does not provide past 30 years data. On the other hand, Landsat image has moderate spatial resolution which is 30 m but it provides past 30 years or beyond that

data. Therefore, the researcher used Landsat images that can provide a smart spatial resolution and also past 30 years data.

Landsat data can be collected at free of cost. The data can be collected from the USGS website. Therefore, the Authors show interest to analyze the LULC as well LST, NDBI and NDVI using Landsat data series. Before 2013, Landsat TM 4-5 data and after that Landsat OLI 8 data are used for the study. All the Landsat images were taken in the month of November because of the availability of low cloud cover and better visibility. Images and also the dates of acquisition are shown in Table 4.1.1 [68].

Table 4.2: Date of Collection and Specification

Satellite data	Date of Acquisition	Sensor	Band No.	Spectral range (Wavelength μm)	Spatial Resolution (m)
Landsat 4-5	November 04, 1989 November 18, 1994; November 16, 1999; November 13, 2004; November 11, 2009;	TM	1	0.45–0.52	30
			2	0.52–0.60	30
			3	0.63–0.69	30
			4	0.76–0.90	30
			5	1.55–1.75	30
			6	10.40 –12.50	120 resampled to 30
			7	2.08 – 2.35	30
Landsat 8	November 25, 2014; November 23, 2019	OLI	1	0.43–0.45	30
			2	0.45–0.51	30
			3	0.64–0.67	30
			4	0.53–0.59	30
			5	0.85–0.88	30
			6	1.57–1.65	30
			7	2.11–2.29	30
			8	1.36–1.38	15
			9	0.50–0.68	30
		TRIS 1	10	10.60–11.19	100 resampled to 30
		TRIS 2	11	11.50–12.51	100 resampled to 30

After downloading the data, sequentially LULC, LST, NDVI and NDBI were calculated. Using the data, LST and LULC were predicted for future 20 years. Meanwhile, the

calculated data were validated using BMD Agargaon Station's data. In addition, frequent field visits were undertaken to validate the measured data by interviewing local respondents. Afterwards, a correlation analysis was done among LST, NDVI and NDBI. The whole methodological steps are given by following flow diagram.

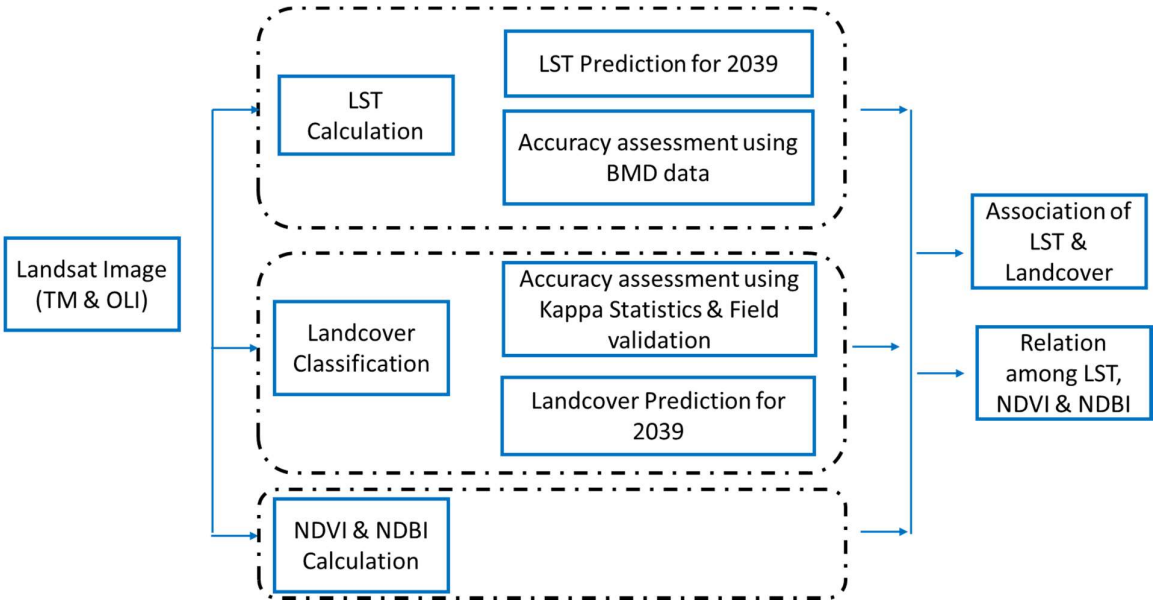

Figure 4.1: Flow Diagram of Methodology

4.3 LULC Classification

The collected satellite images were composited in ArcGIS V10.6.1 software. True Color Composite (TCC) was generated using suitable combinations of bands for all the images to select training samples and identify the different LULC classes [95, 96]. The images were obtained from Landsat, classified into four broad LULC classes (water body, built up area, vegetation and bare land) for the year of 1989, 1994, 1999, 2004, 2014 and 2019 based on Maximum Likelihood Supervised Classification (MLSC) technique (Figure 4.2). Around 25 samples were collected in order to produce LULC maps for each LULC class. Each classified map has been evaluated for accuracy assessment using Kappa index [69, 130, 132].

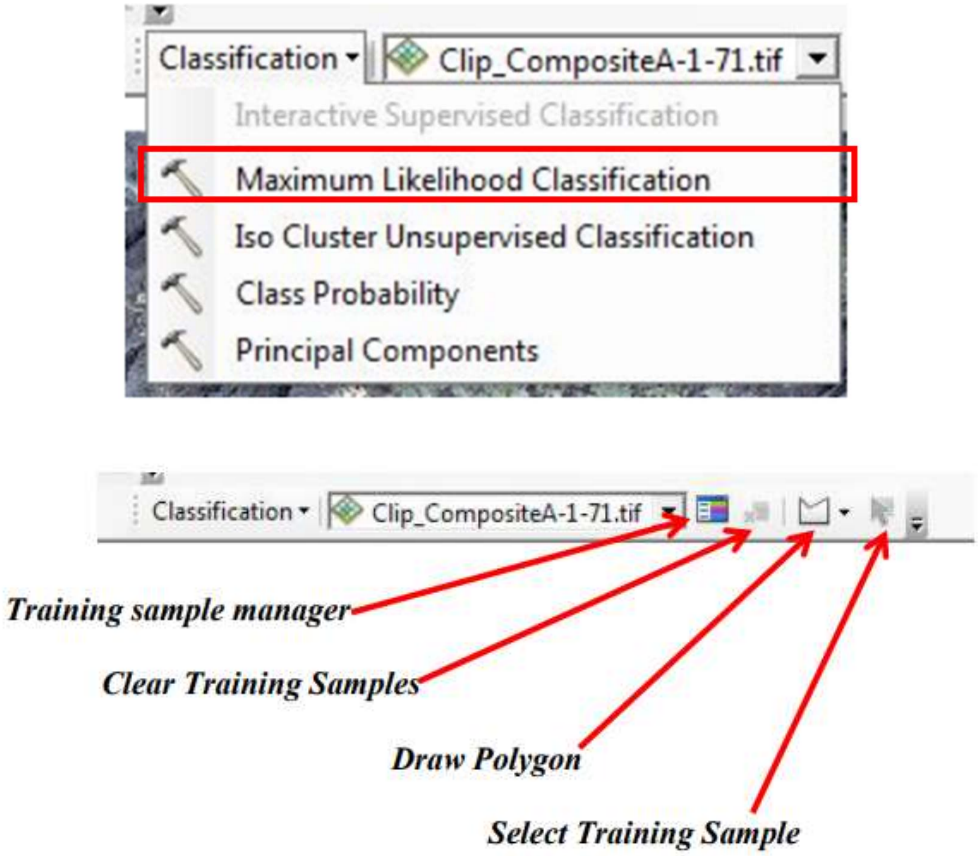

Figure 4.2: MLSC Tools for ArcGIS [Source:Good &Giordano,2010)]

4.4 Estimation of LST

The LST was estimated using different formulas which were collected from several literatures and these were discussed in section 2.2. The whole methodology of retrieving LST was used using the chapter 2.2 formulas.

4.5 Simulation of LULC and LST

The CA-ANN model proposed is designed to simulate land use changes through a multiple output neuron. The network output layer decides the possibilities of multiple land uses with multiple output neurons. The appropriate parameters for the simulation are calculated automatically by the neural network training process. The CA-ANN model does not include specific transfer rules. The only function is to train the neural network to achieve empirical parameter values. Many factors can be added to the model to improve the precise simulation. Combination of Cellular Automata and ANN Models will produce a better LULC and LST transition spatio-temporal pattern [119, 136].

The LST and LULC for the year of 2039 with the help of MOLUSE plug-in in QGIS 2.18 is typically predicted with an ANN. ANN is an effective method that helps to forecast future LST and LULC time series using data sets from previous years [22, 48, 50, 137]. LST simulation was performed in this study using input parameters LULC images, NDVI, NDBI, latitude and longitude and as output parameters for LST [22, 125]. Besides, the CA-ANN model for the future LULC was used in the prediction of input parameters of road layers, NDBI, NDVI, Latitude and Longitude data. The pixel value data of the images were transformed in ArcGIS software V10.6.1 for the better performance of the model. The model was developed using past 20 years data (199-2019) as the input parameters for predicting the future year 2039 data. The LST prediction model architecture is shown in Figure 4.3.

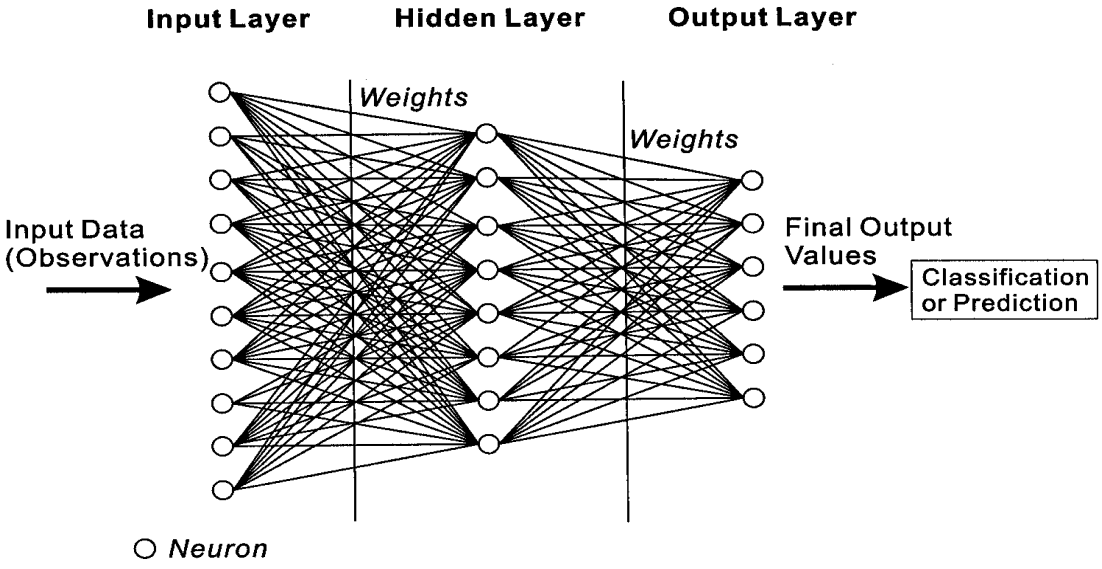

Figure 4.3: ANN Model Architecture (Source: Ullah et al, 2019)

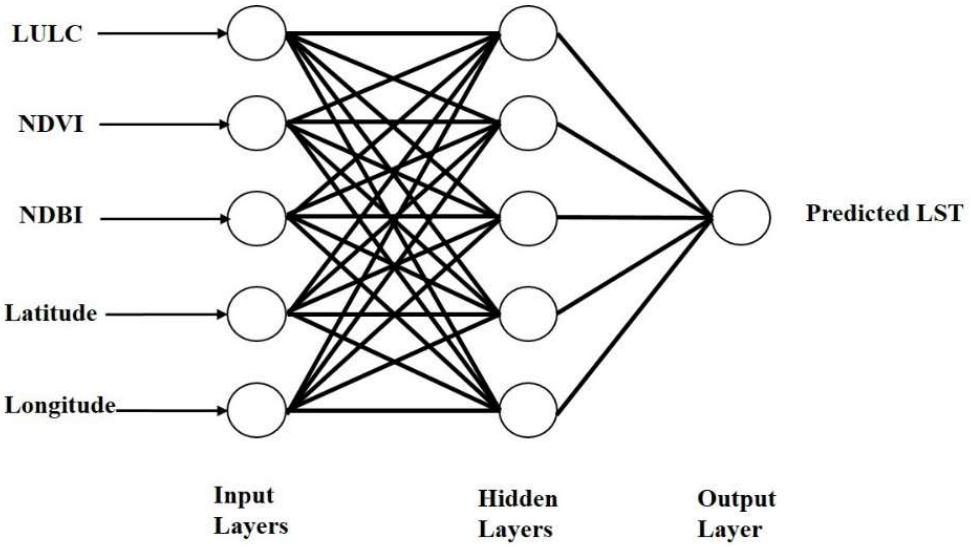

Figure 4.4: CA-ANN Model Architecture (Source: Maduako & Patrick, 2016)

4.5.1 ANN Model Simulation in QGIS

The detail procedure of ANN model simulation in QGIS-MOLUSCE Plugin software is described chronologically. In Figure 4.4, the input variables are LST images for the year 1999 and 2019, NDVI, NDBI, Latitude and longitude values. For LULC prediction, input variables are LULC images for 1999 and 2019, Road Layer for base year (2019), NDVI, NDBI, Latitude and longitude values.

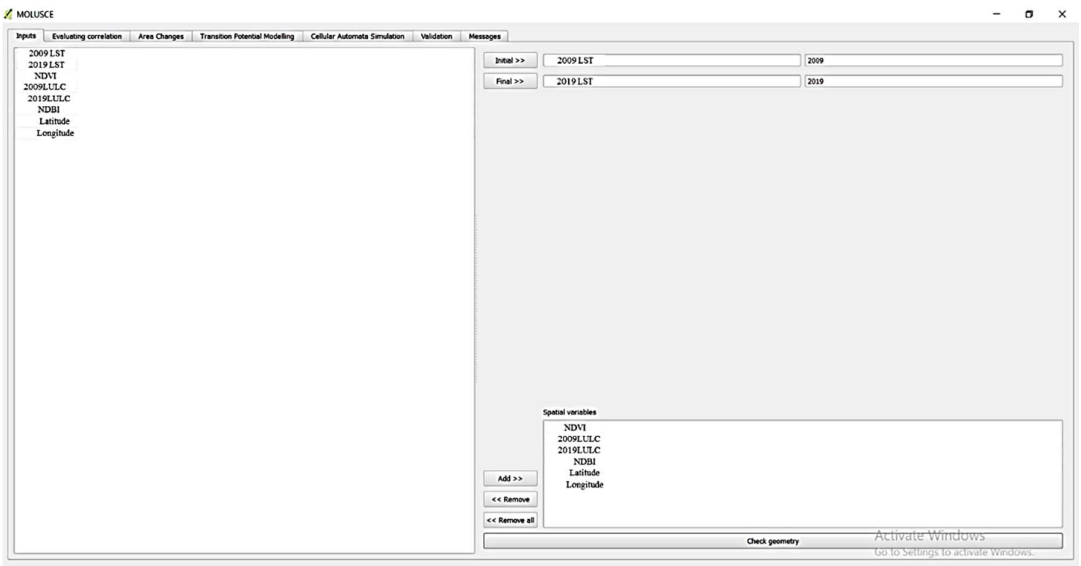

Figure 4.4: MOLUSE plug-in Interface in QGIS

In the second step, transition potential modeling between LST and LULC of 1999 and 2019 with the assistance of other spatial variables performed ANN approach. This process will indicate the potential likelihood of changes in LST and LULC which produce change of LST and LULC maps for future LST simulation.

Then prediction window will come afterwards where some prediction tools are set by dropdown option. As the study focuses on ANN simulation method, therefore, ANN was selected as a method for predicting both LST and LULC, neighborhood pixel was considered as 1 pixel and maximum iteration was set for 1000 and rest of the options were set as default.

After training the data through neural network, the overall accuracy, current kappa validation were automatically measured. Then ANN data and transition data were inserted in the cellular automata tab where combining the CA and ANN method, the ultimate simulation was done.

CHAPTER 05: RESULTS AND DISCUSSIONS

CHAPTER 05: RESULTS AND DISCUSSIONS

5.1 Introduction

This Chapter sequentially discusses about the analyzed results of the classification of LULC and LST, data validation, association of LULC and LST, relationship among LST, NDBI and NDVI, future prediction of LULC and LST and finally validation of predicted result.

5.2 Classification of LULC

MLSC is applied to generate the LULC map for the years 1989, 1994, 1999, 2004, 2009, 2014 and 2019 (Figure 5.1 to 5.7). The total study area is approximately 48.830 km^2. The classified image of year 1989 showed higher percentage of area 35.04%, 27.34% and 24.9% for bare land, water bodies and vegetation, respectively. The built up area recorded only 12.56% for year 1989 (Figure 5.1). The percentage area of each class in 1994 showed that bare land had the largest area (39.20%) followed by water bodies (24.63%) and vegetation (17.04%) (Figure 5.2). There was a moderate increase in built up area (7%) in year 1994 compared to 1989. The continuation of the increasing trend in the bare land (40.45%) and built up area (31.85%) were accelerated in the year 1999 mainly which were influenced by rapid urbanization. Water bodies (8.19%) and vegetation land (19.11%) were facing decreasing trend because of the conversion of natural surfaces to bare land and after then built up area (Figure 5.3). In the year 2004 the bare land (33.15%) was facing decreasing trend because of the conversion of bare land to the urban built area (43.76%). Filling up water bodies (4.77%) and vegetation land (18.32%) in the form of bare land at initial stage and finally were got transferred to built-up area was stared to accelerate in the year 2004 (Figure 5.4).

The classified LULC results for the years 2009, 2014, and 2019 are projected (Figure 5.5 to 5.7) by showing their percentage of changes among different LULC classes. From 2009 to 2019, the amount of bare and vegetation land (-10% approximately) were declined significantly. During the same period, the built up area was increased by (21% of the study area). Finally, the water body slightly decreased by 1% of the study area from 2009 to 2019.

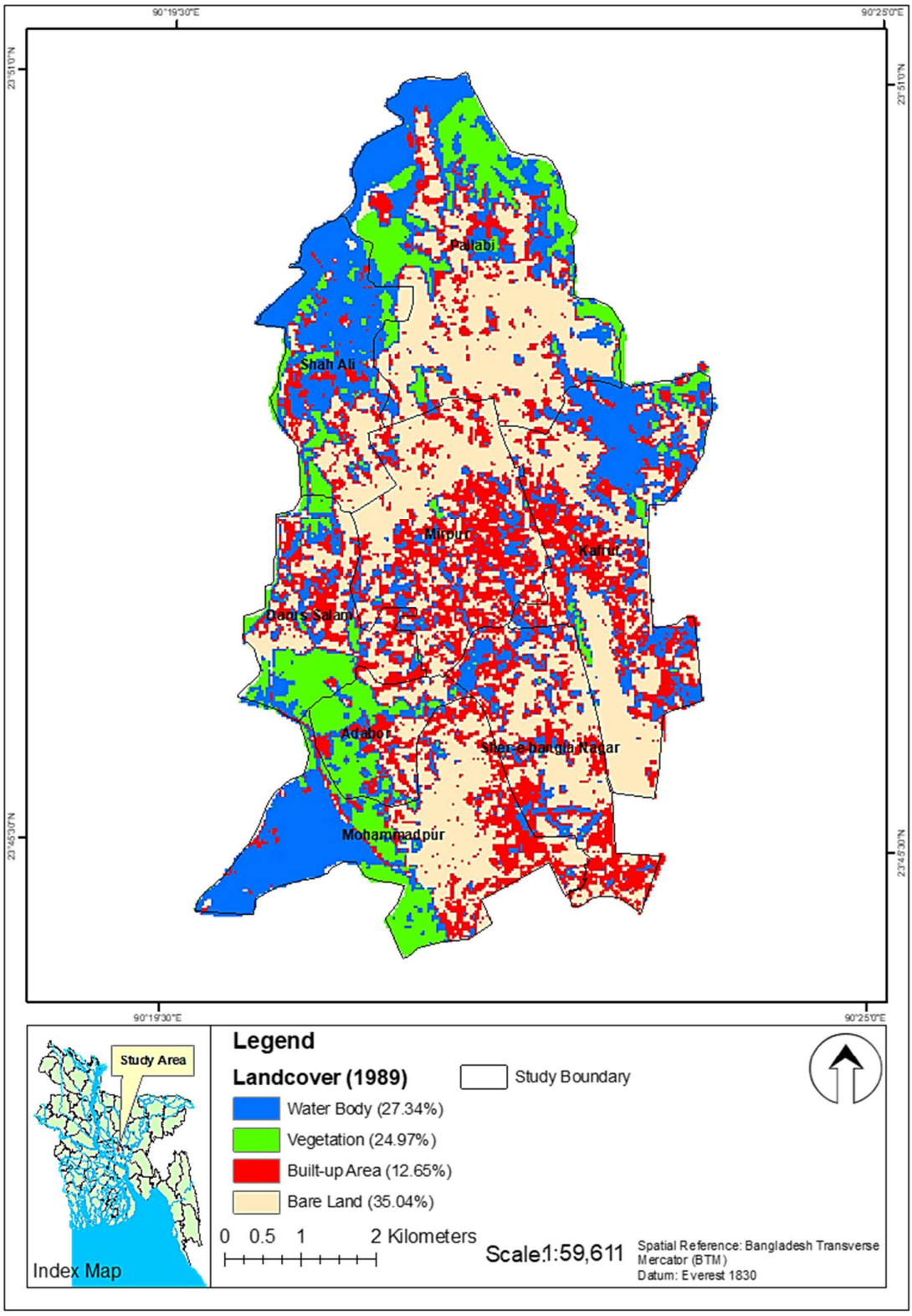

Figure 5.1: Supervised Image Classification Map of the Study Area in 1989

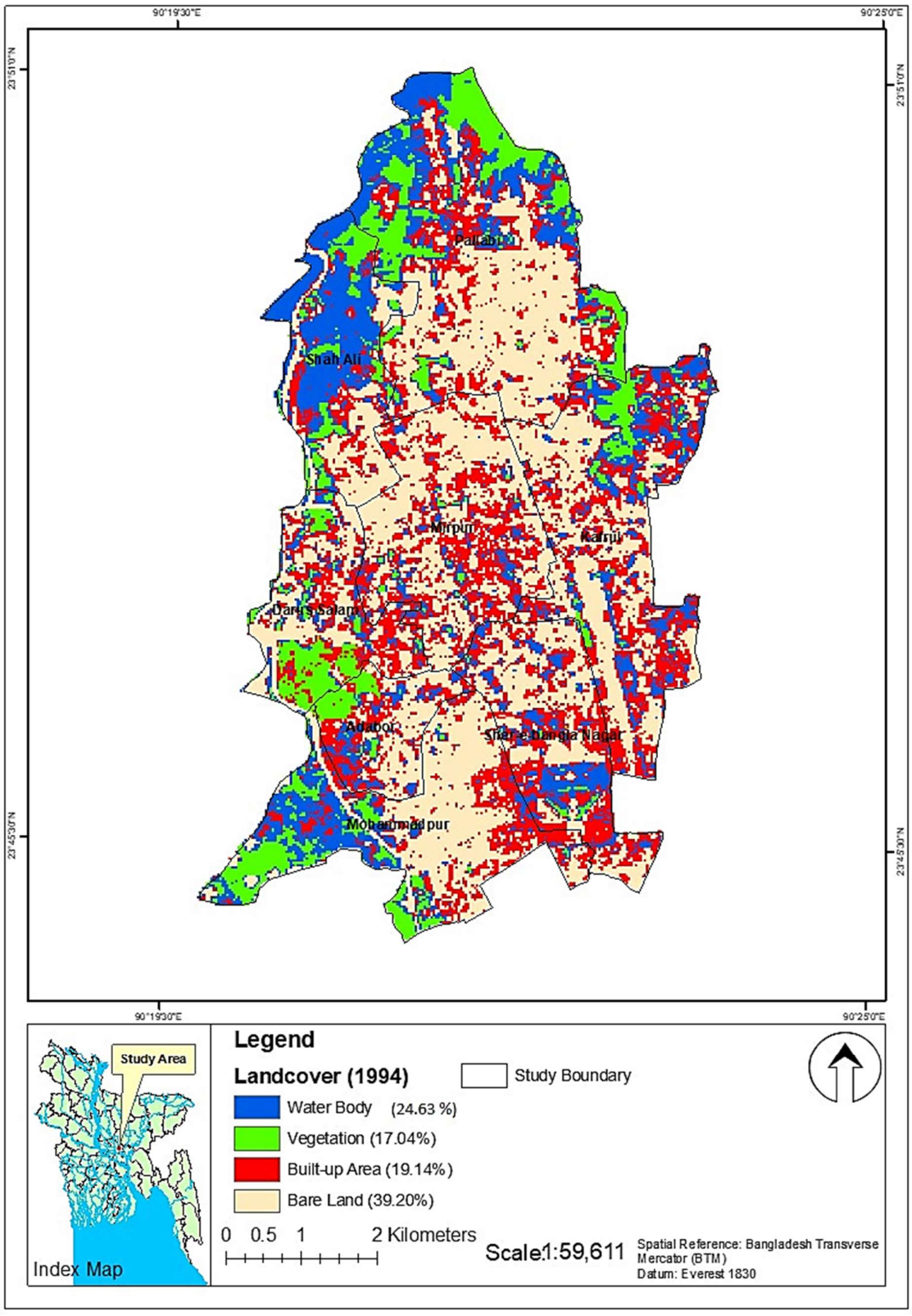

Figure 5.2: Supervised Image Classification Map of the Study Area in 1994

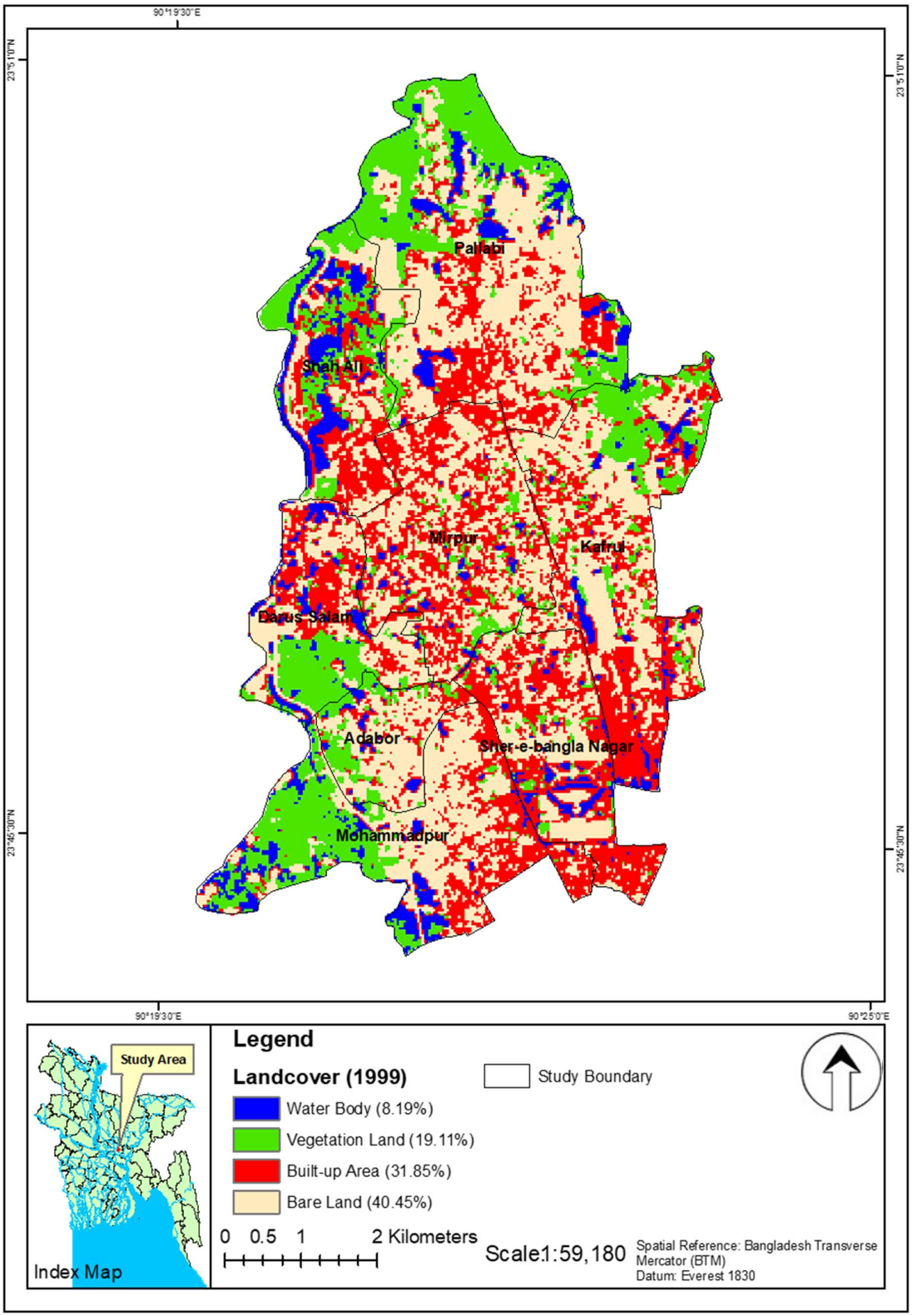

Figure 5.3: Supervised Image Classification Map of the Study Area in 1999

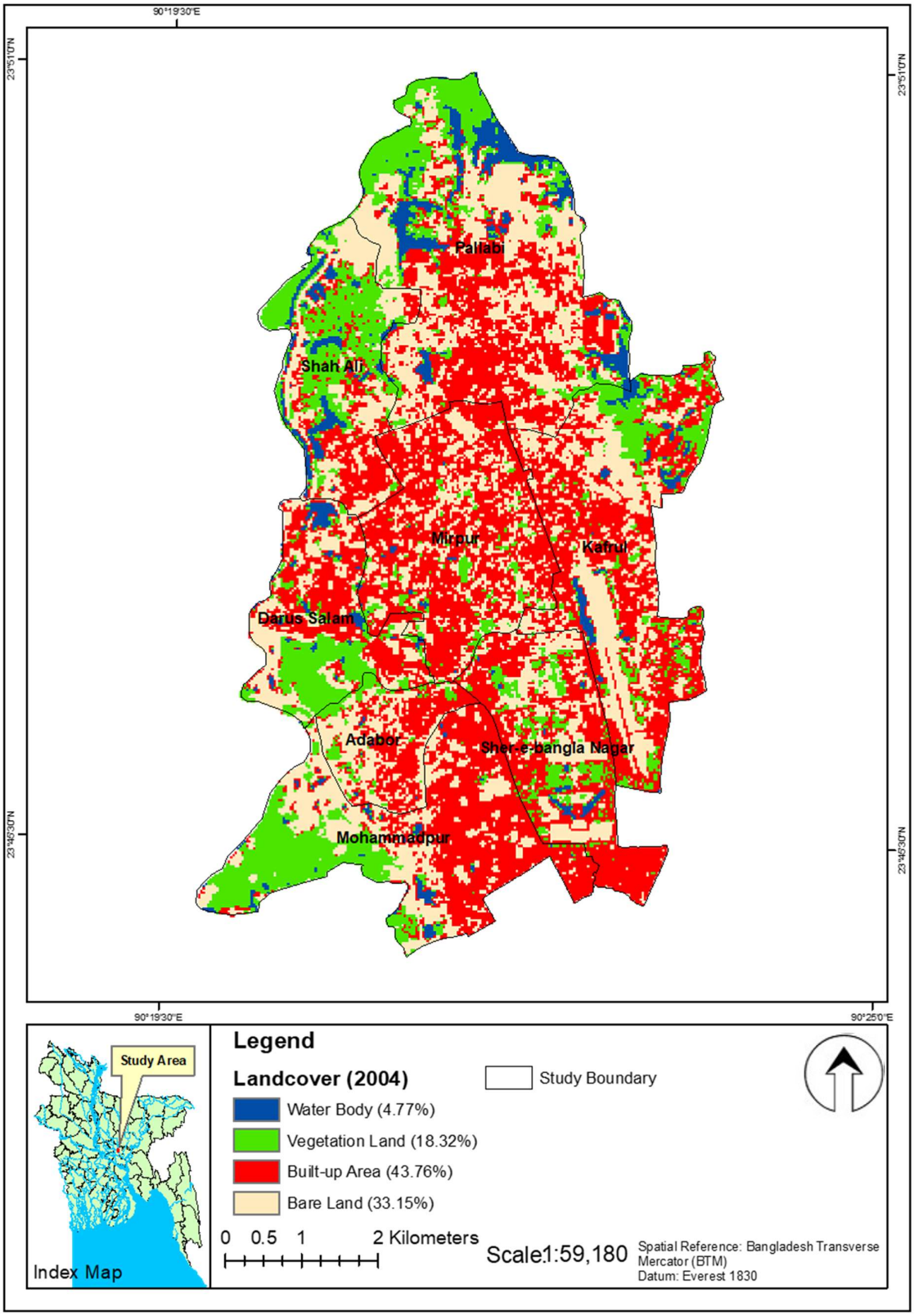

Figure 5.4: Supervised Image Classification Map of the Study Area in 2004

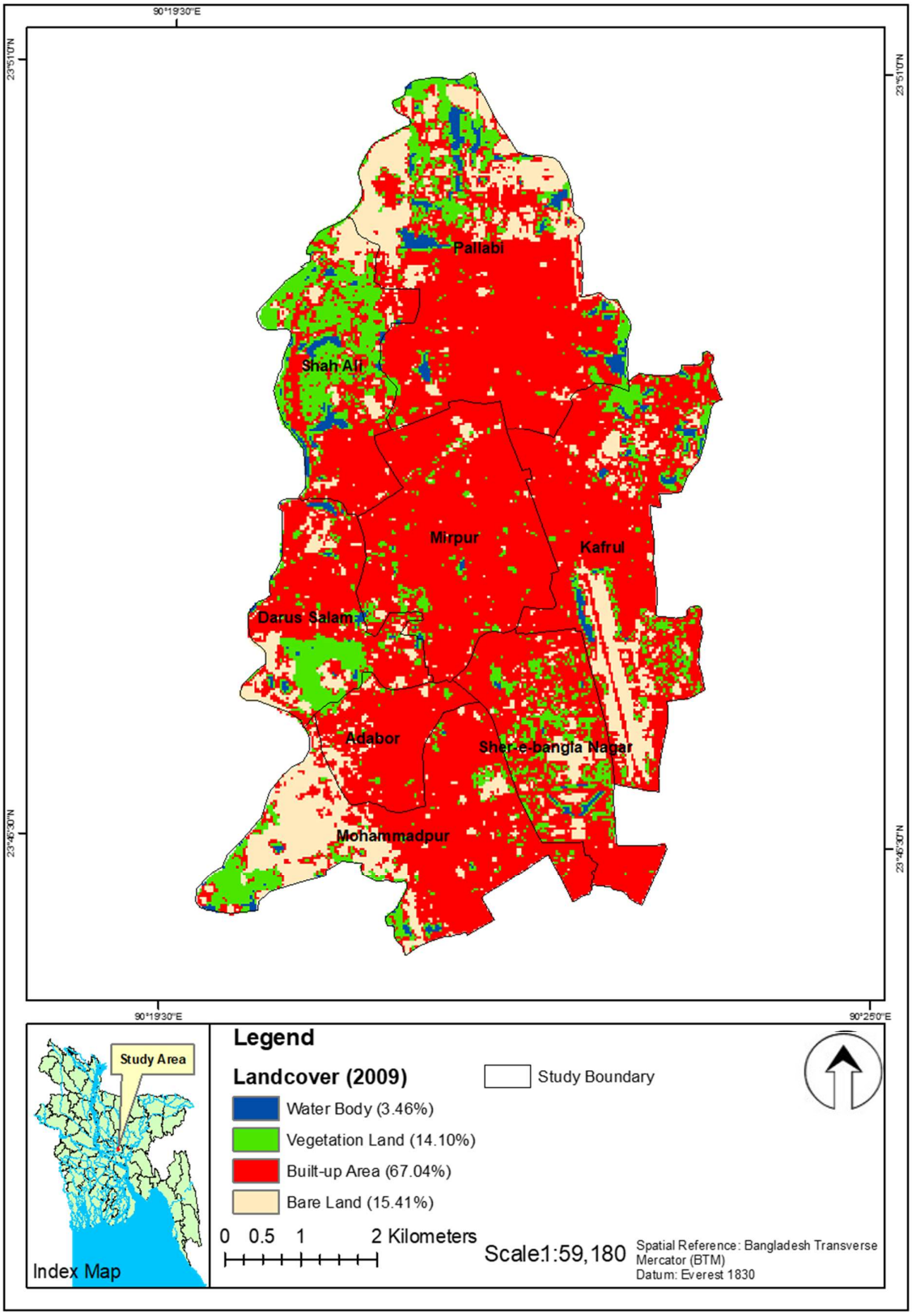

Figure 5.5: Supervised Image Classification Map of the Study Area in 2009

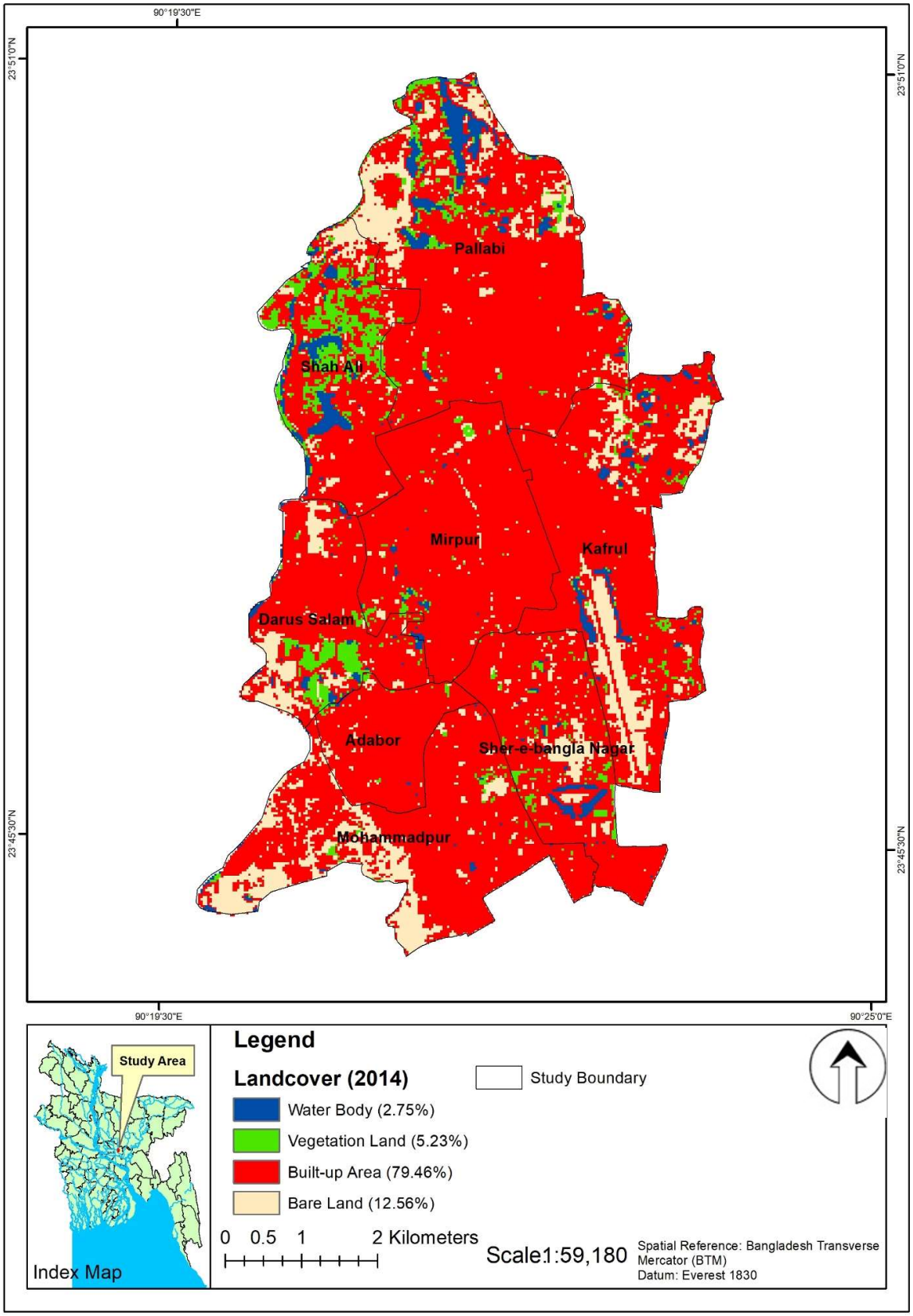

Figure 5.6: Supervised Image Classification Map of the Study Area in 2014

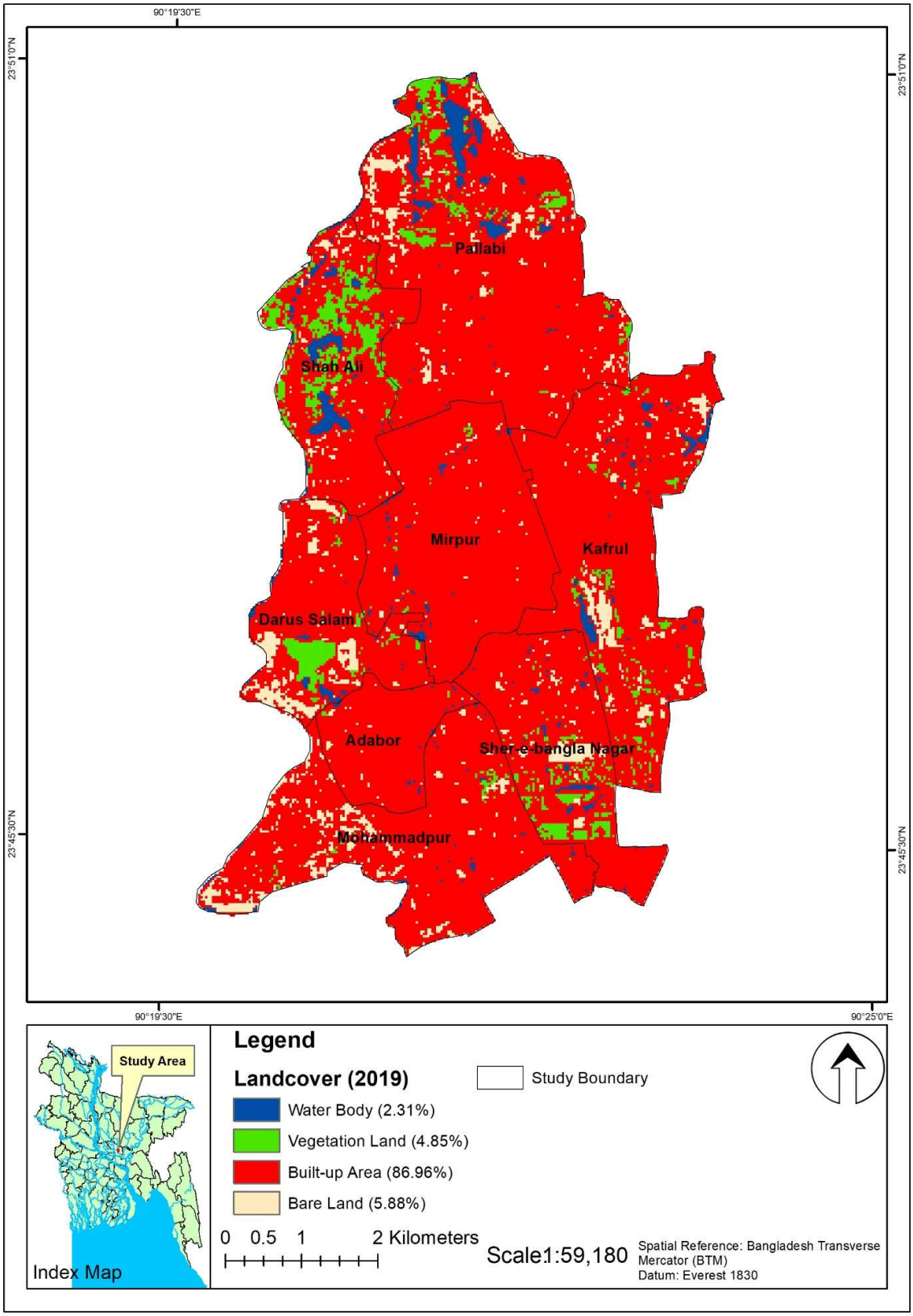

Figure 5.7: Supervised Image Classification Map of the Study Area in 2019

5.2.1 Percent Change Analysis of Different LULC

During the 1989–2019 study period, LULC categories were converted into other categories and thus losses and gains of LULC categories, were also examined (Table 5.1 to 5.6). The results indicate that built up area was generally increasing and water bodies and vegetation land was decreasing significantly during the study period.

For the year 1989 to 1994, built up area and bare land area were gained 6.485% and 4.158% area, respectively, where vegetation and water bodies were lost by 7.930% and 2.713% of its area, respectively (Table 5.1).

Similar for the year 1994-1999, a significant increase in the built up area and a very moderate increase in bare land and vegetation area were found and the percentages were showed by 12.717%, 1.653% and 2.056%, respectively. Only dramatic loss in water bodies by 16.445% was recorded from 1994-1999 (Table 5.2).

Table 5.1: Percentage Change of LULCs in the Study Area from 1989-1994 (km^2)

LULC	Area (1989)	Area in Percentage	Area (1994)	Area in Percentage	Change in Percentage (1994-1989)
Water body	13.4	27.34	12.03	24.63	-2.713
Built up	6.2	12.65	9.34	19.14	6.485
Vegetation	12.2	24.97	8.32	17.04	-7.930
Bare land	17.1	35.04	19.14	39.20	4.158
Total	48.83	100.00	48.83	100.00	0

Table 5.2: Percentage Change of LULCs in the Study Area from 1994-1999 (km^2)

LULC	Area (1994)	Area in Percentage	Area (1999)	Area in Percentage	Change in Percentage (1999-1994)
Water body	12.03	24.63	4.00	8.19	-16.445
Built up	9.34	19.14	15.55	31.85	12.717
Vegetation	8.32	17.04	9.33	19.11	2.075
Bare land	19.14	39.20	19.95	40.85	1.653
Total	48.83	100.00	48.83	100.00	0

From 1999-2004, except built up area other three LULC classes were facing decreasing trend. Built up area gained by 11.906% where bare land, water bodies and vegetation land were lost 7.686 %, 3.421 % and -0.789 % area respectively. From 1999, the percentage of built up area has started to increase because of the conversion of large percentage of bare land to built up area (Table 5.3).

Table 5.3: Percentage Change of LULCs in the Study Area from 1999-2004 (km^2)

LULC	Area (1999)	Area in Percentage	Area (2004)	Area in Percentage	Change in Percentage (2004-1999)
Water body	4.00	8.19	2.33	4.77	-3.421
Built up	15.55	31.85	21.37	43.76	11.906
Vegetation	9.33	19.11	8.95	18.32	-0.789
Bare land	19.95	40.85	16.19	33.15	-7.696
Total	48.83	100.00	48.83	100.00	0

From 2004-2009, significantly built up area gained 23.281 % area where bare land, vegetation and water bodies were reduced to 17.748 %, 4.228 % and -1.305 % respectively (Table 5.4).

Table 5.4: Percentage Change of LULCs in the Study Area from 2004-2009 (km^2)

LULC	Area (2004)	Area in Percentage	Area (2009)	Area in Percentage	Change in Percentage (2009-2004)
Water body	2.3274	4.77	1.69	3.46	-1.305
Built up	21.3687	43.76	32.74	67.04	23.281
Vegetation	8.9478	18.32	6.88	14.10	-4.228
Bare land	16.1901	33.15	7.52	15.41	-17.748
Total	48.83	100.00	48.83	100.00	

From 2009-2014, built up area gained by 12.425 % whereas bare land, vegetation and water bodies reduced to 2.847 %, 8.863 % and 0.715 % respectively (Table 5.5).

Table 5.5: Percentage Change of LULCs in the Study Area from 2009-2014 (km^2)

LULC	Area (2009)	Area in Percentage	Area (2014)	Area in Percentage	Change in Percentage (2014-2009)
Water body	1.6902	3.46	1.34	2.75	-0.715
Built up	32.7375	67.04	38.81	79.46	12.425
Vegetation	6.8832	14.10	2.56	5.23	-8.863
Bare land	7.5231	15.41	6.13	12.56	-2.847
Total	48.83	100.00	48.83	100.00	

Considering the year 2014-2019, built up area gained by 7.499 % whereas bare land, vegetation and water bodies were reduced to 6.679 %, 0.383 % and 0.440 % respectively (Table 5.6).

Table 5.6: Percentage Change of LULCs in the Study Area from 2014-2019 (km^2)

LULC	Area (2014)	Area in Percentage	Area (2019)	Area in Percentage	Change in Percentage (2019-2014)
Water	1.341	2.75	1.13	2.31	-0.440
Built up	38.8053	79.46	42.47	86.96	7.499
Vegetation	2.5551	5.23	2.37	4.85	-0.380
Bare land	6.1326	12.56	2.87	5.88	-6.679
Total	48.83	100.00	48.83	100.00	

Overall, the highest losses (bare land and vegetation) and gains (urban area) were observed in the 2004–2014 period. However, the water body expansively was lost its coverage form 1994–1999.

5.2.2 Field validation of LULC

Table 5.7 demonstrates the classification of overall accuracy, Kappa coefficient, and validation of land use classification. For the year 2019, the overall accuracy was over 90% and the result of the Kappa coefficient was 0.83. The accuracy level is classified as very strong when the Kappa coefficient is greater than 0.75 [69, 130-132]. In order to validate the land use classification, 50 sampling points were compared with the corresponding point on Google Earth images over the same period. In conclusion, the

overall classification accuracy, Kappa coefficient statistics, and validation all show good accuracy which is suitable for LULC simulation.

Table 5.7: Accuracy Assessment for 2019 LULC Map

	Ground Truth					
Classified Class	Water body	Urban	Vegetation	Bare Soil	Total	User Accuracy
Water	10	0	1	0	11	90.91
Built up Area	0	15	0	1	16	93.75
Vegetation	0	0	11	1	12	91.67
Bare Soil	1	1	0	9	11	81.82
Total	11	16	12	11	50	
Producer Accuracy	90.91	93.75	91.67	81.82	Overall Accuracy	Kappa Statistics
					90	83.85

5.3 Estimation of LST

Figure (5.8 to 5.14) indicates the spatial pattern of LST distribution. In all maps bright yellow tone represents higher temperature and greenish tone represents low surface temperature. LST concentration spatial and temporal LST patterns display rapid changes in LULC groups. The core built up area is sensitive to high temperatures. As the images were taken in the month of November which is generally winter season in Bangladesh, therefore, displayed data will show the temperature of corresponding winter season of the years.

Figure (5.8 and 5.9) focuses on annual surface temperature conditions of 1989 and 1994 and LST varied within the range of less than 20 – 24^0C. From 1999 and 2004 temperature decreased slightly and the reason is Bangladesh went under massive flood during that period. In that period, surface water existed for a long period. For that temperature was comparatively lower than the previous year and LST varied 20 – 32^0C (Figure 5.10 and 5.11). In the year of 2009 the LST varied 20 – 32^0C (Figure 5.12). For 2014 and 2019, the LST were found at the highest peak because of the significant increase of built up area and reduction of water bodies and vegetation land. From 2014 to 2019 LST varied from 24^0C to more than 34^0C (Figure 5.13 to 5.14). The north-western part of the study area exhibited lowering in temperature due to higher vegetation and agricultural land whereas the south eastern part exhibits the rise in LST due to rapid urban expansion and declining of water bodies as well as vegetation land.

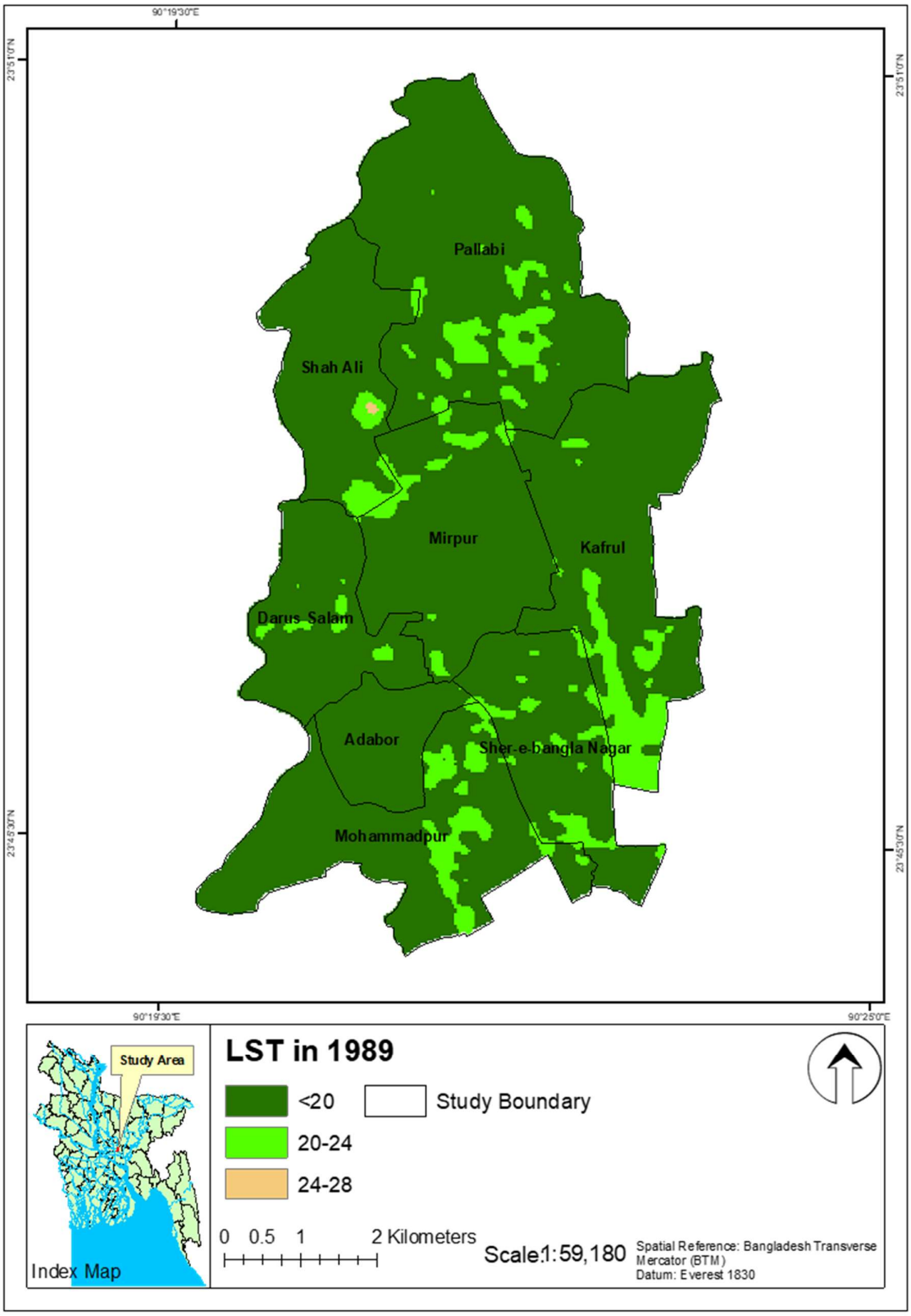

Figure 5.8: Distribution of LST for the Year 1989

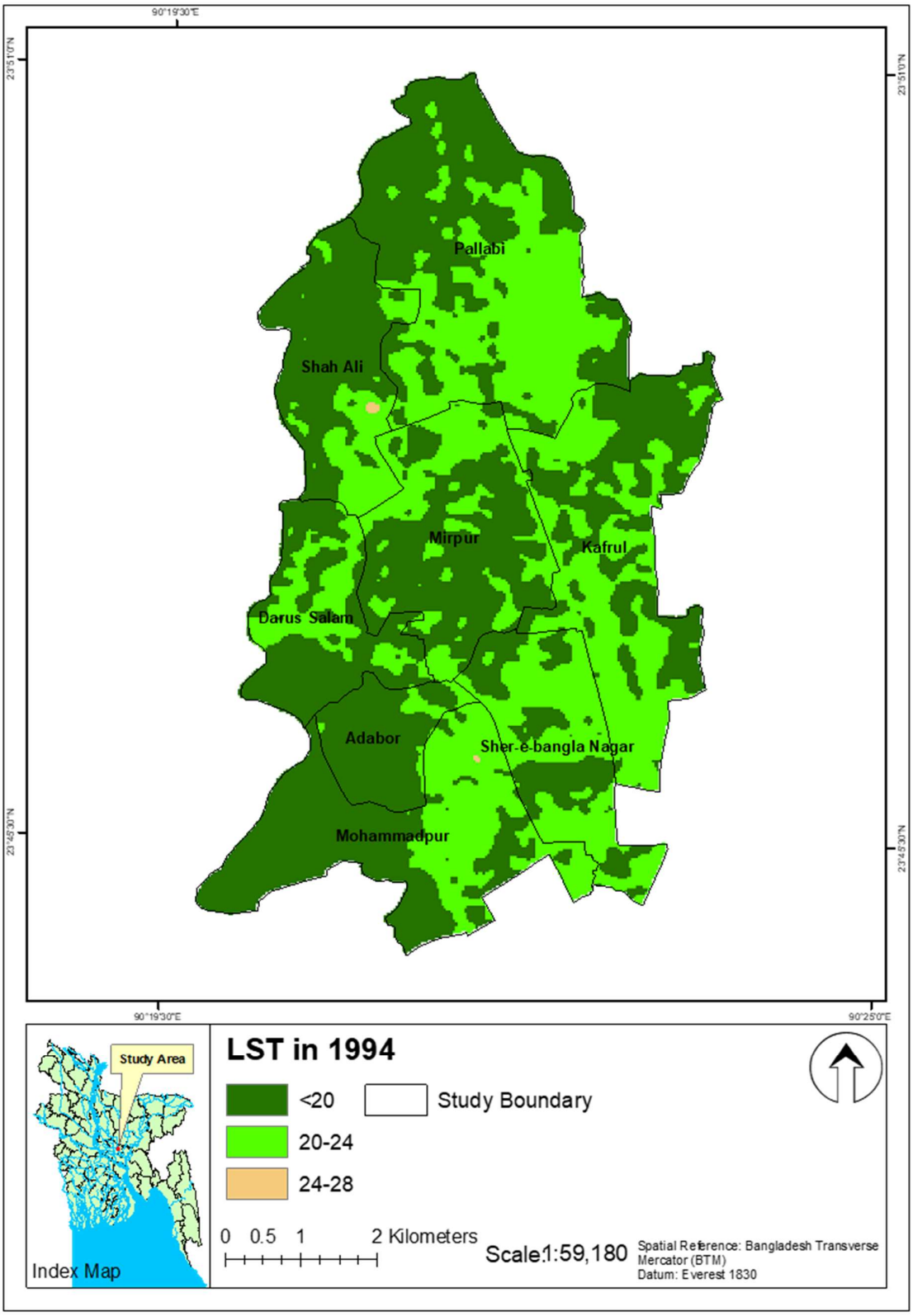

Figure 5.9: Distribution of LST for the Year 1994

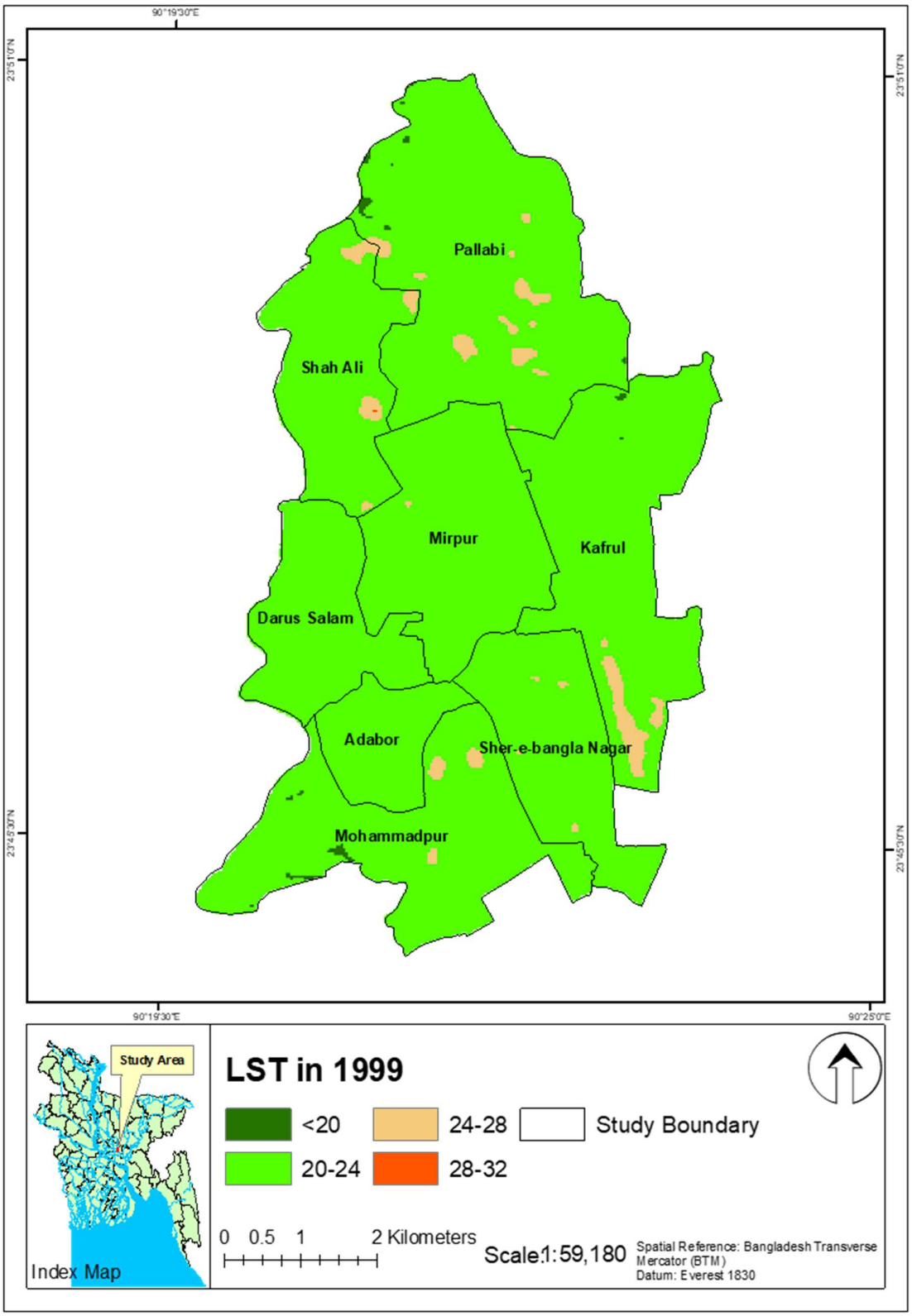

Figure 5.10: Distribution of LST for the Year 1999

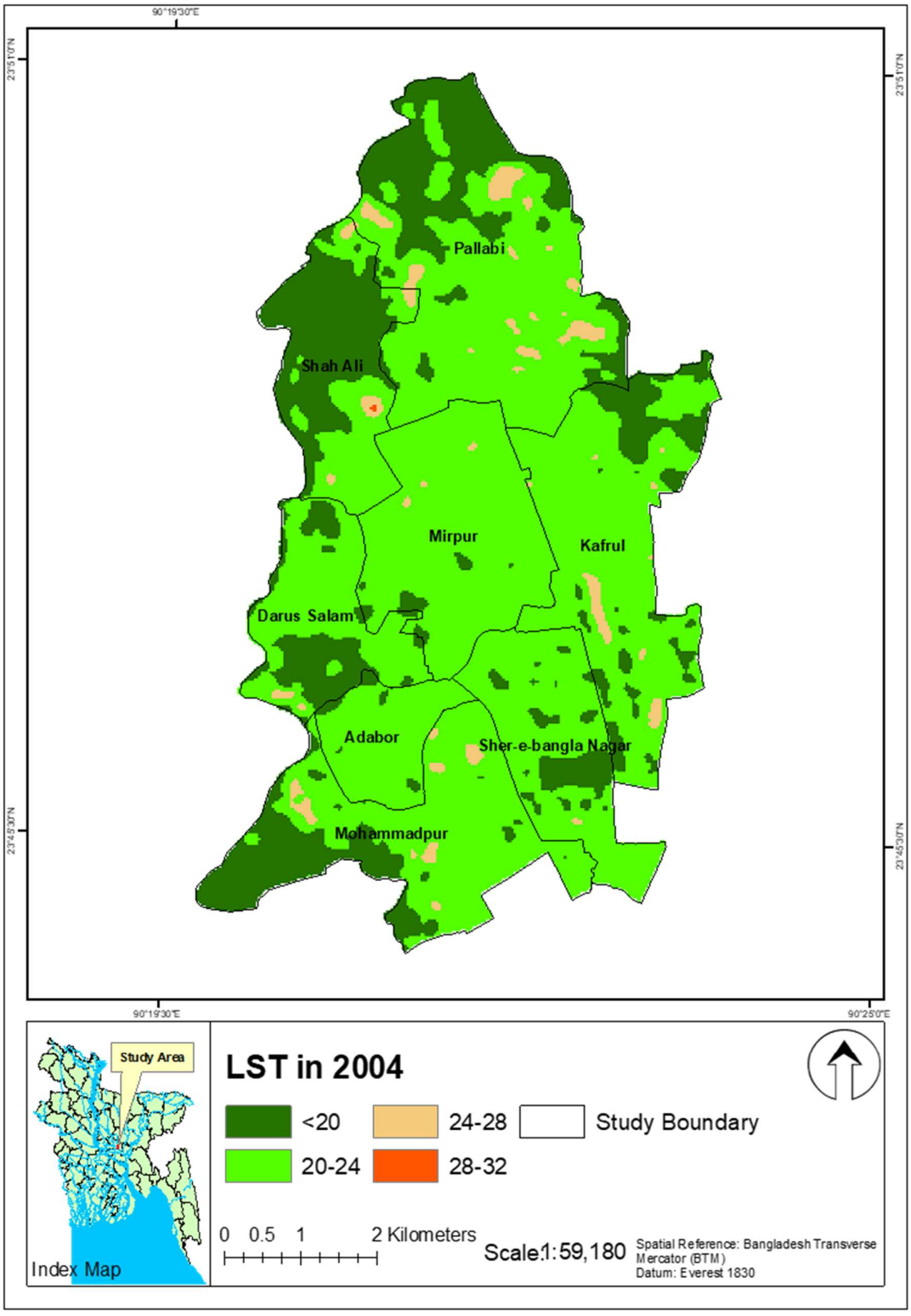

Figure 5.11: Distribution of LST for the Year 2004

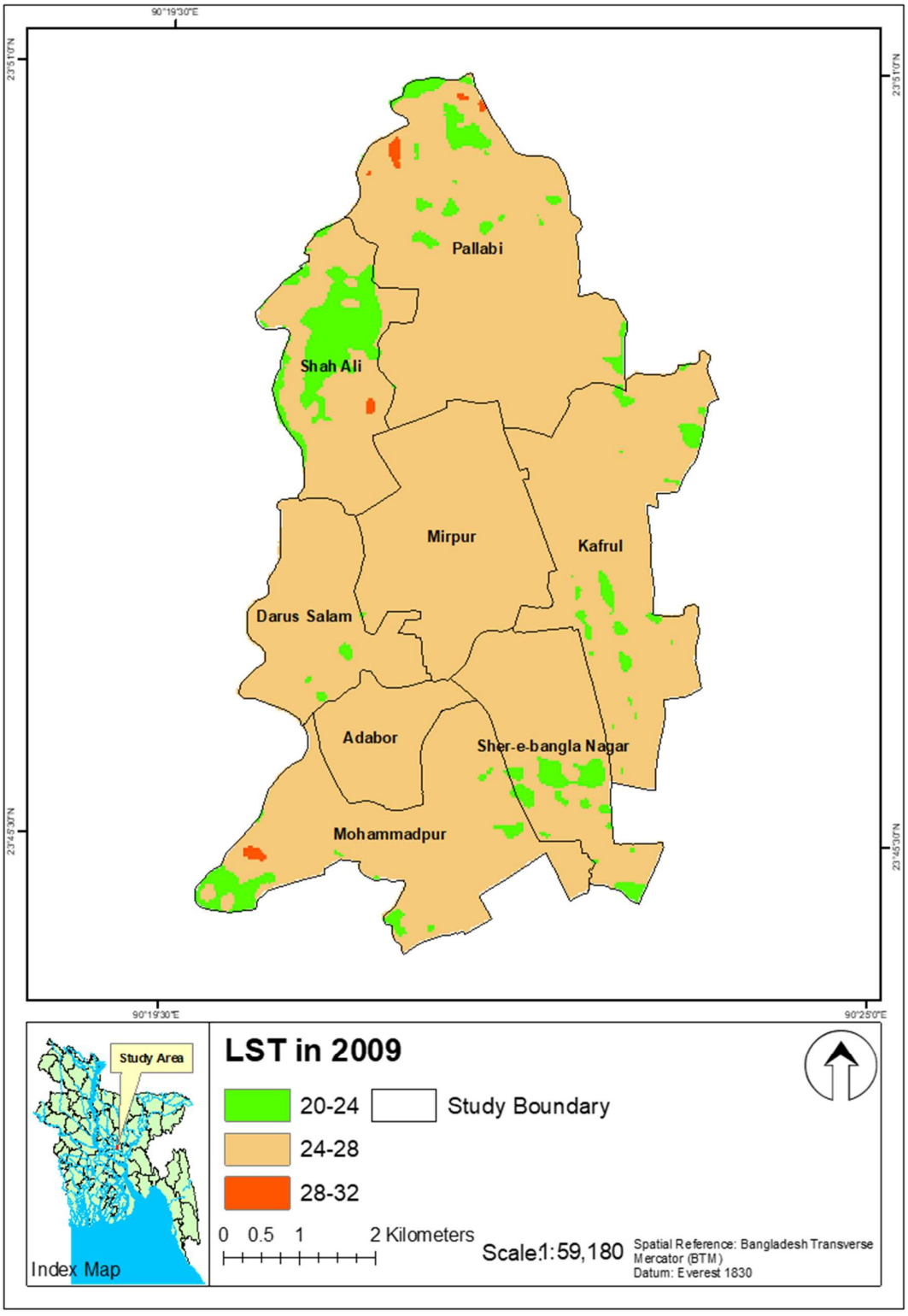

Figure 5.12: Distribution of LST for the Year 2009

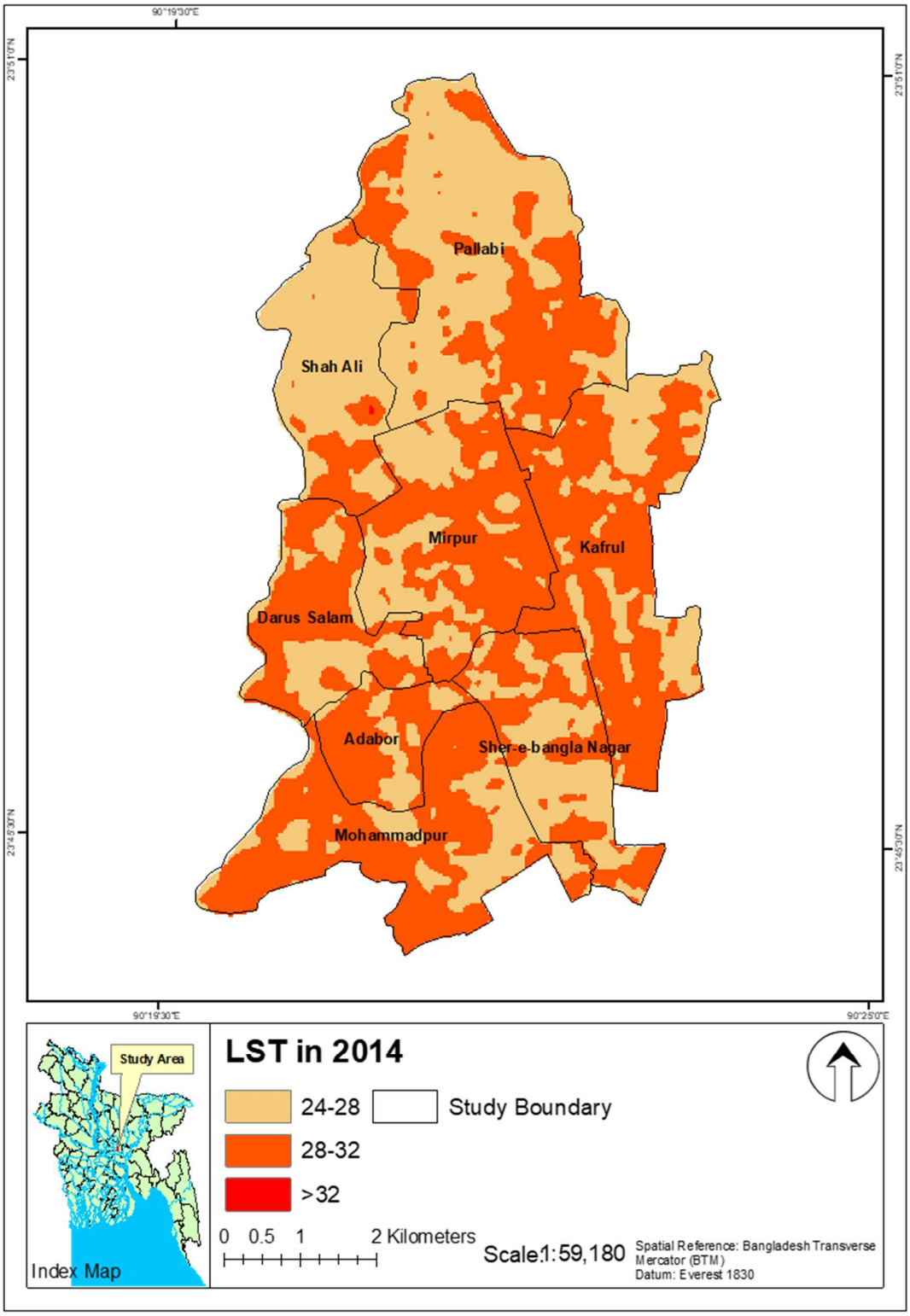

Figure 5.13: Distribution of LST for the Year 2014

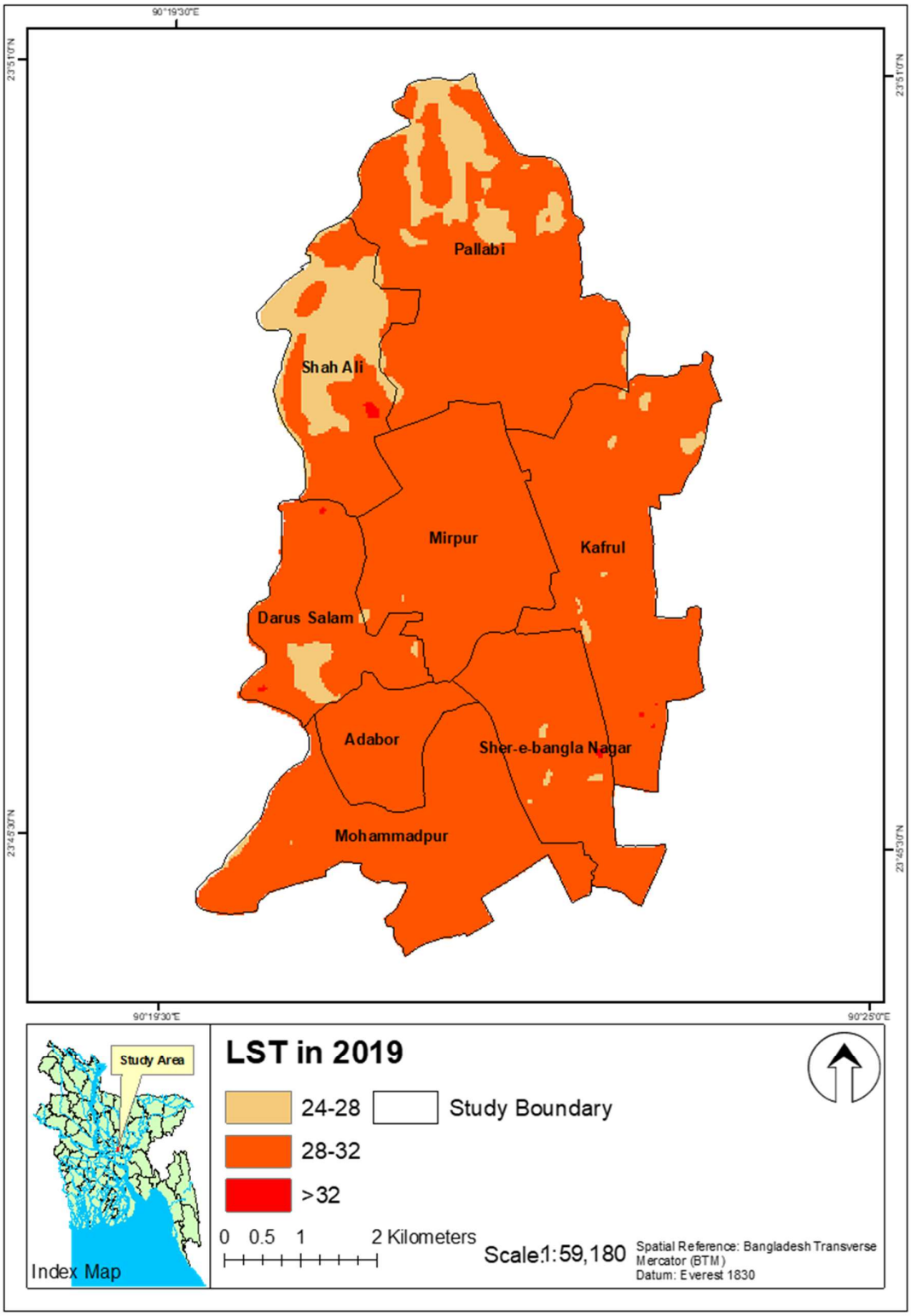

Figure 5.14: Distribution of LST for the Year 2019

5.3.1 Percentage Change in LST

The percentage change in LST will provide a better insight about the temperature variation at different ranges of LST.

Table 5.8: Percentage Change of LSTs in the Study Area from 1989-1994 (km^2)

Range	1989		1994		Change (%) (1994-1989)
	Area km^2	Area in (%)	Area km^2	Area in (%)	
$< 20^0C$	43.109	88.284	27.998	57.338	-30.946
$20\text{-}24^0C$	5.017	10.274	20.119	41.201	30.928
$24\text{-}28^0C$	0.704	1.442	0.713	1.461	0.018
$28\text{-}32^0C$	0.000	0.000	0.000	0.000	0.000
$> 32^0C$	0.000	0.000	0.000	0.000	0.000
Total	48.830	100	48.830	100	

From 1989 to 1994, the highest percentage of area (30.946%) was lost in having LST below 20^0C range. Also, 30.928% area increased within the rage of $20\text{-}24^0C$. Due to abundance vegetation and water bodies temperature range above 28^0C found unavailable (Table 5.8).

Table 5.9: Percentage Change of LSTs in the Study Area from 1994-1999 (km^2)

Range	1994		1999		Change (%) (1999-1994)
	Area km^2	Area in (%)	Area km^2	Area in (%)	
$< 20^0C$	27.998	57.338	0.134	0.275	-57.063
$20\text{-}24^0C$	20.119	41.201	46.892	96.031	54.829
$24\text{-}28^0C$	0.713	1.461	1.118	2.289	0.828
$28\text{-}32^0C$	0.000	0.000	0.686	1.405	1.405
$> 32^0C$	0.000	0.000	0.000	0.000	0.000
Total	48.830	100	48.830	100	

From 1989 to 1994, the highest percentage of area (57.063%) was lost in having LST below 20^0C range. Also, 54.829% area increased within the rage of $20\text{-}24^0C$. Due to abundance vegetation and water bodies temperature range above 32^0C found unavailable (Table 5.9).

Table 5.10: Percentage Change of LSTs in the Study Area from 1999-2004 (km^2)

Range	1999		2004		Change (%) (2004-1999)
	Area km^2	Area in %)	Area km^2	Area in %)	
< 20^0C	0.134	0.275	12.012	24.600	24.326
20-24^0C	46.892	96.031	34.925	71.524	-24.506
24-28^0C	1.118	2.289	1.202	2.461	0.171
28-32^0C	0.686	1.405	0.691	1.415	0.009
> 32^0C	0.000	0.000	0.000	0.000	0.000
Total	48.830	100.000	48.830	100.000	

Due to heavy flood in 2004 LST reduced to less than < 20^0C from 1999 to 2004 (Table 5.10). But, from the year 2004 to 2009, maximum percentage of area increased to 89.09% within the LST range of 24-28^0C. During this period significant increase of built up area, reduction of water bodies and vegetation area were noticed (Table 5.11).

Table 5.11: Percentage Change of LSTs in the Study Area from 2004-2009 (km^2)

Range	2004		2009		Change (%) (2009-2004)
	Area km^2	Area in (%)	Area km^2	Area in (%)	
< 20^0C	12.012	24.600	0.000	0.000	-24.600
20-24^0C	34.925	71.524	3.301	6.761	-64.764
24-28^0C	1.202	2.461	44.708	91.559	89.099
28-32^0C	0.691	1.415	0.820	1.680	0.265
> 32^0C	0.000	0.000	0.000	0.000	0.000
Total	48.830	100.000	48.830	100.000	

Table 5.12: Percentage Change of LST in the Study Area from 2009-2014 (km2)

Range	2009		2014		Change (%) (2014-2009)
	Area km^2	Area in (%)	Area km^2	Area in (%)	
< 20^0C	0.000	0.000	0.000	0.000	0.000
20-24^0C	3.301	6.761	0.000	0.000	-6.761
24-28^0C	44.708	91.559	21.930	44.912	-46.648
28-32^0C	0.820	1.680	26.278	53.816	52.136
> 32^0C	0.000	0.000	0.621	1.273	1.273
Total	48.830	100.000	48.830	100.000	

Built up area continued to increase from 2009 to 2014 (Table 5.12) and from 2014 to 2019 (Table 5.13) which resulted in the increase of LST more than 32^0C. Maximum area of temperature found within 28-32^0C (35.784% area) and it was 52.136% area in 2009 to 2014. Here, 1.273% and 0.238% area increased to more than 32^0C from the year 2009 to 2014. The increase of built up area, reduction of water bodies and vegetation land were dominant from the year 2009 which contributed to increase of LST more than 32^0C from 2009.

Table 5.13: Percentage Change of LSTs in the Study Area from 2014-2019 (km^2)

	2014		2019		Change in Percentage (2019-2014)
Range	Area km^2	Area in (%)	Area km^2	Area in (%)	
< 20^0C	0.000	0.000	0.000	0.000	0.000
20-24^0C	0.000	0.000	0.000	0.000	0.000
24-28^0C	21.930	44.912	4.457	9.127	-35.784
28-32^0C	26.278	53.816	43.636	89.362	35.547
> 32^0C	0.621	1.273	0.738	1.511	0.238
Total	48.830	100.000	48.830	100.000	

5.3.2 Validation of LST Using BMD Data

As the simulation of future LST pattern was estimated on the basis of 1989 to 2019 data at 5 years interval period and BMD Agargaon station's data was available from 2013 to 2018 therefore only LST data of 2014 could be validated. Estimated LST data has minimum and maximum LST value and BMD data also had minimum and maximum LST data. Therefore, the percentage of error was calculated in two ways considering maximum and minimum LST values. After validating both source data, the minimum and maximum temperature error was estimated as 3.678% and 4.982%, respectively. The percentage of error was negligible and therefore the estimation of LST was acceptable for further processing by considering a little limitation (Table 5.14).

Table 5.14: Validation of Simulated LST Based on BMD Data For 2014

Year	LST of Satellite Image	LST of BMD Data	% of Error
2014	Minimum Temperature (^{0}C)		
	24.883	24.000	3.678
	Maximum Temperature (^{0}C)		
	32.545	31.000	4.982

5.4 Association of LST and LULC

5.4.1 Cross Sectional Profile of LULC vs LST

Best way to understand the impact of LULC on LST is to investigate the links between the thermal signatures and land cover types. The radiative energy emitted from the surface of the ground, including roofs, pavement surfaces, vegetation, bare soil and water bodies, were recorded from the remote sensed LST. In order to represent the LULC wise LST, two cross-sections were made across the study area and the average LST of each LULC type was shown in Fig. 5.15 to 5.21. Two cross-sections from northwest to southeast (AB) and northeast to southwest (CD) were considered.

From the profile, it was found that congested built up area experienced average LST more than 24°C in 1989 (Figure 5.15), > 27°C in 1994 (Figure 5.16), > 28°C in 1999 (Figure 5.17), 29°C in 2004 (Figure 5.18), > 30°C in 2009 (Figure 5.19), > 32°C in 2014 (Figure 5.20) and > 34°C in 2019 (Figure 5.21). Also, high LST was recorded as 22°C in 1989, > 25°C in 1994, > 27°C in 1999, 28°C in 2004, > 30°C in 2009, > 31°C in 2014 and > 33°C in 2019 for bare land in seven different year cross-sections. Besides, other two LULC (water bodies and vegetation) were recorded as the lowest temperature ranging from < 16°C - < 27°C.

The findings signify that built up area increases LST by replacing natural vegetation with non-evaporating, non-transpiring surfaces.

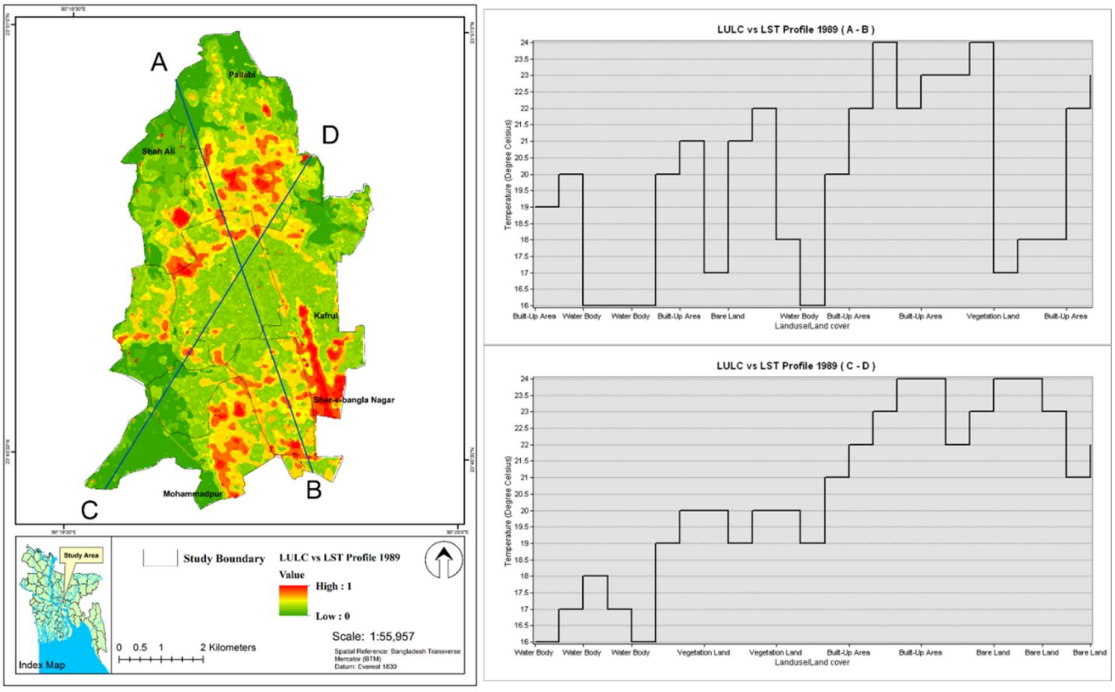

Figure 5.15: Cross Sectional Profile of LULC vs LST for the Year 1989

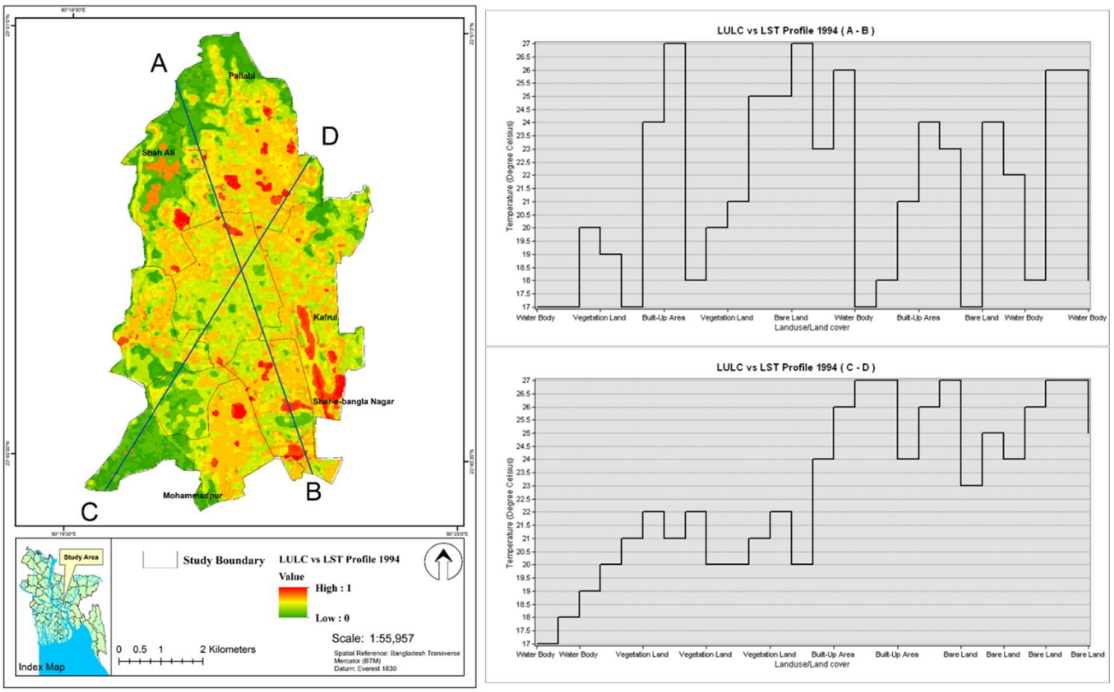

Figure 5.16: Cross Sectional Profile of LULC vs LST for the Year 1994

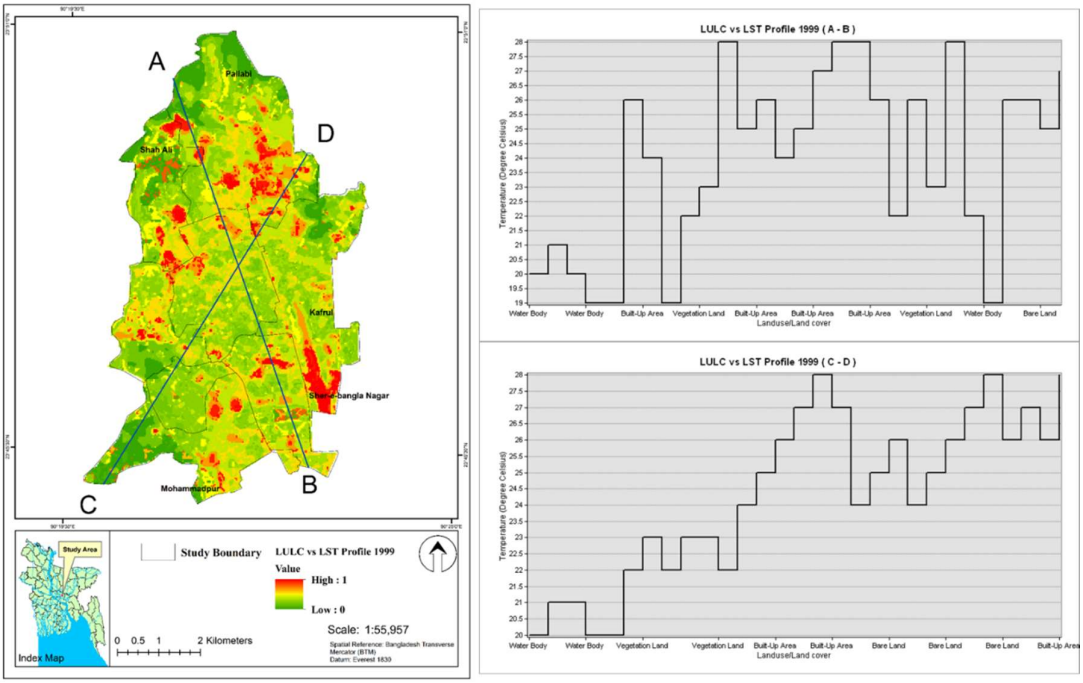

Figure 5.17: Cross Sectional Profile of LULC vs LST for the Year 1999

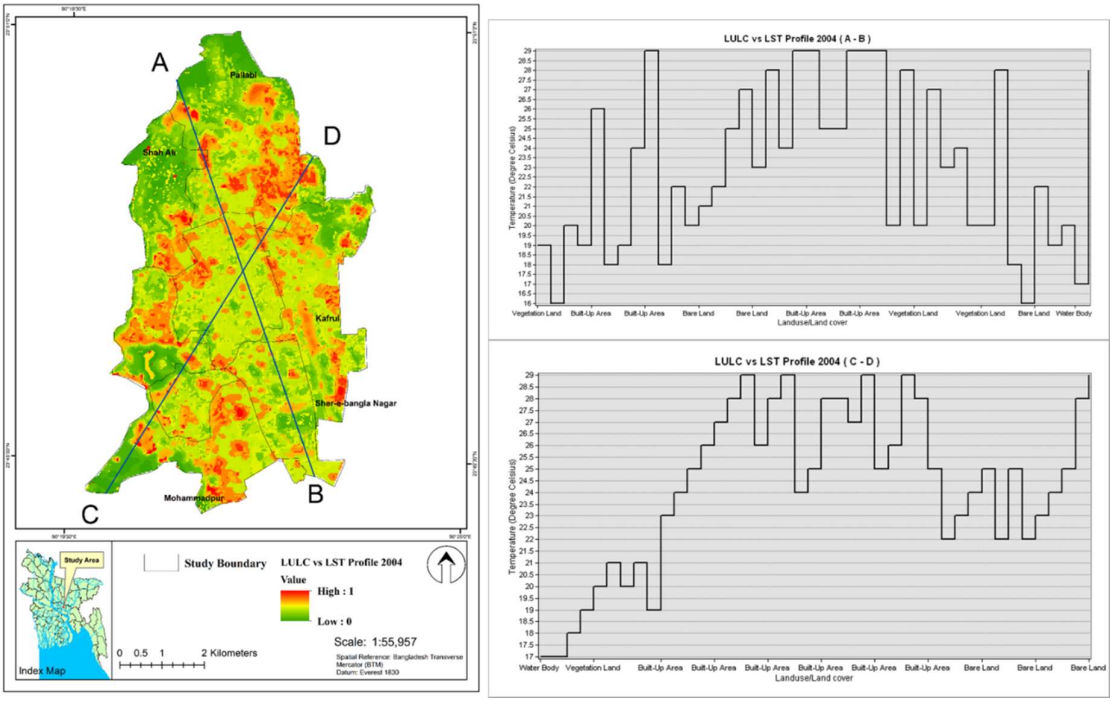

Figure 5.18: Cross Sectional Profile of LULC vs LST for the Year 2004

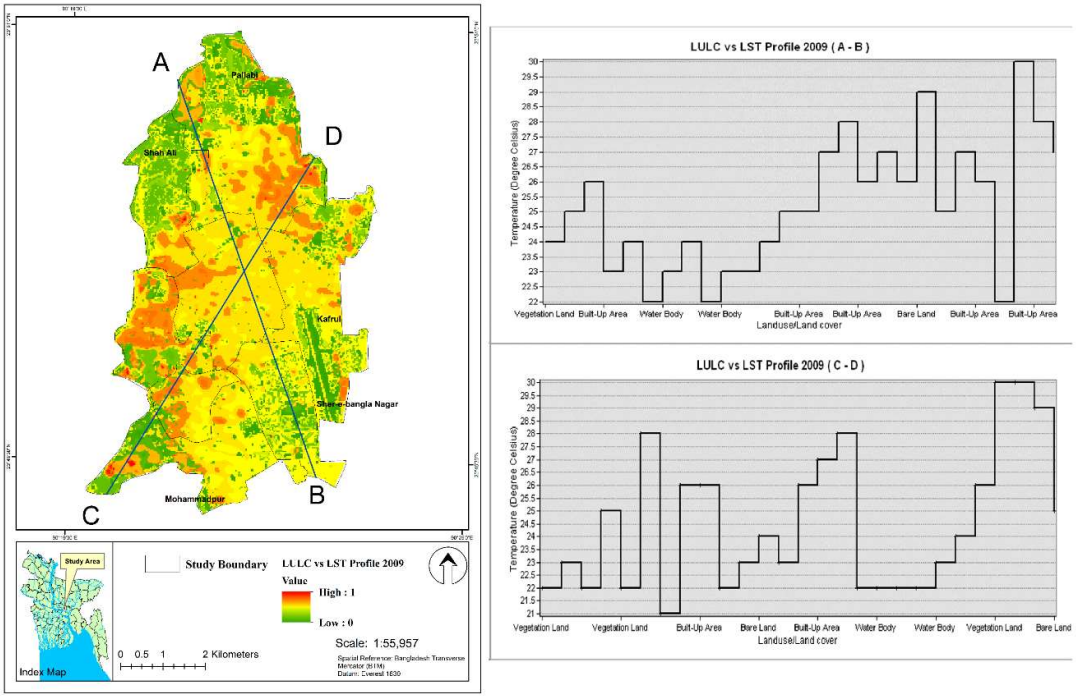

Figure 5.19: Cross Sectional Profile of LULC vs LST for the Year 2009

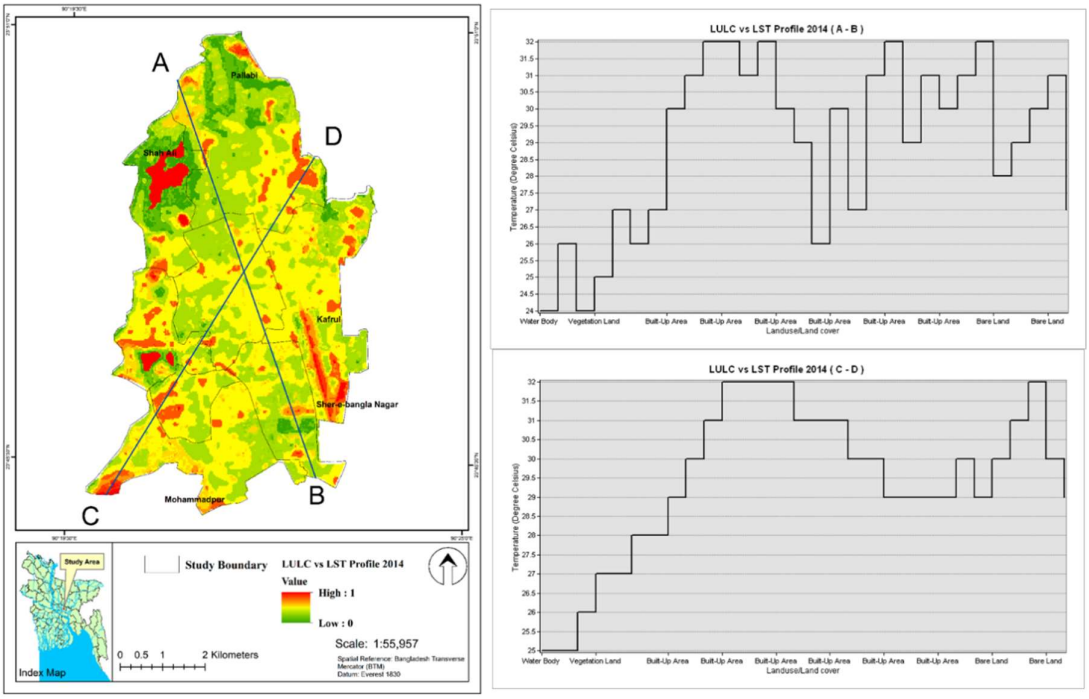

Figure 5.20: Cross Sectional Profile of LULC vs LST for the Year 2014

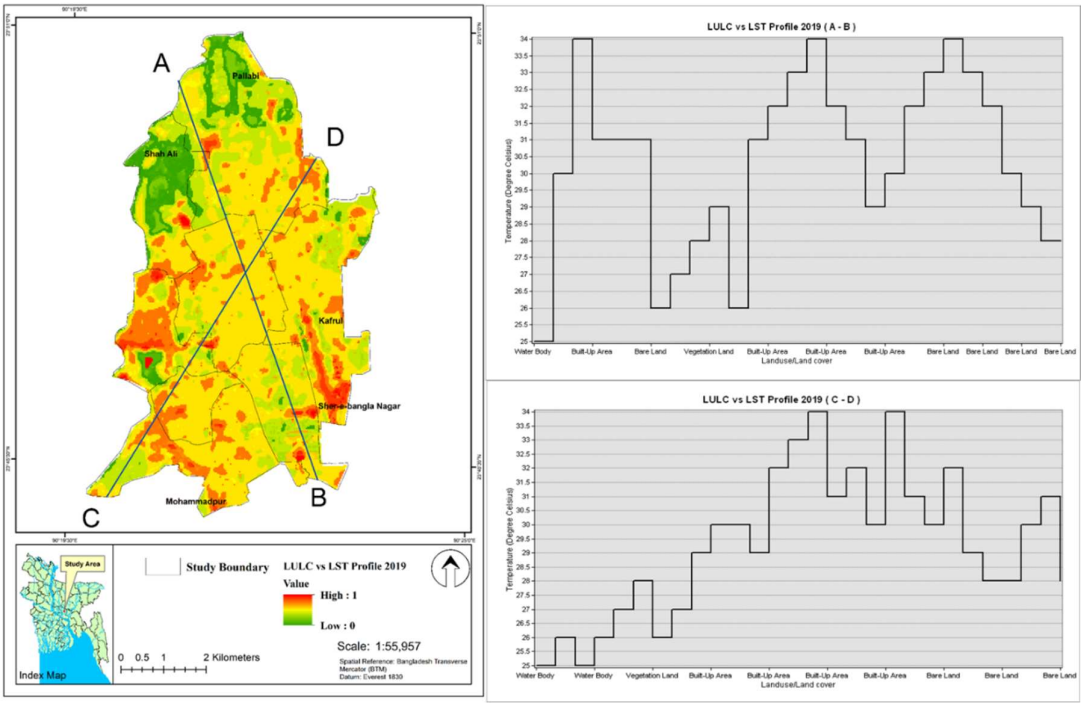

Figure 5.21: Cross Sectional Profile of LULC vs LST for the Year 2019

5.4.2 LULC wise LST Distribution

The distribution of LST in different LULC classes in various ranges demonstrates the LULC wise LST concentration in the study area. Considering the LST distribution in different LULC classes for the year 1989, most of the area was experienced below 20^0C in every LULC class and the covered area under 20^0C was 15.40 km^2 in water bodies, 12.27 km^2 in bare land, 3.24 km^2 in built up area and 12.20 km^2 in vegetation cover (Table 5.15).

Table 5.15: LULC Wise LST Distribution in Year 1989

Temperature	**< 20^0C**	**20-24^0C**	**24-28^0C**	**28-32^0C**	**> 32^0C**
Land cover	**1989 (area km2)**				
Water Body	15.40	0.00	-	-	-
Built up Area	3.24	2.89	0.70	-	-
Vegetation Land	12.20	0.00	-	-	-
Bare Land	12.27	2.12	-	-	-

Table 5.16: LULC Wise LST Distribution in Year 1994

Temperature	< 20^{0}C	20-24^{0}C	24-28^{0}C	28-32^{0}C	> 32^{0}C
Landover	**1994 (area km2)**				
Water Body	10.35	1.68	-	-	-
Built up Area	0.66	7.97	0.71	-	-
Vegetation Land	2.91	5.41	-	-	-
Bare Land	14.08	5.06		-	-

In 1994 most of the area experienced below 20^{0}C for all LULC and the dominated LULC was bare land (14.08 km^2), water bodies (10.35 km^2), and vegetation (2.91 km^2). At LST range 20-24^{0}C, 7.97 km^2, 5.41 km^2 and 5.06 km^2 area were recorded as built up area, vegetation land and bare land respectively (Table 5.16).

Table 5.17: LULC wise LST Distribution in Year 1999

Temperature	< 20^{0}C	20-24^{0}C	24-28^{0}C	28-32^{0}C	> 32^{0}C
Landover	**1999 (area km2)**				
Water Body	0.09	3.91	0.00	0.00	-
Built up Area	0.00	14.54	0.32	0.69	-
Vegetation Land	0.04	9.33	0.00	0.00	-
Bare Land	0.00	19.11	0.84	0.00	-

For the year 1999, the highest range was 20-24^{0}C and the maximum coverage of LULC class was bare land (19.11 km^2), followed by built up area (15.75 km^2) and vegetation land (5.30 km^2) (Table 5.17).

Table 5.18: LULC wise LST Distribution in Year 2004

Temperature	< 20^{0}C	20-24^{0}C	24-28^{0}C	28-32^{0}C	> 32^{0}C
Land cover	**2004 (area km2)**				
Water Body	1.42	0.39	0.00	0.00	-
Built up Area	1.94	18.05	1.20	0.69	-
Vegetation Land	4.59	4.36	0.00	0.00	-
Bare Land	4.06	12.13	0.00	0.00	-

In 2004, the highest range of LST was 20-24^{0}C and the maximum LULC classes were built up area (18.05 km^2), followed by bare land area (12.13 km^2). The lowest LST found at water bodies (1.42 km^2) which was below 20^{0}C (Table 5.19).

Table 5.19: LULC wise LST Distribution in Year 2009

Temperature	**< 20^{0}C**	**20-24^{0}C**	**24-28^{0}C**	**28-32^{0}C**	**> 32^{0}C**
Land cover			**2009 (area km2)**		
Water Body	-	1.32	0.37	0	-
Built up Area	-	0.02	31.90	0.82	-
Vegetation Land	-	1.45	5.43	0	-
Bare Land	-	0.51	6.75	0	-

In year 2009, the highest range of temperature was 24-28^{0}C and the maximum coverage of LULC class was in urban area (31.90 km^2), followed by bare land area (6.75 km^2). The lowest temperature was recorded urban area (0.02 km^2) under 20-24^{0}C temperature (Table 5.19).

Table 5.20: LULC wise LST Distribution in Year 2014

Temperature	**< 20^{0}C**	**20-24^{0}C**	**24-28^{0}C**	**28-32^{0}C**	**> 32^{0}C**
Land cover			**2014 (area km2)**		
Water Body	-	-	1.33	0.01	0.00
Built up Area	-	-	15.18	23.04	0.59
Vegetation Land	-	-	1.23	1.33	0.00
Bare Land	-	-	4.19	1.89	0.03

As the built up area is continuously increasing, therefore, LST values got a momentum from 2014 to 2019. In 2014, highest percentage of built up areas were found in the range of 28-32^{0}C and 24-28^{0}C with corresponding areas of 23.04 km^2 and 15.15 km^2 respectively. In 2019, 0.61 km^2 and 40.94 km^2 of built up areas were found having more than 32^{0}C and 28-32^{0}C respectively (Table 5.20 – 5.21).

Table 5.21: LULC wise LST Distribution in Year 2019

Temperature	< 20^0C	20-24^0C	24-28^0C	28-32^0C	> 32^0C
Land cover			**2019 (area km2)**		
Water Body	-	-	0.92	0.21	0.00
Built up Area	-	-	0.92	40.94	0.61
Vegetation Land	-	-	1.84	0.53	0.00
Bare Land	-	-	0.78	1.95	0.14

5.5 Relation among LST, NDVI and NDBI

Two land cover indices, namely the NDVI and NDBI were derived in order to establish quantifiable relationships between LST and the indices. In this research, the lower NDVI value was identified with higher LST level. In addition, the NDVI value in the study area was found to be decreasing from -0.1 to -0.3 over 1989 to 2019. The lower NDVI value represents paved earth, bare soil, and rock producing high surface temperatures. The low values of NDVI (0.2 to 0.3) are shrub and grassland, while the high values indicate green surfaces.

On the contrary, the NDBI value was gradually increasing and leading towards higher LST values. The result of linear regression and multiple correlation indicate that LST represents strong and positive correlation with NDBI and strongly negative correlation with NDVI from the year 1989 to 2019 (Figure 5.4.1 – 5.4.7). In all the correlation analysis, the R^2 was more than 0.75 that means strongly correlated with each other. The generated linear regression formula gave an equation of predicting dependent variable NDVI or NDBI by putting independent variable value such as LST for every year. The equation varies year by year and the equation can be utilized for further complex relationship among LST, NDBI and NDVI. Furthermore, the correlation coefficient of each equation having complex relationship between variables which can be discussed in further studies.

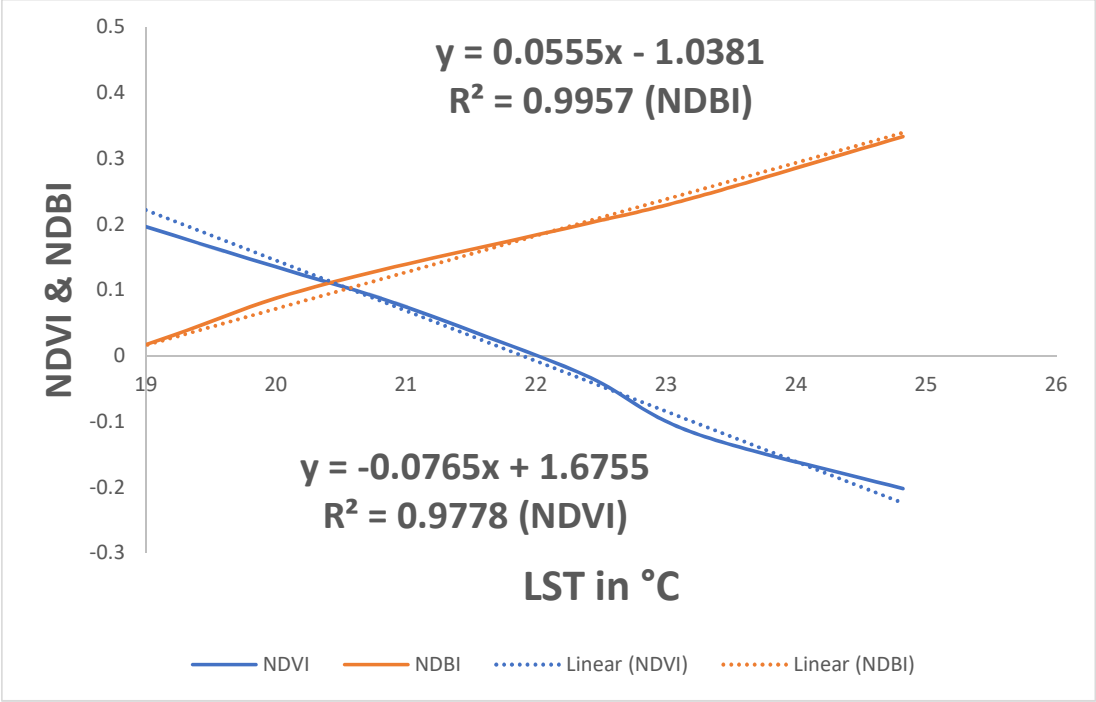

Figure 5.22: Correlation between LST vs NDVI & NDBI in the year 1989

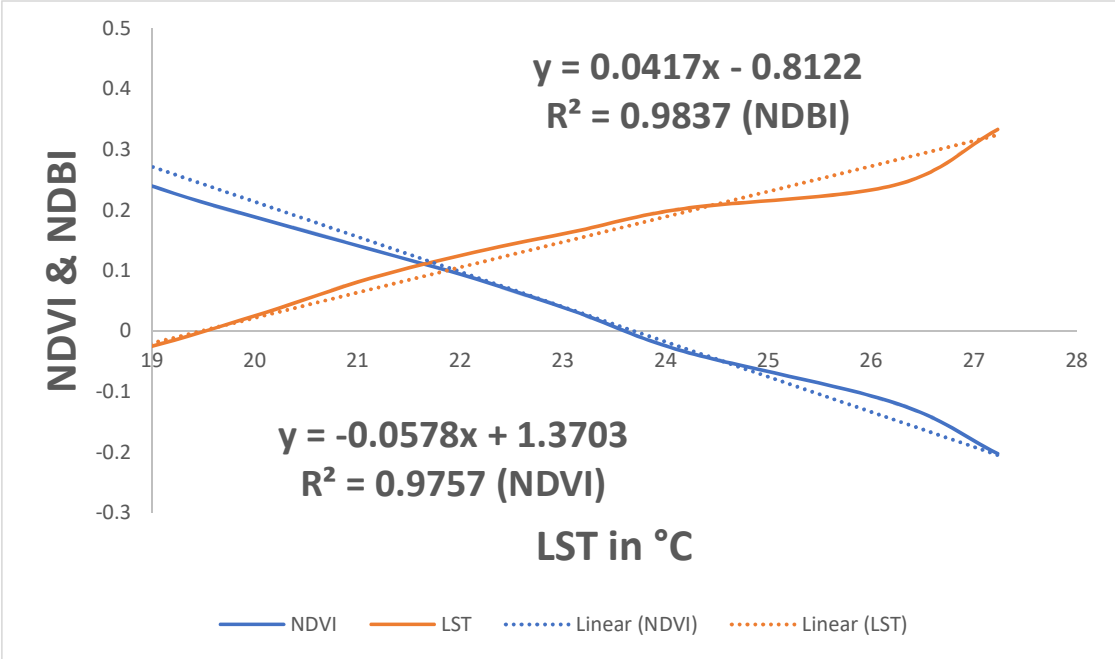

Figure 5.23: Correlation between LST vs NDVI & NDBI in the year 1994

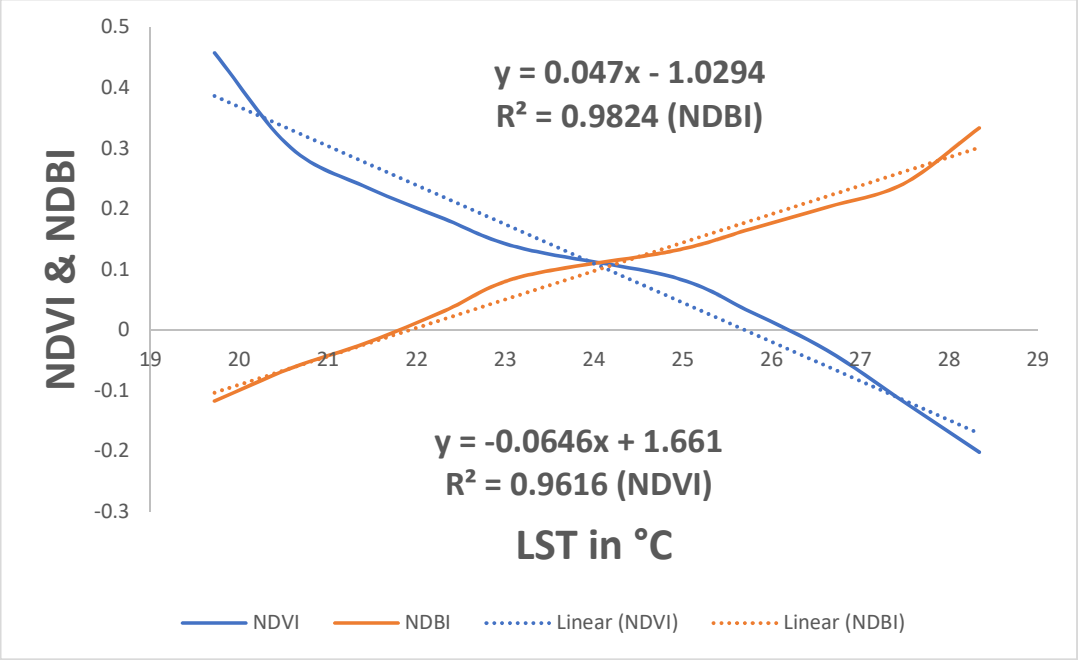

Figure 5.24: Correlation between LST vs NDVI & NDBI in the year 1999

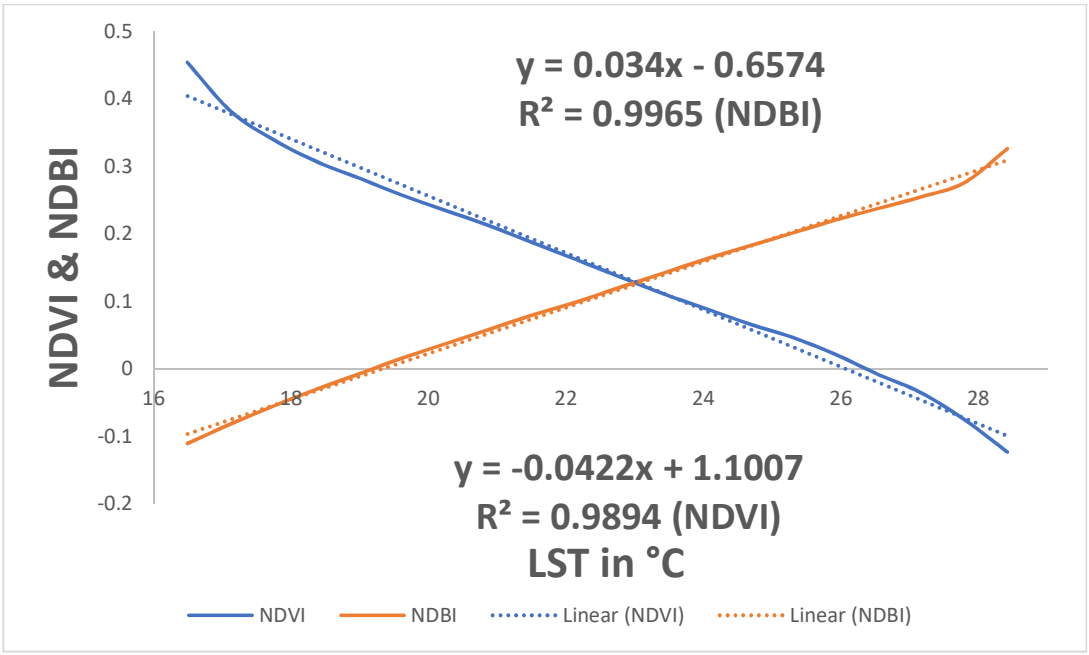

Figure 5.25: Correlation between LST vs NDVI & NDBI in the year 2004

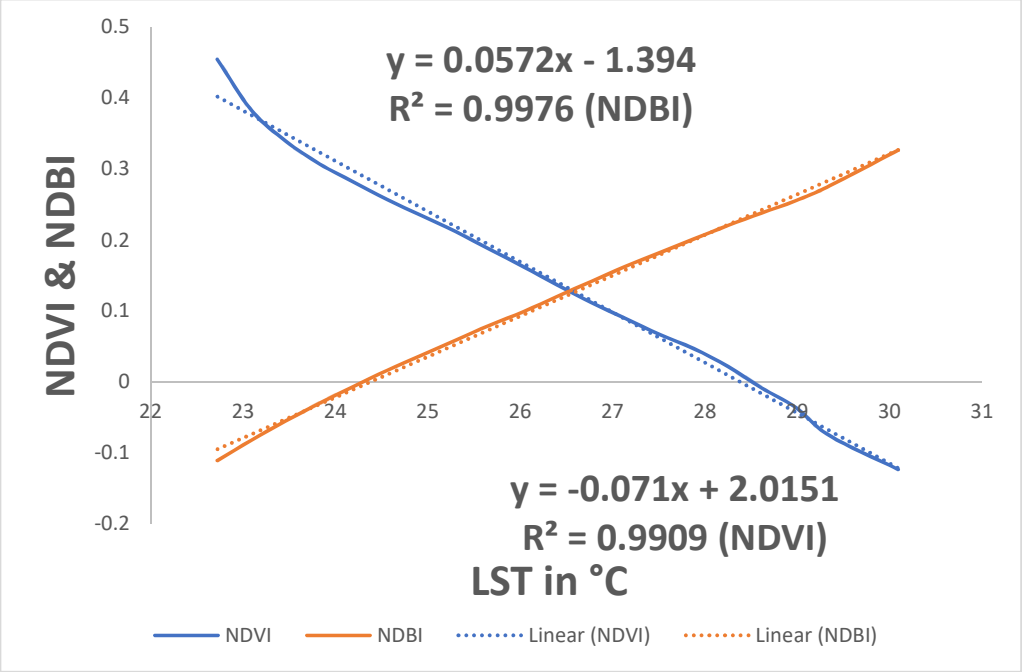

Figure 5.26: Correlation between LST vs NDVI & NDBI in the year 2009

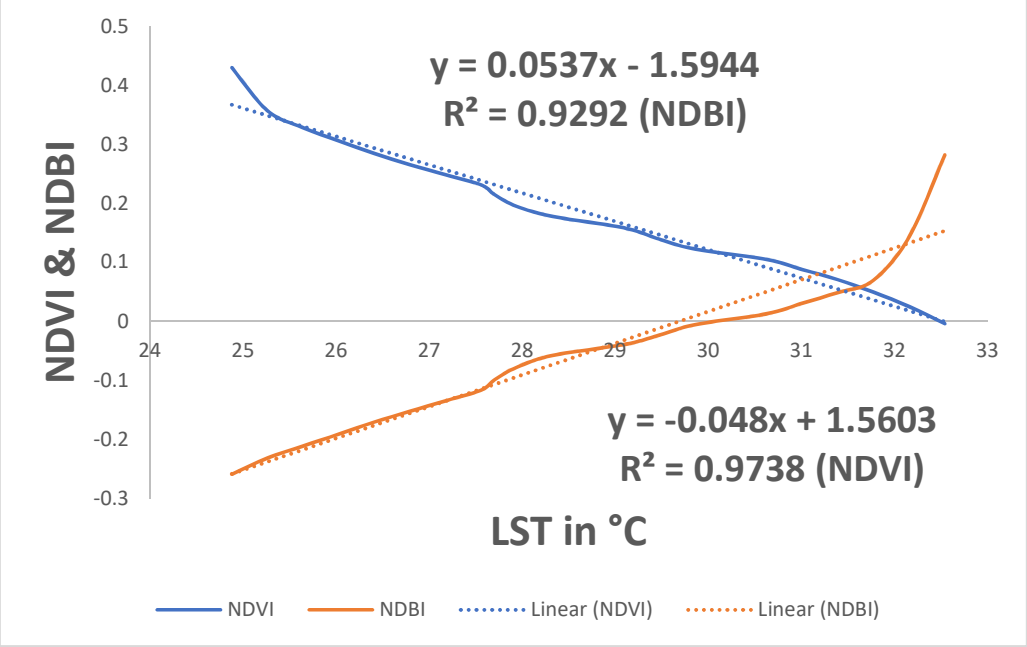

Figure 5.27: Correlation between LST vs NDVI & NDBI in the year 2014

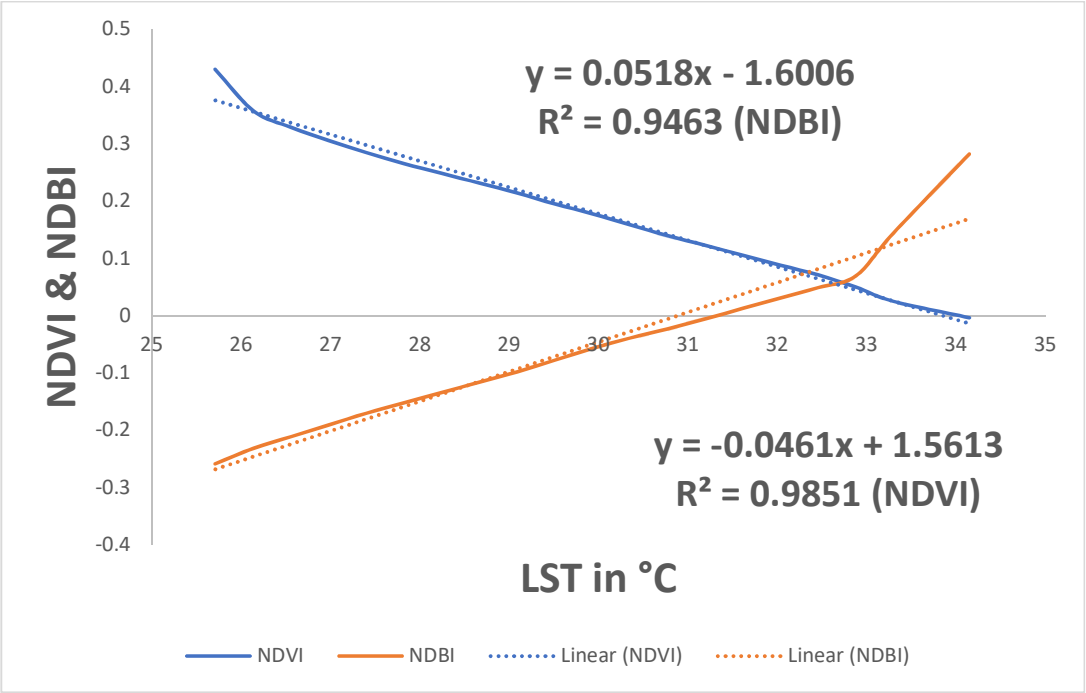

Figure 5.28: Correlation between LST vs NDVI & NDBI in the year 2019

5.6 Artificial Neural Network (ANN) Algorithm

ANN is used to make a system learn a mapping for attribute values that can be applied to classify new and hidden anomalous behaviors. Being inspired by the architecture of the human brain, ANN is composed of inter-connected nodes and weighted links. Nodes in an ANN are called neurons as an analogy with biological neurons [139]. Various network architectures have been designed depending on actual activity fields. The most widely used one is made up of three layers called the input layer, hidden layer, and output layer, where each of them consists of one or more nodes represented by the rectangles in Figure 5.29. The information flow is symbolized by the lines between one node and the next one. The nodes in the input layer receive a single value on their input and duplicate the value to the multiple outputs without modifying data. Meanwhile, the nodes in the hidden and output layers actively modify the data. These simple functional units are composed of networks that have the ability to learn a classification problem after they are trained with sufficient data. The ANN is suitable for user activity recognition and prediction. In order to recognize user activities, the Multilayer-Perceptron learning method is chosen. Figure 5.29 illustrates its common architecture.

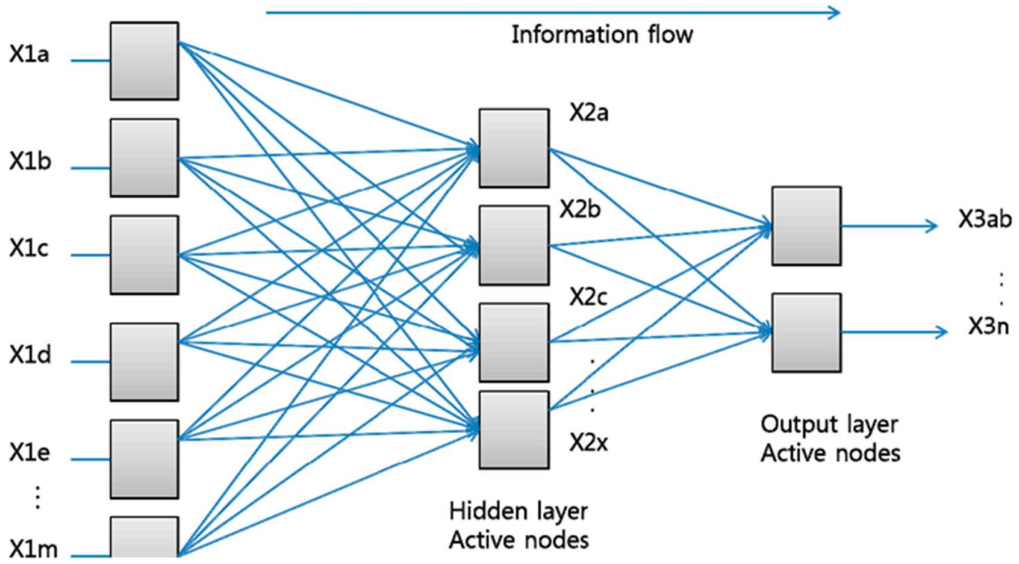

Figure 5.29: Multilayered Artificial Neural Network (Liao et al, 2005)

The pseudo code for the study of methodology is defined in Algorithms 1–3 below. The frequent activity patterns and number of clusters are entered, while the cluster set is the algorithm output as illustrated in Figure 5.30.

```
Algorithm 1: K-PATTERN CLUSTERING (NC, cP)
Input: NC- Number of Clusters        - Initially is zero
       C1set- set of Cluster Centers
       P1set- set of Input Patterns
Output: Set of Clusters
1 Read the Input dataset
2 begin
3     for each Pattern P in dataset do
4         if NC= 0 then
5             C1 ← P1                  - First Pattern as Cluster Center
6               i ← 1                  - Index of the Pattern
7             NC ← 1
8         else
9               i ← i+1
10            Get next Pattern Pi
11            Assign Pi to Cluster
12            Cluster (NC, Ci, Pi)
13 return Cluster
```

Figure 5.30: Process of Forming Frequent Activity Patterns (Sukanya & Gayathri, 2013)

Two patterns belong to the same cluster if the distance between them is less than a specified threshold. In that case, a new cluster center has to be computed as Lines 3–6 in Figure 5.31. In Figure 5.32, the computation of a new cluster center firstly needs to compare the sequence length to get the common items from both the input pattern and the cluster center (Line 7). The second stage gets different items from this input pattern and

the cluster center to check the priority table in order to get the sequence with the highest priority (Lines 8–9). Finally, the items formed at Lines 8 and 9 are combined to create a new cluster center (Line 11).

```
Algorithm 2: CLUSTER (NC, Ci, Pi)

Input:   NC- Number of Clusters
         C- set of Cluster Centers
         P- Input Pattern
Output: Patterns are assigned to Clusters
1   l: Cluster label for each pattern
2   for each Cluster center Ci do
3      if dif f <= threshold then
4         lc ← cluster id
5         recompute cluster center
6         center (Ci, Pi)
7      else
8         Assign it as a new cluster
9         nc ← nc+1
10     return clusters              - Patterns are assigned to clusters
```

Figure 5.31: Process of Forming Clustering [Source:140]

```
Algorithm 3: CENTER (Ci,Pi)

  Input: Ci- Clusters Center
         Pi- Input Pattern
  Output: new cluster center
1 q: common sequence in both patterns
2 pq: Priority table of the sequence
3 s: itemsets that differ in both sequence
4 g: length of the pattern
5 begin
6     for g do
7         q ←  compare Ci and Pi      - Common sequence in both patterns
8         s ←  itemsets differ
9         d ←  compare q and pq       - Get sensor items with high priority
10        Form the new cluster center
11        C[i] ← q+d
12    return Ci                       - new Cluster Center
```

Figure 5.32: Process of Re-computing New Center (Source: Sukanya &Gayathri, 2013)

5.7 LULC and LST Prediction for 2039

LULC classes significantly changed during the study period (1989–2019) in the study area. It was therefore important to simulate the future LULC dynamics because if the past trends persist, LST will be changed which may alter both biodiversity and micro-climate

of the study area. The future LULC prediction is also important as it provides framework for sustainable urban planning.

Moreover, the variation of LST analysis from 1999 to 2019 displayed a significant change. Therefore, it was essential to predict future LST patterns. The CA-ANN model was applied to predict the future LULC and LST for the year 2039 by analyzing the past patterns of LULC and LST of the study area. The accuracy of the prediction was validated by using percentage of correctness, overall Kappa value, Kappa location and Kappa history value based on the predicted variables.

5.8 Simulation of LULC for 2039

In the Transition potential modeling, the model validation results showed that overall Kappa index and %-correctness value was 84% (Table 5.22) which is an acceptable accuracy level for LULC modeling.

Table 5.22: ANN Model Validation for LULC in QGIS MOLUSCE Plugin

Prediction Year	ANN model validation for LULC prediction			
	QGIS-MOLUSCE Plugin module			
2039	%-correctness	Overall Kappa Value	Kappa- location	Kappa- histo
	84.56%	0.84508	0.8529	0.8852

Figure 5.33 indicates the model validation result which was generated from QGIS software.

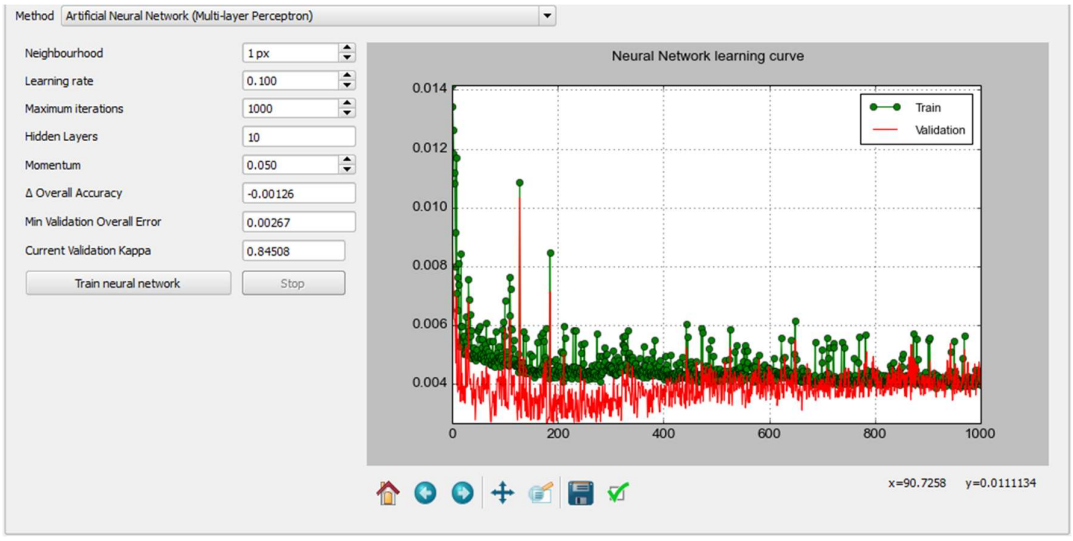

Figure 5.33: LULC Prediction Model Validation Result for the Year 2039

In the Transition potential modeling, the current validation Kappa value for represents excellent Kappa value (0.9136) and neural network learning curve. The ultimate output of the approach was simulated LST for the year 2039.

The simulated result showed a strong agreement that confirmed the accuracy of the ANN model's prediction for 2039 with 91.856% correctness and 0.9362 overall Kappa value (Table 5.23). Based on the ANN model validation in other researches, the percentage of correctness value over 80% demonstrates strong agreement of accuracy.

Table 5.23: ANN Model Validation for LST in QGIS MOLUSCE Plugin

Prediction Year	ANN model validation for LST prediction			
	QGIS-MOLUSCE Plugin module			
2039	%-correctness	Overall Kappa Value	Kappa- location	Kappa- histo
	91.856	0.9362	0.9037	0.92582

The validation provided an excellent accuracy with more than 90% of correctness for simulated LST map in 2039 (Figure 5.34).

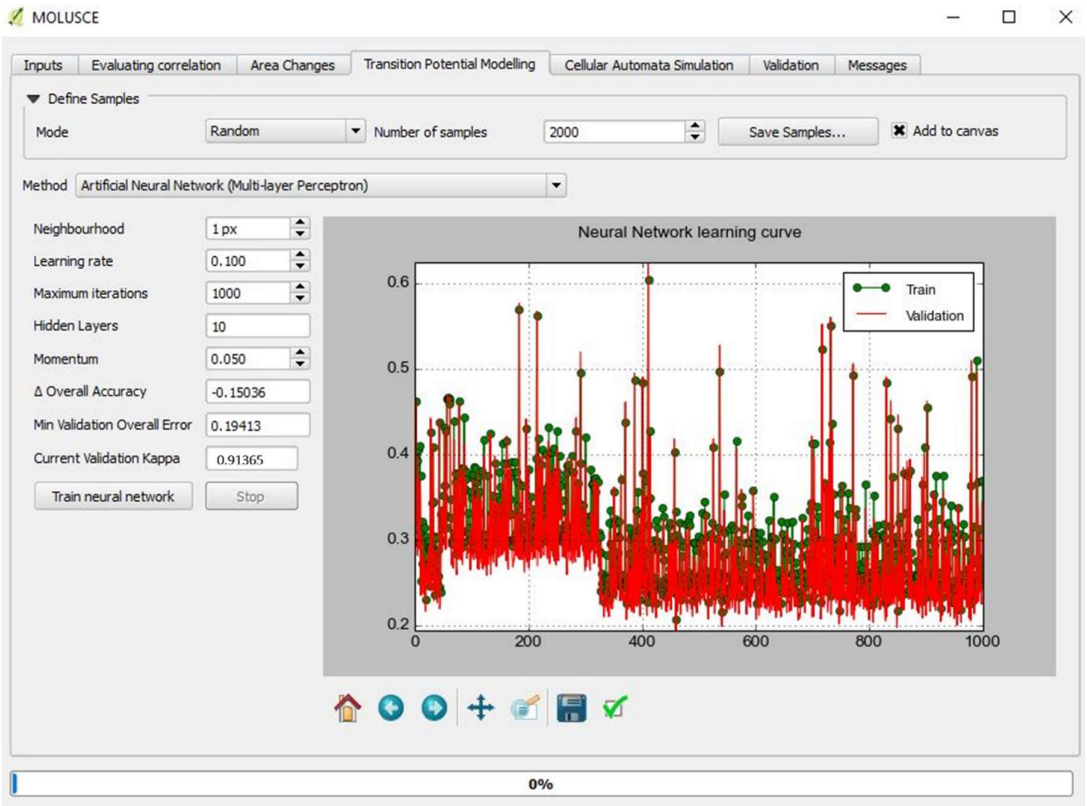

Figure 5.34: Transition Potential Modeling for LST Simulation for the Year 2039

In the final step, validation of ANN model was performed based on the reference map and simulated map. The reference map was set as the LST map for year 2019 and simulated map for year 2039 which was achieved from transition potential modeling process.

Simulation results showed that approximately 92% of the area will be converted into built up area in 2039 (Figure 5.35). Predicted LULC change in future could adversely affect the environment altering both climate and biodiversity of the area.

Table 5.24: Percentage Change of LULCs in the Study Area from 2019-2039 (km^2)

LULC	Area km^2 (2019)	Area in %	Area km^2 (2039)	Area in %	Change in % (2039-2019)
Water body	1.1259	2.31	1.12	2.29	-0.012
Built up area	42.4674	86.96	45.13	92.42	5.459
Vegetation	2.3697	4.85	2.05	4.19	-0.664
Bare land	2.871	5.88	0.53	1.09	-4.788
Total	48.83	100.00	48.83	100.00	

The percentage of change indicates that in 2039 built up area would increase about 5.5% higher than the 2019 if this pattern continues. Moreover 92.42% of Mirpur and surrounding area would convert in to built up area and there will be drastic reduction of other LULC such as vegetation, bare land and water bodies (Table 5.24).

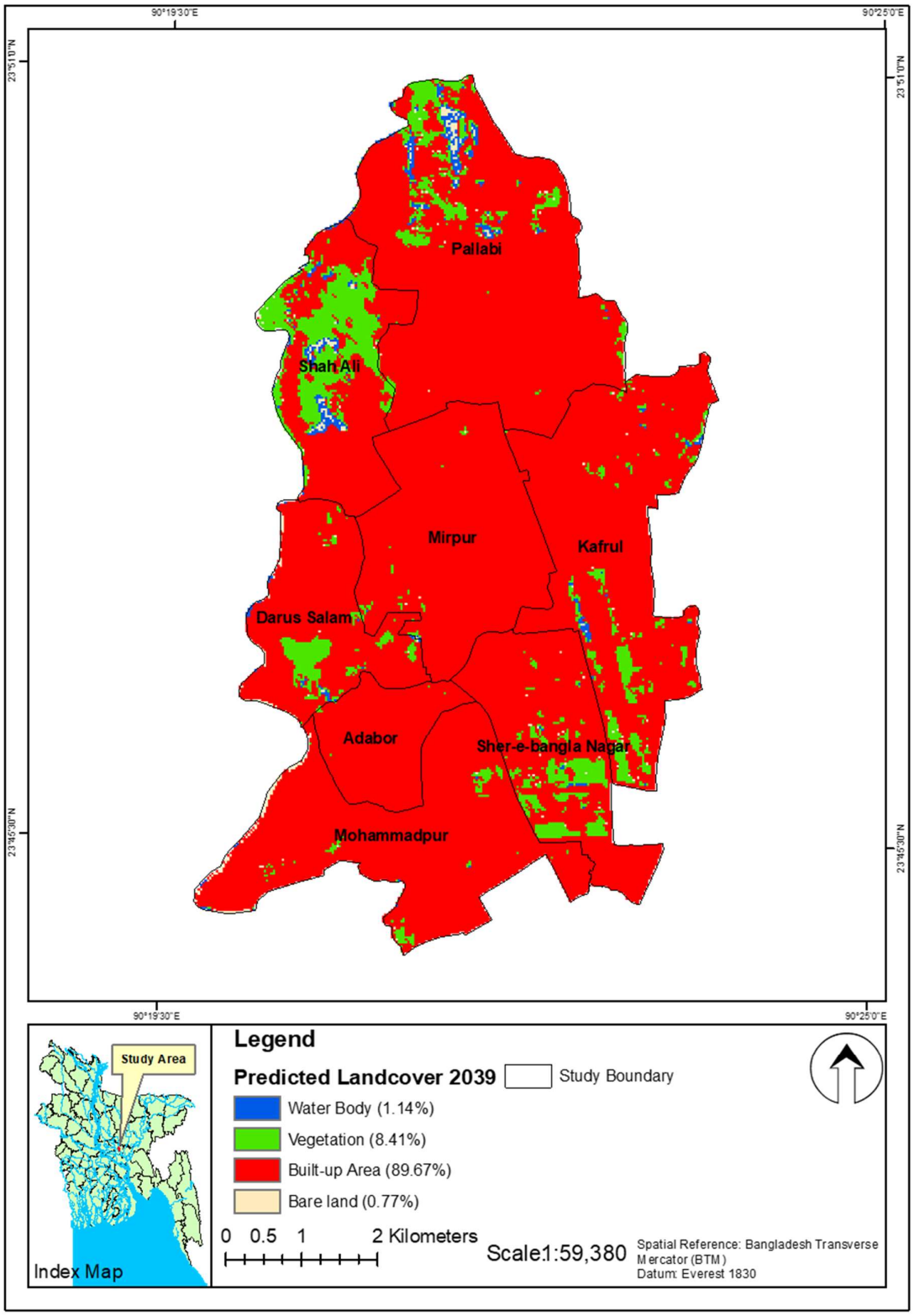

Figure 5.35: Simulated LULC Map for the year 2039

5.9 Simulation of LST for 2039

Similar to the LULC for the study period from 1989–2019 LST also shows a substantial amount of change. Accordingly, LST is simulated for 2039. The past trends of estimated LST data are used in the ANN model to predict the future LST trends of the study area.

The prediction exhibited that approximately 23.69% of Mirpur area likely to have LST greater than 32°C and 72.62% area is likely to remain 28-32°C LST range. There may not be any temperature area that might experience below 28°C LST. Change of percentage of area is around 22.18% which will fall within the range of LST greater than 32°C in 2039 (Table 5.25). The prediction results demonstrate that most of the LST remains below-32°C. Figure 5.36 shows the rising trend of LST in the study area for the year 2039.

Table 5.25: Percentage Change of LSTs in the Study Area from 2019-2039 (km^2)

Range	Area (2019)	Area in Percentage	Area (2039)	Area in Percentage	Change in Percentage (2039-2019)
< 20°C	-	-	-	-	-
20-24°C	-	-	-	-	-
24-28°C	4.46	9.13	1.80	3.69	-5.44
28-32°C	43.64	89.36	35.46	72.62	-16.74
> 32°C	0.74	1.51	11.57	23.69	22.18
Total	48.83	100	48.83	100	

This effect of high LST is going to be a worrying problem for the study area. The temperature effect depends on the city geometry and Dhaka City's unexpected growth triggers this devastating impact of the increase of LST.

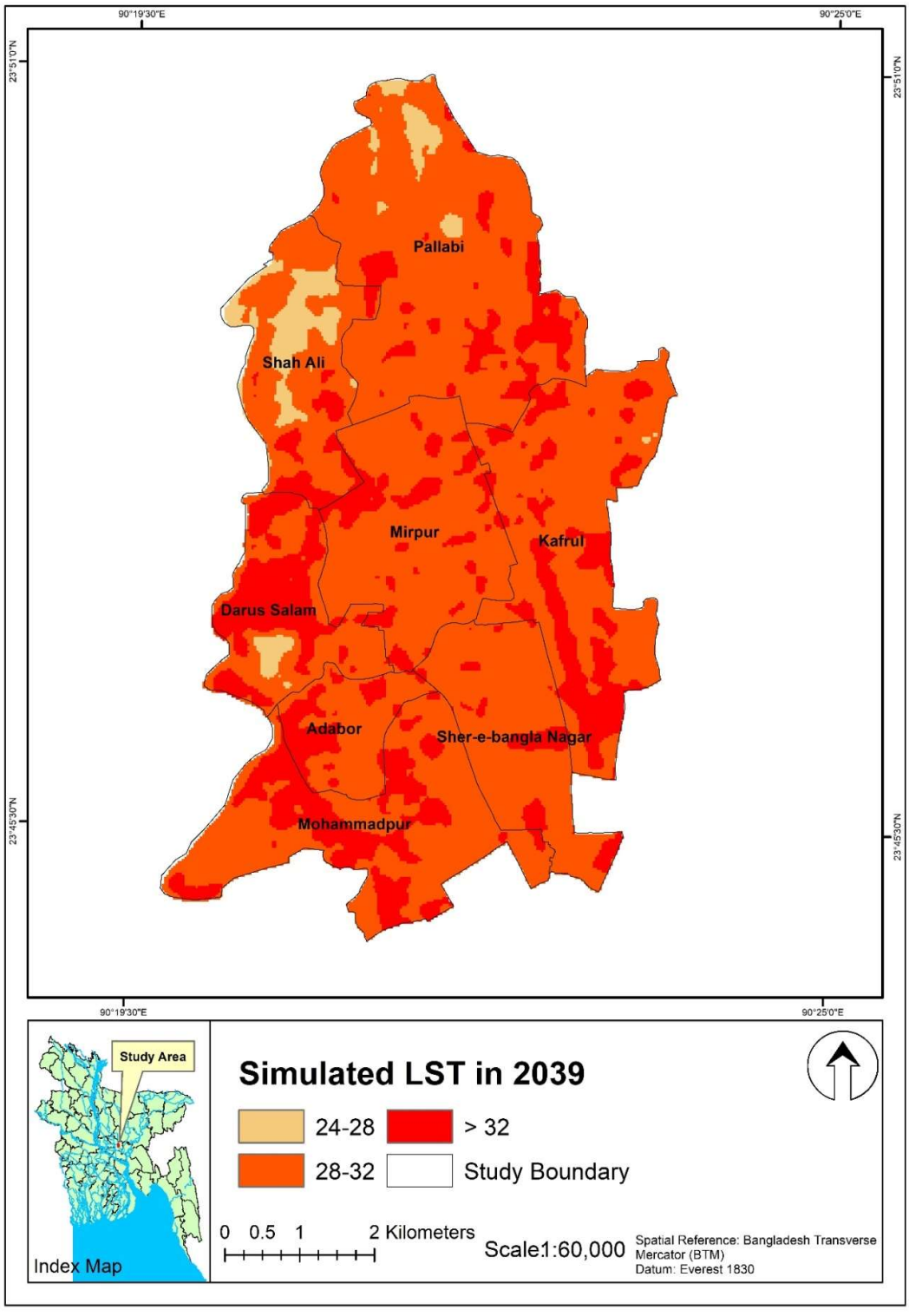

Figure 5.36: Simulated LST Map for the Year 2039

CHAPTER 06: CONCLUSIONS & RECOMMENDATIONS

CHAPTER 06: CONCLUSIONS & RECOMMENDATIONS

6.1 Conclusions

The LST classification analysis on Landsat image shows that it could provide useful and efficient remote sensed data for LST retrieval for any area. In order to assess the LST dynamics and environmental impacts an in depth study of Landsat satellite images over a period of thirty years from 1989 to 2019 was carried out at a 5 years interval period. Furthermore, CA-ANN based prediction for both LULC and LST were analyzed to realize what will be the consequences if this increasing trend continues. Some key outputs from this analysis are stated below.

The study area faced tremendous increase of built up area. Increasing impervious layers trend to reflect and generate higher surface temperature. Considering the year 2014-2019, built up area gained 7.5 % area where bare land, vegetation and water bodies were lost 6.68%, 0.38% and 0.44% area, respectively. The maximum losses (bare land and vegetation) and gains (built up area) were observed in the 2004 to 2014 period. However, the water body expansively was lost its coverage in the 1994 to 1999 periods.

The average surface temperature increasing rate is high in 5 years interval period. In 1989, 88.28% of area was covered under 20^0C temperature. Later, maximum area of temperature was increased to the range of 28 to 32^0C at 52.14% from the year 2009 to 2014. Here, 1.27% and 0.24% area were increased to more than 32^0C from the year 2009 to 2014 and from 2014 to 2019, respectively. The increase of built up area, reduction of surface water bodies and vegetation land were dominant from the year 2009 which contribute to the increase in the LST up to more than 32^0C from the year 2009. Validation of LST estimated data with BMD data was pretty much impressive and the percentage of error is 3% to 4%.

Prediction indicates that in the year 2039 approximately 92.42% of Mirpur and surrounding areas will be covered by built-up area and corresponding predicted LST range will be greater than 32°C. The prediction exhibited that approximately 23.69% of Mirpur area likely to have LST greater than 32°C and 72.62% area is likely to remain 28 to 32°C LST range. There may not be any temperature area that might experience below 28°C LST. Change of percentage of area is around 22.18% which will fall within the

range of LST greater than 32°C in 2039. The prediction results demonstrate that most of the LST remains below 32°C. A rising trend of LST was observed for the year 2039.

Cross section profile of LULC vs LST shows higher temperature existed in built up area in all time periods. In the year 2019, 0.61 km^2 of urban area was fallen more than 32^0C temperature range followed by 40.94 km^2 in the range of 28 to 32^0C. LST has strong positive correlation with NDBI. LST has strong negative correlation with NDVI. In all the correlation analysis, the R^2 value was found more than 0.9 that means the variables are strongly correlated with each other. The study shows a clear past and present situation of the negative consequence of unplanned rapid urbanization as well as predicts the future scenario of the study region.

6.2 Recommendations

The overall result shows a high LST change in the study area. Mirpur area is located in the DMP area which is the most economically productive area of this country. Therefore, preparation steps to reduce LST as well as UHI effects is important. The seasonal change of LST in the study area, which in a tropical country is very uncertain, needs cloud-free satellite images. In summer region, cloud contains the whole study region. If summer images could be collected, then actual LST effects can easily be realized. In addition, to understand the magnitude, it is necessary to evaluate UHI locally and nationwide.

This is the first study, to the knowledge of the Author that demonstrated a method of deriving future LST of urban areas based on the simulation from observed relationships between land cover and LST changes in the study area. Therefore, future city planning should focus more on urban greening as the study area is gradually shifting towards the highest temperature zone due to the expansion of urban areas. If the current trend continues then almost the entire study area will be an UHI in 2039. A compact-town like decentralization of urban areas (satellite-towns) is, therefore, a possible way forward in order to prevent the formation of large-scale UHI effect in the future. The study used LULC indices (NDVI and NDBI) and applied a simple regression equation for the derivation of future LST. It is possible that the different land cover indices can be used together as independent factors in a multiple regression equation model in order to derive the LST in a more robust way, possibly through undertaking a factor analysis. Future study should seek to incorporate these and improve upon the model presented here.

REFERENCES

[1] E. F. Lambin, "Land-use and land-cover Change (LUCC)-implementation strategy," *A core project of the International Geosphere-Biosphere Programme and the International Human Dimensions Programme on Global Environmental Change,* 1999.

[2] B. L. Turner, D. Skole, S. Sanderson, G. Fischer, L. Fresco, and R. Leemans, "Land-use and land-cover change: science/research plan," *[No source information available],* 1995.

[3] J. Liu, W. Kuang, Z. Zhang, X. Xu, Y. Qin, J. Ning*, et al.*, "Spatiotemporal characteristics, patterns, and causes of land-use changes in China since the late 1980s," *Journal of Geographical Sciences,* vol. 24, pp. 195-210, 2014.

[4] A. M. Dewan and Y. Yamaguchi, "Land use and land cover change in Greater Dhaka, Bangladesh: Using remote sensing to promote sustainable urbanization," *Applied geography,* vol. 29, pp. 390-401, 2009.

[5] W. B. Meyer and B. L. Turner, "Human population growth and global land-use/cover change," *Annual review of ecology and systematics,* vol. 23, pp. 39-61, 1992.

[6] R. J. Corner, A. M. Dewan, and S. Chakma, "Monitoring and prediction of land-use and land-cover (LULC) change," in *Dhaka megacity*, ed: Springer, 2014, pp. 75-97.

[7] M. S. Rahman, H. Mohiuddin, A.-A. Kafy, P. K. Sheel, and L. Di, "Classification of cities in Bangladesh based on remote sensing derived spatial characteristics," *Journal of Urban Management,* 2018.

[8] A. M. Dewan, M. H. Kabir, K. Nahar, and M. Z. Rahman, "Urbanisation and environmental degradation in Dhaka Metropolitan Area of Bangladesh," *International Journal of Environment and Sustainable Development,* vol. 11, pp. 118-147, 2012.

[9] A. Lilly Rose, Devadas, M.D., "Analysis of Land Surface Temperature and Land Use/Land Cover Types Using Remote Sensing Imagery - A Case In Chennai City, India," presented at the The seventh International Conference on Urban Climate., held on 29 June – 3 July 2009, Yokohama, Japan., 2009.

[10] IPCC, "Mitigation of climate change," *Contribution of Working Group III to the Fifth Assessment Report of the Intergovernmental Panel on Climate Change,* vol. 1454, 2014.

[11] X.-L. Chen, H.-M. Zhao, P.-X. Li, and Z.-Y. Yin, "Remote sensing image-based analysis of the relationship between urban heat island and land use/cover changes," *Remote sensing of environment,* vol. 104, pp. 133-146, 2006.

[12] M. L. McKinney, "Urbanization, biodiversity, and conservation. Bioscience 52: 883890McKinney ML (2006) Urbanization as a major cause of biotic homogenization," *Biol Conserv,* vol. 127, p. 247260, 2002.

[13] D. X. Tran, F. Pla, P. Latorre-Carmona, S. W. Myint, M. Caetano, and H. V. Kieu, "Characterizing the relationship between land use land cover change and land surface temperature," *ISPRS journal of photogrammetry and remote sensing,* vol. 124, pp. 119-132, 2017.

[14] B. Ahmed, "Modelling spatio-temporal urban land cover growth dynamics using remote sensing and GIS techniques: A case study of Khulna City," *Journal of Bangladesh institute of Planners,* vol. 4, pp. 15-32, 2011.

[15] I. Balogun and K. Ishola, "Projection of future changes in landuse/landcover using cellular automata/markov model over Akure city, Nigeria," *Journal of Remote Sensing Technology,* vol. 5, pp. 22-31, 2017.

[16] M. Rahman, A. S. Aldosary, and M. Mortoja, "Modeling future land cover changes and their effects on the land surface temperatures in the Saudi Arabian eastern coastal city of Dammam," *Land,* vol. 6, p. 36, 2017.

[17] R. T. Handayanto, S. M. Kim, and N. K. Tripathi, "Land use growth simulation and optimization in the urban area," 2017, pp. 1-6.

[18] B. Celik, S. Kaya, U. Alganci, and D. Z. Seker, "Assessment of the Relationship Between Land Use/Cover Changes and Land Surface Temperatures: A case study of Thermal Remote Sensing," *FEB-FRESENIUS ENVIRONMENTAL BULLETIN,* vol. 3, p. 541, 2019.

[19] A. Kafy, M. Islam, L. Ferdous, A. R. Khan, and M. M. Hossain, "Identifying Most Influential Land Use Parameters Contributing Reduction of Surface Water Bodies in Rajshahi City, Bangladesh: A Remote Sensing Approach," *Remote Sensing of Land,* vol. 2, pp. 87-95, 2019.

[20] S. Ullah, A. A. Tahir, T. A. Akbar, Q. K. Hassan, A. Dewan, A. J. Khan*, et al.*, "Remote sensing-based quantification of the relationships between land use land

cover changes and surface temperature over the lower Himalayan region," *Sustainability,* vol. 11, p. 5492, 2019.

[21] S. U. E. Grimmond, "Urbanization and global environmental change: local effects of urban warming," *Geographical Journal,* vol. 173, pp. 83-88, 2007.

[22] I. D. Maduako, Z. Yun, and B. Patrick, "Simulation and prediction of land surface temperature (LST) dynamics within Ikom City in Nigeria using artificial neural network (ANN)," *Journal of Remote Sensing & GIS,* vol. 5, pp. 1-7, 2016.

[23] A. A. A. Al-sharif and B. Pradhan, "Monitoring and predicting land use change in Tripoli Metropolitan City using an integrated Markov chain and cellular automata models in GIS," *Arabian journal of geosciences,* vol. 7, pp. 4291-4301, 2014.

[24] M. Rahman, "Detection of land use/land cover changes and urban sprawl in Al-Khobar, Saudi Arabia: An analysis of multi-temporal remote sensing data," *ISPRS International Journal of Geo-Information,* vol. 5, p. 15, 2016.

[25] H. W. Zheng, G. Q. Shen, H. Wang, and J. Hong, "Simulating land use change in urban renewal areas: A case study in Hong Kong," *Habitat International,* vol. 46, pp. 23-34, 2015.

[26] E. M. Zine El Abidine, Y. E. Mohieldeen, A. A. Mohamed, O. Modawi, and M. H. Al-Sulaiti, "Heat wave hazard modelling: Qatar case study," *QScience connect,* p. 9, 2014.

[27] M. Maimaitiyiming, A. Ghulam, T. Tiyip, F. Pla, P. Latorre-Carmona, Ü. Halik*, et al.*, "Effects of green space spatial pattern on land surface temperature: Implications for sustainable urban planning and climate change adaptation," *ISPRS Journal of Photogrammetry and Remote Sensing,* vol. 89, pp. 59-66, 2014.

[28] C. Mozumder and N. K. Tripathi, "Geospatial scenario based modelling of urban and agricultural intrusions in Ramsar wetland Deepor Beel in Northeast India using a multi-layer perceptron neural network," *International Journal of Applied Earth Observation and Geoinformation,* vol. 32, pp. 92-104, 2014.

[29] X. Yu, X. Guo, and Z. Wu, "Land surface temperature retrieval from Landsat 8 TIRS—Comparison between radiative transfer equation-based method, split window algorithm and single channel method," *Remote Sensing,* vol. 6, pp. 9829-9852, 2014.

[30] R. Thapa and Y. Murayama, "Examining spatiotemporal urbanization patterns in Kathmandu Valley, Nepal: Remote sensing and spatial metrics approaches," *Remote Sensing,* vol. 1, pp. 534-556, 2009.

[31] M. T. Rahman, A. S. Aldosary, and M. Mortoja, "Modeling future land cover changes and their effects on the land surface temperatures in the Saudi Arabian eastern coastal city of Dammam," *Land,* vol. 6, p. 36, 2017.

[32] M. T. Rahman and T. Rashed, "Urban tree damage estimation using airborne laser scanner data and geographic information systems: An example from 2007 Oklahoma ice storm," *Urban Forestry & Urban Greening,* vol. 14, pp. 562-572, 2015.

[33] B. Ahmed, M. Kamruzzaman, X. Zhu, M. S. Rahman, and K. Choi, "Simulating land cover changes and their impacts on land surface temperature in Dhaka, Bangladesh," *Remote Sensing,* vol. 5, pp. 5969-5998, 2013.

[34] M. Scarano and J. A. Sobrino, "On the relationship between the sky view factor and the land surface temperature derived by Landsat-8 images in Bari, Italy," *International Journal of Remote Sensing,* vol. 36, pp. 4820-4835, 2015.

[35] Q. Zhi-hao, L. Wen-juan, Z. Ming-hua, A. Karnieli, and P. Berliner, "Estimating of the essential atmospheric parameters of mono-window algorithm for land surface temperature retrieval from Landsat TM 6," *Remote Sensing for Land & Resources,* vol. 15, pp. 37-43, 2011.

[36] W. Zhou, G. Huang, and M. L. Cadenasso, "Does spatial configuration matter? Understanding the effects of land cover pattern on land surface temperature in urban landscapes," *Landscape and urban planning,* vol. 102, pp. 54-63, 2011.

[37] C. T. van Scheltinga, D. A. Quadir, and F. Ludwig, "Baseline Study Climate Change–Bangladesh Delta Plan," Bangladesh Delta Plan2015.

[38] J. Li and H. Zhao, "Detecting urban land-use and land-cover changes in Mississauga using Landsat TM images," *Journal of Environmental Informatics,* vol. 2, pp. 38-47, 2003.

[39] V. N. Mishra and P. K. Rai, "A remote sensing aided multi-layer perceptron-Markov chain analysis for land use and land cover change prediction in Patna district (Bihar), India," *Arabian Journal of Geosciences,* vol. 9, p. 249, 2016.

[40] M. A. Hart and D. J. Sailor, "Quantifying the influence of land-use and surface characteristics on spatial variability in the urban heat island," *Theoretical and applied climatology,* vol. 95, pp. 397-406, 2009.

[41] M. S. Islam and R. Ahmed, "Land use change prediction in Dhaka city using GIS aided Markov chain modeling," *Journal of Life and Earth Science,* vol. 6, pp. 81-89, 2011.

[42] P. Fu and Q. Weng, "Responses of urban heat island in Atlanta to different land-use scenarios," *Theoretical and applied climatology,* vol. 133, pp. 123-135, 2018.

[43] H. Bahi, H. Rhinane, A. Bensalmia, U. Fehrenbach, and D. Scherer, "Effects of urbanization and seasonal cycle on the surface urban heat island patterns in the coastal growing cities: A case study of Casablanca, Morocco," *Remote Sensing,* vol. 8, p. 829, 2016.

[44] D. R. Streutker, "Satellite-measured growth of the urban heat island of Houston, Texas," *Remote Sensing of Environment,* vol. 85, pp. 282-289, 2003.

[45] G. Chander, B. L. Markham, and D. L. Helder, "Summary of current radiometric calibration coefficients for Landsat MSS, TM, ETM+, and EO-1 ALI sensors," *Remote sensing of environment,* vol. 113, pp. 893-903, 2009.

[46] R. Amiri, Q. Weng, A. Alimohammadi, and S. K. Alavipanah, "Spatial–temporal dynamics of land surface temperature in relation to fractional vegetation cover and land use/cover in the Tabriz urban area, Iran," *Remote sensing of environment,* vol. 113, pp. 2606-2617, 2009.

[47] G. Gutman, C. Huang, G. Chander, P. Noojipady, and J. G. Masek, "Assessment of the NASA–USGS global land survey (GLS) datasets," *Remote sensing of environment,* vol. 134, pp. 249-265, 2013.

[48] N. Shatnawi and H. Abu Qdais, "Mapping urban land surface temperature using remote sensing techniques and artificial neural network modelling," *International Journal of Remote Sensing,* pp. 1-16, 2019.

[49] Q. Weng, D. Lu, and J. Schubring, "Estimation of land surface temperature–vegetation abundance relationship for urban heat island studies," *Remote sensing of Environment,* vol. 89, pp. 467-483, 2004.

[50] D. L. Civco, "Artificial neural networks for land-cover classification and mapping," *International journal of geographical information science,* vol. 7, pp. 173-186, 1993.

[51] B. C. Pijanowski, D. G. Brown, B. A. Shellito, and G. A. Manik, "Using neural networks and GIS to forecast land use changes: a land transformation model," *Computers, environment and urban systems,* vol. 26, pp. 553-575, 2002.

[52] J. F. Mas and J. J. Flores, "The application of artificial neural networks to the analysis of remotely sensed data," *International Journal of Remote Sensing,* vol. 29, pp. 617-663, 2008.

[53] B. Ahmed, "Urban land cover change detection analysis and modeling spatio-temporal Growth dynamics using Remote Sensing and GIS Techniques: A case study of Dhaka, Bangladesh," 2011.

[54] V. N. Mishra, P. K. Rai, R. Prasad, M. Punia, and M.-M. Nistor, "Prediction of spatio-temporal land use/land cover dynamics in rapidly developing Varanasi district of Uttar Pradesh, India, using geospatial approach: a comparison of hybrid models," *Applied Geomatics,* vol. 10, pp. 257-276, 2018.

[55] A. Rasul, H. Balzter, and C. Smith, "Spatial variation of the daytime Surface Urban Cool Island during the dry season in Erbil, Iraqi Kurdistan, from Landsat 8," *Urban climate,* vol. 14, pp. 176-186, 2015.

[56] I. Santé, A. M. García, D. Miranda, and R. Crecente, "Cellular automata models for the simulation of real-world urban processes: A review and analysis," *Landscape and Urban Planning,* vol. 96, pp. 108-122, 2010.

[57] J. J. Arsanjani, M. Helbich, W. Kainz, and A. D. Boloorani, "Integration of logistic regression, Markov chain and cellular automata models to simulate urban expansion," *International Journal of Applied Earth Observation and Geoinformation,* vol. 21, pp. 265-275, 2013.

[58] M. M. Hassan, "Monitoring land use/land cover change, urban growth dynamics and landscape pattern analysis in five fastest urbanized cities in Bangladesh," *Remote Sensing Applications: Society and Environment,* vol. 7, pp. 69-83, 2017.

[59] M. M. Hassan and M. N. I. Nazem, "Examination of land use/land cover changes, urban growth dynamics, and environmental sustainability in Chittagong city, Bangladesh," *Environment, development and sustainability,* vol. 18, pp. 697-716, 2016.

[60] A. A. Kafy, M. S. Rahman, A. A. Faisal, M. M. Hasan, and M. Islam, "Modelling future land use land cover changes and their impacts on land surface temperatures in Rajshahi, Bangladesh," *Remote Sensing Applications: Society and Environment,* 2020.

[61] H. Wang, Y. Zhang, J. Y. Tsou, and Y. J. S. Li, "Surface urban heat island analysis of Shanghai (China) based on the change of land use and land cover," vol. 9, p. 1538, 2017.

[62] U. N. Habitat, "Urbanization and development: emerging futures," *World cities report,* vol. 3, pp. 4-51, 2016.

[63] J. Mallick, Y. Kant, and B. Bharath, "Estimation of land surface temperature over Delhi using Landsat-7 ETM+," *J. Ind. Geophys. Union,* vol. 12, pp. 131-140, 2008.

[64] M. Bokaie, M. K. Zarkesh, P. D. Arasteh, and A. Hosseini, "Assessment of urban heat island based on the relationship between land surface temperature and land use/land cover in Tehran," *Sustainable Cities and Society,* vol. 23, pp. 94-104, 2016.

[65] A. Gaur, M. K. Eichenbaum, and S. P. Simonovic, "Analysis and modelling of surface Urban Heat Island in 20 Canadian cities under climate and land-cover change," *Journal of environmental management,* vol. 206, pp. 145-157, 2018.

[66] M. T. Rahman, A. S. Aldosary, and M. J. L. Mortoja, "Modeling future land cover changes and their effects on the land surface temperatures in the Saudi Arabian eastern coastal city of Dammam," vol. 6, p. 36, 2017.

[67] A. F. Alqurashi, L. Kumar, and P. Sinha, "Urban land cover change modelling using time-series satellite images: A case study of urban growth in five cities of Saudi Arabia," *Remote Sensing,* vol. 8, p. 838, 2016.

[68] G. Chaudhuri and N. B. Mishra, "Spatio-temporal dynamics of land cover and land surface temperature in Ganges-Brahmaputra delta: A comparative analysis between India and Bangladesh," *Applied Geography,* vol. 68, pp. 68-83, 2016.

[69] G. M. Foody, "Status of land cover classification accuracy assessment," *Remote sensing of environment,* vol. 80, pp. 185-201, 2002.

[70] M. K. Islam and S. Chowdhury, "Analysis of changing land cover in Chittagong City Corporation Area (CCC) by Remote Sensing and GIS," *International Journal of Innovation and Applied Studies,* vol. 8, p. 1193, 2014.

[71] H. N. Beevi, S. Sivakumar, and R. Vasanthi, "Land use / land cover classification of Kanniykumari Coast, Tamilnadu, India. Using remote sensing and GIS techniques," *International Journal of Engineering Research and Applications,* vol. 5, 2015// 2015.

[72] A. S. Hadeel, M. T. Jabbar, and C. Xiaoling, "Remote sensing and GIS application in the detection of environmental degradation indicators," *Geo-spatial Information Science,* vol. 14, 2011// 2011.

[73] K. W. Mubea, T. G. Ngigi, and C. N. Mundia, "Assessing application of Markov chain analysis in predicting land cover change: a case study of Nakuru

municipality," *Journal of Agriculture, Science and Technology,* vol. 12, 2010// 2010.

[74] D. Fanelli and F. Piazza, "Analysis and forecast of COVID-19 spreading in China, Italy and France," *Chaos, Solitons & Fractals,* vol. 134, p. 109761, 2020.

[75] A. A. Kafy, L. Ferdous, M. S. Ali, and P. Sheel, "Using Contingent Valuation Method to Determine Economic Value of Padma River Wetland in Rajshahi District, Bangladesh," in *1st National Conference on Water Resources Engineering (NCWRE 2018)*, Chittagong, Bangladesh, 2018, pp. 180-185.

[76] D. Lu, P. Mausel, E. Brondizio, and E. Moran, "Change detection techniques," *International Journal of Remote Sensing,* vol. 25, 2003// 2003.

[77] B. L. Turner, E. F. Lambin, and A. Reenberg, "The emergence of land change science for global environmental change and sustainability," *Proceedings of the National Academy of Sciences,* vol. 104, 2007// 2007.

[78] P. H. Verburg, J. R. V. Eck, T. C. D. Hijs, M. J. Dijst, and P. Schot, "Determination of land use change patterns in the Netherlands," *Environment and Planning B: Urban Analytics and City Science,* vol. 31, 2004// 2004.

[79] I. Ogashawara and V. d. S. B. Bastos, "A quantitative approach for analyzing the relationship between urban heat islands and land cover," *Remote Sensing,* vol. 4, pp. 3596-3618, 2012.

[80] S. Pal and S. Ziaul, "Detection of land use and land cover change and land surface temperature in English Bazar urban centre," *The Egyptian Journal of Remote Sensing and Space Science,* vol. 20, pp. 125-145, 2017.

[81] J. He, J. Liu, D. Zhuang, W. Zhang, and M. Liu, "Assessing the effect of land use/land cover change on the change of urban heat island intensity," *Theoretical and Applied Climatology,* vol. 90, pp. 217-226, 2007.

[82] Z. Hu and C. Lo, "Modeling urban growth in Atlanta using logistic regression," *Computers, Environment and Urban Systems,* vol. 31, pp. 667-688, 2007.

[83] A. M. Rizwan, L. Y. Dennis, and L. Chunho, "A review on the generation, determination and mitigation of Urban Heat Island," *Journal of Environmental Sciences,* vol. 20, pp. 120-128, 2008.

[84] R. Xiao, Q. Weng, Z. Ouyang, W. Li, E. W. Schienke, and Z. Zhang, "Land surface temperature variation and major factors in Beijing, China," *Photogrammetric Engineering & Remote Sensing,* vol. 74, pp. 451-461, 2008.

[85] X. Li, W. Zhou, Z. Ouyang, W. Xu, and H. Zheng, "Spatial pattern of greenspace affects land surface temperature: evidence from the heavily urbanized Beijing metropolitan area, China," *Landscape ecology,* vol. 27, pp. 887-898, 2012.

[86] B. Dousset and F. Gourmelon, "Satellite multi-sensor data analysis of urban surface temperatures and landcover," *ISPRS journal of photogrammetry and remote sensing,* vol. 58, pp. 43-54, 2003.

[87] M. Lazzarini, P. R. Marpu, and H. Ghedira, "Temperature-land cover interactions: The inversion of urban heat island phenomenon in desert city areas," *Remote Sensing of Environment,* vol. 130, pp. 136-152, 2013.

[88] H. Radhi and S. Sharples, "Quantifying the domestic electricity consumption for air-conditioning due to urban heat islands in hot arid regions," *Applied energy,* vol. 112, pp. 371-380, 2013.

[89] C. Rinner and M. Hussain, "Toronto's urban heat island—Exploring the relationship between land use and surface temperature," *Remote Sensing,* vol. 3, pp. 1251-1265, 2011.

[90] K. P. Gallo and T. W. Owen, "Assessment of urban heat Islands: A multi-sensor perspective for the Dallas-Ft. worth, USA region," *Geocarto International,* vol. 13, pp. 35-41, 1998.

[91] K. S. Kumar, P. U. Bhaskar, and K. Padmakumari, "Estimation of land surface temperature to study urban heat island effect using LANDSAT ETM+ image," *International journal of Engineering Science and technology,* vol. 4, pp. 771-778, 2012.

[92] C. Coll, J. M. Galve, J. M. Sanchez, and V. Caselles, "Validation of Landsat-7/ETM+ thermal-band calibration and atmospheric correction with ground-based measurements," *IEEE Transactions on Geoscience and Remote Sensing,* vol. 48, pp. 547-555, 2009.

[93] L. Liu and Y. Zhang, "Urban heat island analysis using the Landsat TM data and ASTER data: A case study in Hong Kong," *Remote Sensing,* vol. 3, pp. 1535-1552, 2011.

[94] R. I. Sholihah and S. Shibata, "Retrieving Spatial Variation of Land Surface Temperature Based on Landsat OLI/TIRS: A Case of Southern part of Jember, Java, Indonesia," in *IOP Conference Series: Earth and Environmental Science*, 2019, p. 012125.

[95] R. P. d'Entremont and L. W. Thomason, "Interpreting meteorological satellite images using a color-composite technique," *Bulletin of the American Meteorological Society,* vol. 68, pp. 762-768, 1987.

[96] T. Good and P. A. Giordano, "Methods for constructing a color composite image," ed: Google Patents, 2019.

[97] Y. Xiong, S. Huang, F. Chen, H. Ye, C. Wang, and C. Zhu, "The impacts of rapid urbanization on the thermal environment: A remote sensing study of Guangzhou, South China," *Remote sensing,* vol. 4, pp. 2033-2056, 2012.

[98] U. Avdan and G. Jovanovska, "Algorithm for automated mapping of land surface temperature using LANDSAT 8 satellite data," *Journal of Sensors,* vol. 2016, 2016.

[99] F. Yuan and M. E. Bauer, "Comparison of impervious surface area and normalized difference vegetation index as indicators of surface urban heat island effects in Landsat imagery," *Remote Sensing of environment,* vol. 106, pp. 375-386, 2007.

[100] I. Dar, J. Qadir, and A. Shukla, "Estimation of LST from multi-sensor thermal remote sensing data and evaluating the influence of sensor characteristics," *Annals of GIS,* pp. 1-19, 2019.

[101] M. Neteler, "Estimating daily land surface temperatures in mountainous environments by reconstructed MODIS LST data," *Remote sensing,* vol. 2, pp. 333-351, 2010.

[102] C. P. Durand, M. Andalib, G. F. Dunton, J. Wolch, and M. A. Pentz, "A systematic review of built environment factors related to physical activity and obesity risk: implications for smart growth urban planning," *Obesity reviews,* vol. 12, pp. e173-e182, 2011.

[103] E. ArcGIS, "Environmental Systems Research Institute: Redlands," *CA, USA,* 2012.

[104] J. Eastman, F. Sangermano, E. Machado, J. Rogan, and A. Anyamba, "Global trends in seasonality of normalized difference vegetation index (NDVI), 1982–2011," *Remote Sensing,* vol. 5, pp. 4799-4818, 2013.

[105] B.-C. Gao, "NDWI—A normalized difference water index for remote sensing of vegetation liquid water from space," *Remote sensing of environment,* vol. 58, pp. 257-266, 1996.

[106] M. Maki, M. Ishiahra, and M. Tamura, "Estimation of leaf water status to monitor the risk of forest fires by using remotely sensed data," *Remote Sensing of Environment,* vol. 90, pp. 441-450, 2004.

[107] H. Zhao and X. Chen, "Use of normalized difference bareness index in quickly mapping bare areas from TM/ETM+," in *International geoscience and remote sensing symposium*, 2005, p. 1666.

[108] E. Kalnay and M. Cai, "Impact of urbanization and land-use change on climate," *Nature,* vol. 423, p. 528, 2003.

[109] Y. Zha, J. Gao, and S. Ni, "Use of normalized difference built-up index in automatically mapping urban areas from TM imagery," *International journal of remote sensing,* vol. 24, pp. 583-594, 2003.

[110] S. D. G. UN. (2015, 25th November). *UN, "Sustainable Development Goals," 2015*.

[111] R. G. Pontius Jr and J. Spencer, "Uncertainty in extrapolations of predictive land-change models," *Environment and Planning B: Planning and design,* vol. 32, pp. 211-230, 2005.

[112] C. Dereczynski, W. L. Silva, and J. Marengo, "Detection and projections of climate change in Rio de Janeiro, Brazil," *American Journal of Climate Change,* vol. 2, pp. 25-33, 2013.

[113] M. Hilferink and P. Rietveld, "Land Use Scanner: An integrated GIS based model for long term projections of land use in urban and rural areas," *Journal of Geographical Systems,* vol. 1, pp. 155-177, 1999.

[114] P. H. Verburg, T. C. M. de Nijs, J. R. van Eck, H. Visser, and K. de Jong, "A method to analyse neighbourhood characteristics of land use patterns," *Computers, Environment and Urban Systems,* vol. 28, pp. 667-690, 2004.

[115] J.-C. Castella, S. Boissau, T. N. Trung, and D. D. Quang, "Agrarian transition and lowland–upland interactions in mountain areas in northern Vietnam: application of a multi-agent simulation model," *Agricultural systems,* vol. 86, pp. 312-332, 2005.

[116] B. Pijanowski, S. Gage, D. Long, and W. Cooper, "A land transformation model: integrating policy, socioeconomics and environmental drivers using a geographic information system," *Landscape ecology: a top down approach,* pp. 183-198, 2000.

[117] H. Balzter, "Markov chain models for vegetation dynamics," *Ecological modelling,* vol. 126, pp. 139-154, 2000.

[118] W. J. McConnell, S. P. Sweeney, and B. Mulley, "Physical and social access to land: spatio-temporal patterns of agricultural expansion in Madagascar," *Agriculture, Ecosystems & Environment,* vol. 101, pp. 171-184, 2004.

[119] V. A. Parsa, A. Yavari, and A. Nejadi, "Spatio-temporal analysis of land use/land cover pattern changes in Arasbaran Biosphere Reserve: Iran," *Modeling Earth Systems and Environment,* vol. 2, pp. 1-13, 2016.

[120] D. Ozturk, "Urban growth simulation of Atakum (Samsun, Turkey) using cellular automata-Markov chain and multi-layer perceptron-Markov chain models," *Remote Sensing,* vol. 7, pp. 5918-5950, 2015.

[121] R. Regmi, S. Saha, and M. Balla, "Geospatial analysis of land use land cover change predictive modeling at Phewa Lake Watershed of Nepal," *Int. J. Curr. Eng. Tech,* vol. 4, pp. 2617-2627, 2014.

[122] P. Bhowmick, S. Mukhopadhyay, and V. Sivakumar, "A review on GIS based Fuzzy and Boolean logic modelling approach to identify the suitable sites for Artificial Recharge of Groundwater," *Scholars Journal of Engineering and Technology,* vol. 2, pp. 316-319, 2014.

[123] M. H. Hassoun, *Fundamentals of artificial neural networks*: MIT press, 1995.

[124] M. Van Gerven and S. Bohte, "Artificial neural networks as models of neural information processing," *Frontiers in Computational Neuroscience,* vol. 11, p. 114, 2017.

[125] S. Gopal and C. Woodcock, "Remote sensing of forest change using artificial neural networks," *IEEE Transactions on Geoscience and Remote Sensing,* vol. 34, pp. 398-404, 1996.

[126] G. Spellman, "An application of artificial neural networks to the prediction of surface ozone concentrations in the United Kingdom," *Applied Geography,* vol. 19, pp. 123-136, 1999.

[127] X. Yao, "Evolving artificial neural networks," *Proceedings of the IEEE,* vol. 87, pp. 1423-1447, 1999.

[128] S. Ullah, K. Ahmad, R. U. Sajjad, A. M. Abbasi, A. Nazeer, and A. A. J. J. o. e. m. Tahir, "Analysis and simulation of land cover changes and their impacts on land surface temperature in a lower Himalayan region," vol. 245, pp. 348-357, 2019.

[129] S. Mansour, M. Al-Belushi, and T. Al-Awadhi, "Monitoring land use and land cover changes in the mountainous cities of Oman using GIS and CA-Markov modelling techniques," *Land Use Policy,* vol. 91, p. 104414, 2020.

[130] M. Story and R. G. Congalton, "Accuracy assessment: a user's perspective," *Photogrammetric Engineering and remote sensing,* vol. 52, pp. 397-399, 1986.

[131] R. G. Congalton and K. Green, *Assessing the accuracy of remotely sensed data: principles and practices*: CRC press, 2008.

[132] R. G. Pontius Jr and M. Millones, "Death to Kappa: birth of quantity disagreement and allocation disagreement for accuracy assessment," *International Journal of Remote Sensing,* vol. 32, pp. 4407-4429, 2011.

[133] B. Ahmed and R. Ahmed, "Modeling urban land cover growth dynamics using multi-temporal satellite images: a case study of Dhaka, Bangladesh," *ISPRS International Journal of Geo-Information,* vol. 1, pp. 3-31, 2012.

[134] A. Dewan and R. Corner, *Dhaka megacity: Geospatial perspectives on urbanisation, environment and health*: Springer Science & Business Media, 2013.

[135] W. Bank, "Climate Change & Sustainable Report- Bangladesh," 2016.

[136] M. S. Mondal, N. Sharma, P. Garg, and M. Kappas, "Statistical independence test and validation of CA Markov land use land cover (LULC) prediction results," *The Egyptian Journal of Remote Sensing and Space Science,* vol. 19, pp. 259-272, 2016.

[137] Z.-L. Li, B.-H. Tang, H. Wu, H. Ren, G. Yan, Z. Wan*, et al.*, "Satellite-derived land surface temperature: Current status and perspectives," *Remote sensing of environment,* vol. 131, pp. 14-37, 2013.

[138] K. Patil, M. C. Deo, S. Ghosh, and M. Ravichandran, "Predicting sea surface temperatures in the North Indian Ocean with nonlinear autoregressive neural networks," *International Journal of Oceanography,* vol. 2013, 2013.

[139] L. Liao, D. Fox, and H. A. Kautz, "Location-Based Activity Recognition using Relational Markov Networks," in *IJCAI*, 2005, pp. 773-778.

[140] P. Sukanya and K. Gayathri, "An Unsupervised Pattern Clustering Approach for Identifying Abnormal User Behaviors in Smart Homes 1," 2013.

APPENDIX

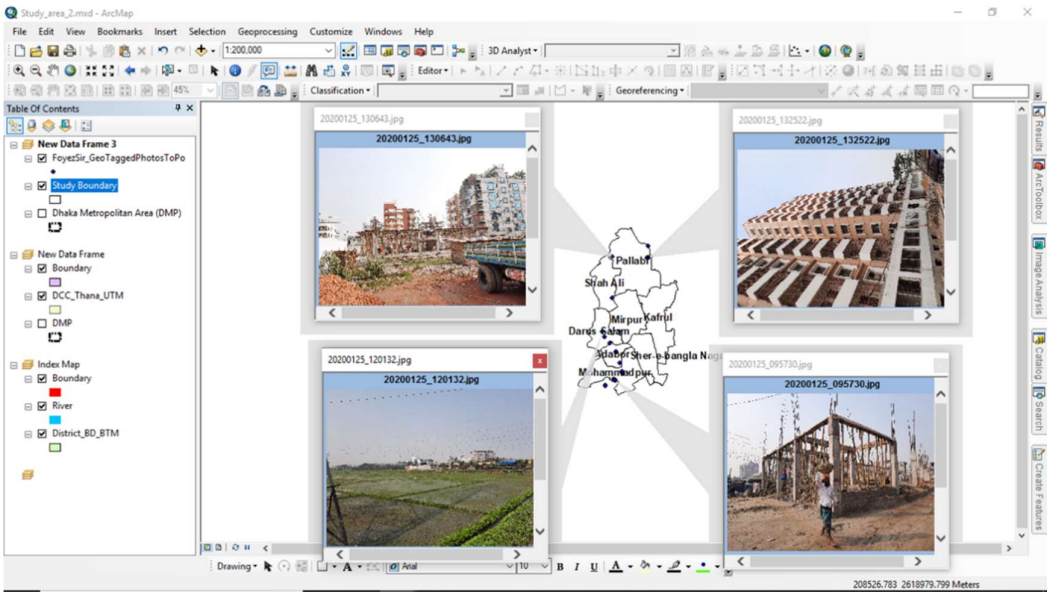

Figure A1: Field visit data analysis using ArcGIS

Figure A3: Open Land of Bangladesh Agricultural Development Corporation

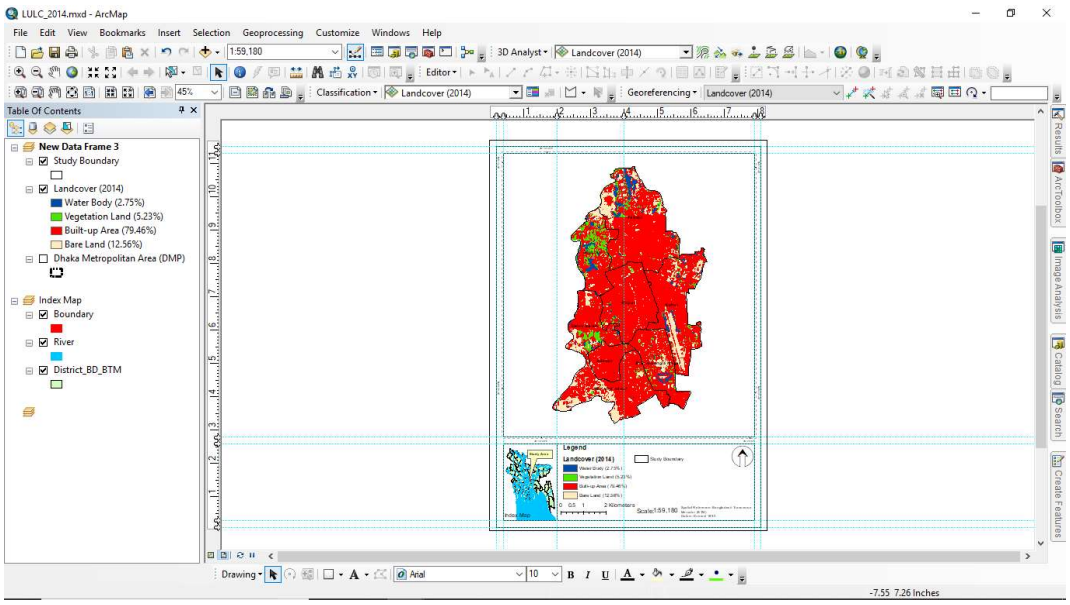

Figure A4: Satellite Image Processing using ArcGIS

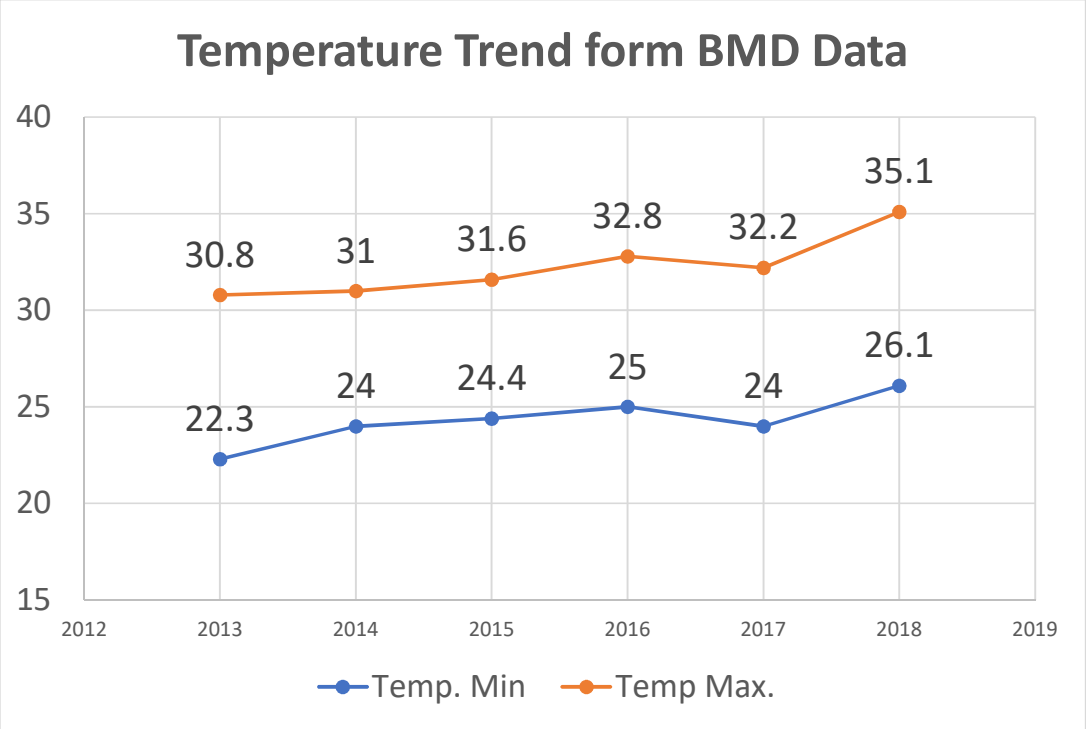

Figure A5: Temperature Trend form BMD Data

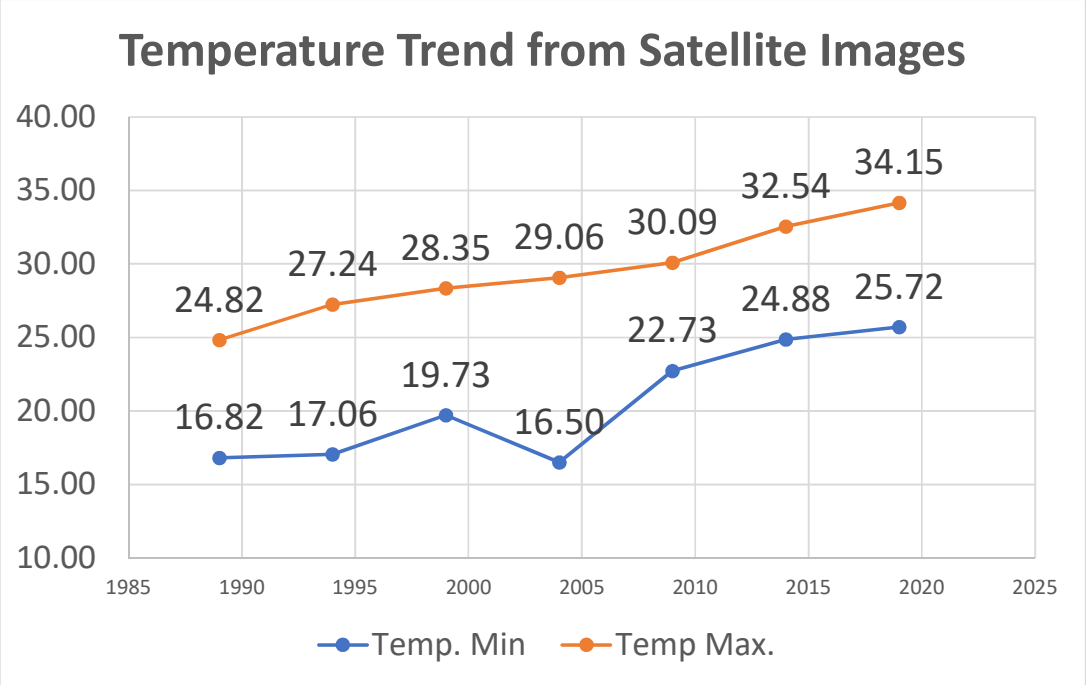

Figure A6: Temperature Trend from Satellite Images

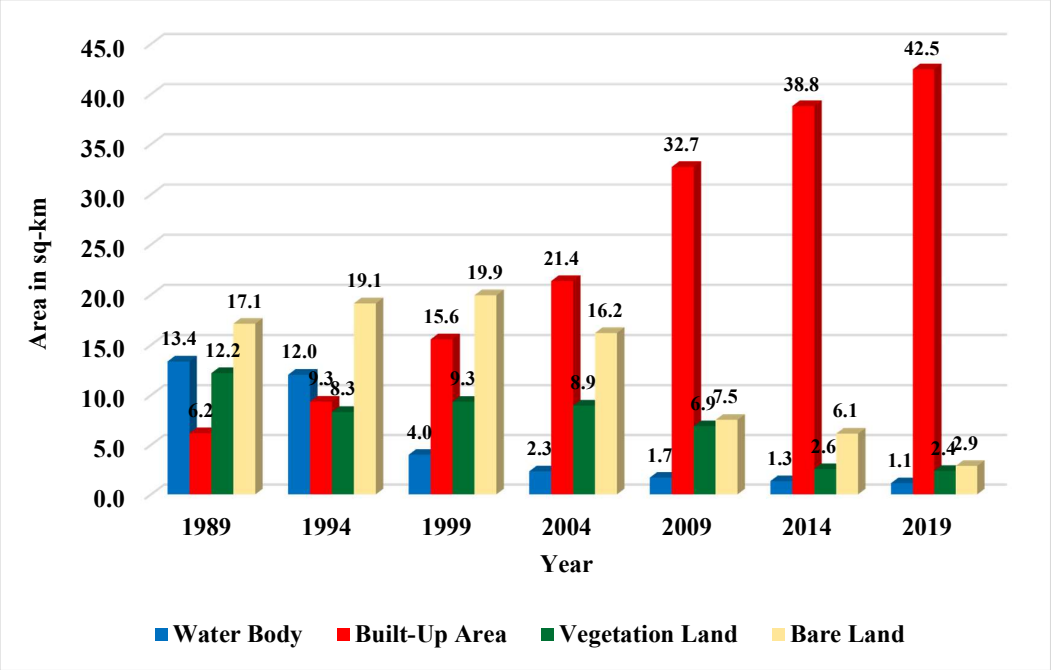

Figure A7: Changing Pattern of Different LULC Classes From 1989 To 2019 in the Study Area

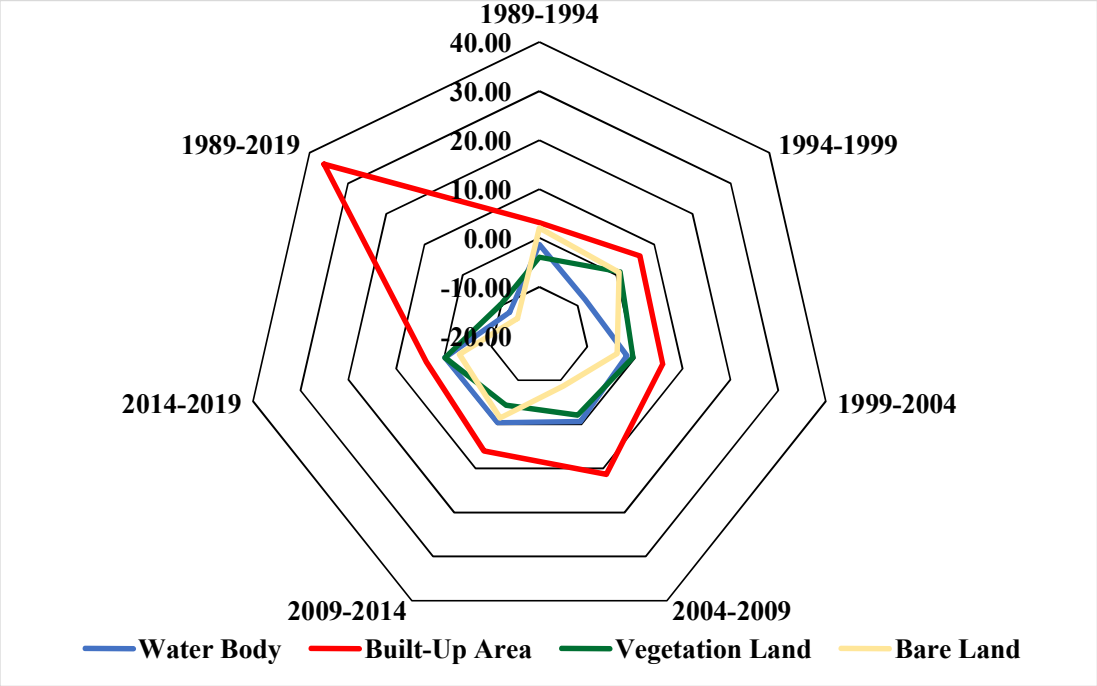

Figure A8: Spatial Pattern of LULC Change in Different Direction from Year 1989 to 2019